School of Molecular and Life Sciences

Characterisation of Gelation by Atomic Force Microscopy

Emily Clare Barker
0000-0002-7564-1449

This thesis is presented for the Degree of
Doctor of Philosophy
of
Curtin University

December 2020

Declaration

To the best of my knowledge and belief this thesis contains no material previously published by any other person except where due acknowledgment has been made.

This thesis contains no material which has been accepted for the award of any other degree or diploma in any university.

(Include where applicable)

Human Ethics (For projects involving human participants/tissue, etc) The research presented and reported in this thesis was conducted in accordance with the National Health and Medical Research Council National Statement on Ethical Conduct in Human Research (2007) – updated March 2014. The proposed research study received human research ethics approval from the Curtin University Human Research Ethics Committee (EC00262), Approval Number #.....

or

Animal Ethics (For projects involving animal use) The research presented and reported in this thesis was conducted in compliance with the National Health and Medical Research Council Australian code for the care and use of animals for scientific purposes 8th edition (2013). The proposed research study received animal ethics approval from the Curtin University Animal Ethics Committee, Approval Number #.....

Signature: ……

Date: 04/12/2020……...

Acknowledgements

First and foremost I'd like to thank my primary supervisor, Dr. Thomas Becker, who's patience and generosity have made my PhD a smooth and fulfilling experience. The six years I spent working with you have been the highlight of my education at Curtin University and I have greatly enjoyed all of our time on the scanning probe microscopes as well as our meetings. I could spend decades working in that lab and still not learn everything you have to teach about these instruments but I will be eternally grateful for what I have been taught. I was never the most patient student in return but I hope it was not too arduous an experience for you!

The second person I must thank is Prof. Mark Ogden who has also supervised me for the last six years or more. Your enduring passion for chemistry has been an inspiration to me during my research and has driven me to delve further into other areas which I find interesting, rather than just the research I am conducting. Your continued advice regarding academic life has been indispensable and I'm sure will continue to guide me in my career. You have been the perfect example of a research group leader and a professor, with your constant time for students and, above all, fairness and reliability.

My third supervisor, Dr. Adam Martin, also deserves a huge thank you. I didn't know you well when you came onto this project but it has always been a pleasure to work with you and I am so grateful you agreed to come on board! I have learnt everything I know about small angle neutron scattering and rheometry from you which is not a small portion of this project. Your trust in my abilities has pushed me further than I would have gone had you not been a part of this

team. It has been invaluable to my PhD and early research career to be able to have you as my supervisor.

I would also like to thank my short term supervisor, Prof. Karin Jacobs, who allowed me into her research group for three months in Germany. I cannot describe how important it was to have a female supervisor and the academic knowledge you so generously passed on while I was in your group will continue to motivate me for years to come. The experience of working in another country cannot be taught and I would not have had this opportunity had you not provided it.

Brendan Ennis, Nicholas Tan, Braden Cunningham, Ching Yong Goh and Caitlin Duncan, your chemical synthesis wizardry has made this research possible. I cannot express how afraid I am of conducting chemical synthesis and how thankful I am to you for doing it for me.

A huge thank you to Peter Chapman and Grant Cope, the chemistry department couldn't run without you and you are both saints for putting up with everything and everyone. Benjamin Austen and Shakawan Beebany, thank you for being courteous and engaging office buddies and for going through PhD life with me. Thanks to Dr. Calum McCulkin, Dr. Rhys Tilbury, Dr. Natalya Garcia, Dr. Buddhika Dorakumbura and everyone else who I went through my PhD with on the scanning probe microscopes. Your enthusiasm and condolences were greatly appreciated during and after experiments.

Lastly thank you to my partner, Nathanael Borbely, my family and friends for putting up with my crazy schedule during this time. You've all always understood when I could not attend events and when I needed someone to be excited about my work, even when you couldn't understand why.

Abstract

This work presents investigations into supramolecular gels by Atomic Force Microscopy (AFM), rheometry and Small Angle Neutron Scattering (SANS). Supramolecular gels are an interesting sub-set of gels due to their reversible nature which can be easily switched from liquid to gel using external stimuli. The assembly and disassembly of these gels is not well understood and most gels have been serendipitously found. The properties of gels define what uses they can be applied to, which is currently impossible to predict prior to synthesising a gel.

Gels of proline calix[4]arene were analysed to study the annealing behaviour when formed with the electrolyte magnesium chloride. This gel was shown by rheometry to become stronger and more brittle with each assembly and disassembly cycle. Imaging by *ex situ* and *in situ* AFM showed larger structures forming during the second assembly of the gel. An investigation by SANS showed the gel reassembling into fibres with a similar length and radius but with a much longer Kuhn length, therefore the fibres were straightening further with each assembly cycle. Gels formed in the presence of lithium chloride did not show this behaviour and were seen to behave fully reversibly by all three methods.

Higher concentration gels of proline calix[4]arene with the electrolyte lithium chloride were seen to form helical structures. These structures were imaged by *ex situ* AFM with the direction of the helices seen to be dependant on the enantiomer of the proline calix[4]arene. This gel was investigated using SANS which showed the radius of the fibres to be slightly larger than in experiments with the lower concentration gel. This indicates a polydisperse system with helices and individual

fibres as a gel comprised of only helical structures should have a radius of at least double that of the lower concentration gel.

Two novel peptide gels were also imaged by AFM. The Fluorenylmethyloxycarbonyl-Gly-Phe-Phe-Arg-Gly-Asp gel was shown to be impossible to image by the *in situ* method used as the Dulbecco's Modified Eagle Medium in which the gel was formed was too viscous. The N,N'-bis-[di-CBZ-L-Lys]-ethylenediamine gel was imaged *ex situ* due to the hazardous solvents in which it gelled. Fibres were imaged with the indication that they may also form helices although these were not further investigated.

Attempts were made to image the assembly and disassembly of a gel, *in situ*, within a thin film but with the AFM cantilever not submerged, to extend the AFM method to opaque gels. However, this was not achieved due to evaporation of the solvent when the gels were heated to initiate disassembly. If a closed cell instrument were available, this may be possible and allow the extension of this method to a greater variety of gels.

A MATLAB script was developed to analyse the properties of gels during their assembly and disassembly as recorded using AFM in PeakForce Quantitative Nanomechanical Mapping. This was not fully tested to find any conclusions in regards to how these properties change during these processes due to time constraints. The values were seen to have a very large error and this is likely due to the low resolution imaging of the experiments used and the heating and cooling processes being too fast causing there to be a large difference in the physical properties of the fibres across the sample in each image.

The rapid developments in AFM instrumentation allow for visualisation of gelation that has barely been investigated. While selected supramolecular hydrogels were quantified in this thesis, the methods developed should allow for a greater understanding of other gels and their properties. There are some barriers to the imaging of certain gels based on their opacity, viscosity and solvents used, however, with the right AFM set up, these should all be able to be overcome.

Supporting publication:

Emily C Barker, Adam D Martin, Christopher J Garvey, Ching Yong Goh, Franca Jones, Mauro Mocerino, Brian W Skelton, Mark I Ogden and Thomas Becker. Thermal annealing behaviour and gel to crystal transition of a low molecular weight hydrogelator. *Soft Matter*, 13(5):1006-1011, 2017.

Contents

List of Figures

List of Tables

List of Abbreviations

AFM	Atomic Force Microscopy.
ANSTO	The Australian Nuclear Science and Technology Organisation.
CLSM	Confocal Laser Scanning Microscopy.
DBS-CO_2H	Dibenzyldiene-D-Sorbitol.
FRET	Fluorescence Resonance Energy Transfer.
FTIR	Fourier Transform Infrared.
HOPG	Highly Ordered Pyrolytic Graphite.
LMW	Low Molecular Weight.
LVER	Linear Viscoelastic Region.
NMR	Nuclear Magnetic Resonance.
SANS	Small Angle Neutron Scattering.
SAXS	Small Angle X-ray Scattering.
SEM	Scanning Electron Microscopy.
SNOM	Scanning Near-field Optical Microscopy.

STM	Scanning Tunnelling Microscopy.
TEM	Transmission Electron Microscopy.
THF	Tetrahydrofuran.
TOF	Time-of-Flight.

Chapter 1

Introduction

1.1 Gels

Gels have been used across many industries for centuries due to their unique but varying properties.[1] They are widely utilised in food science, health industries and materials science.[2–7] Gels are often difficult to categorise as they fall between solid and liquid forms of matter. This has been an ongoing discussion since the initial report of gels in 1861 by Graham.[8] This physical form comes from gels being comprised of two main components; the solvent, or continuous phase, and the gel network, or solid phase, which then locks the solvent in place.[1,9,10] The properties of the resulting gel (such as stiffness and temperature range at which the gel is stable) may be controlled by either the gel network or the solvent.[10,11] Generally, changing the solvent will change the strength of the gel whereas changing the gel network will alter the conditions or stimulus under which the gel forms.[12]

As the assembly process has been shown to change the properties of a gel, it is important to understand how this occurs.[13,14] To form a gel, gelator molecules self-assemble into a solid structure to form the gel network and lock the solvent in place. The self-assembly of these molecules is thought to follow a pattern as seen in Figure 1.1. The gelator molecules first come together to form chains which build the individual fibres. These fibres can then entangle, or further bond, through cross-linking, to form the gel network.[15]

Figure 1.1: Graphical depiction of the assembly of most supramolecular hydrogels.[15]

Classification of gels is often related to the types of solvent used and the type of bonding used to form the gel network. For example, if the solvent is an organic liquid, the gel may be referred to as an organogel.[9,10] These gel definitions are extremely important as most uses for gels have requirements for the system they are used in, such as those used in the medical industry which are often hydrogels so that they are compatible with the human body.[16] Figure 1.2 shows further classifications for gels.[9]

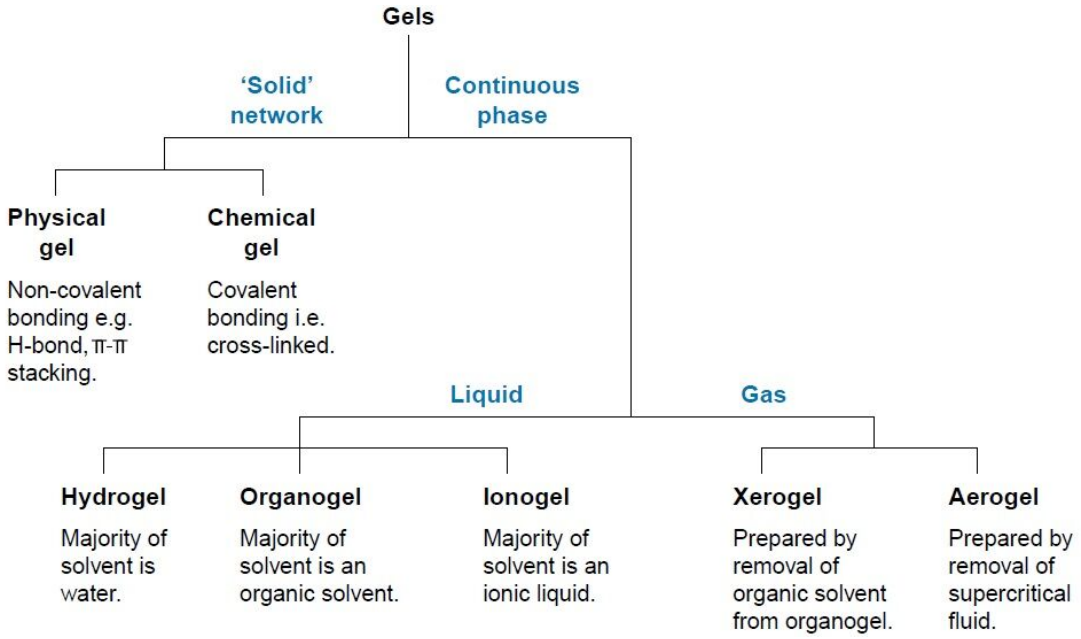

Figure 1.2: Common gel naming conventions.[9]

Despite the large interest in gels and the wide variety of uses for them, it is still very difficult to design and create a gelator for a gel with a specific purpose as for any given gelator molecule it is not possible to predict the properties of the

resulting gel. While gel properties can be modified using additives or by assembling the gel under different conditions, it is often not viable to do so due to the large number of possible variations and the unpredictable nature of the resulting gel.[17–19]

To combat this, gels which are near perfect for a purpose are often modified with the use of additives or changing the conditions during the assembly process. This can either vastly change the properties of a gel or only slightly tweak them.[20–22] Changing the gelator concentration is the most basic, and therefore most common, way to change the properties of a gel. It is assumed that this is due to a larger volume of gel fibres within the gel which will hold the solvent and make the gel stronger. In 2011, Ma *et al.* showed that α-cyclodextrin and poly(ε-caprolactone)–poly(ethylene glycol) block co-polymer would form a gel which would encapsulate chicken egg lysozyme and release it over a period of days.[23] It was shown that modifying the concentration of the α-cyclodextrin and/or the poly(ε-caprolactone)-poly(ethylene glycol) in the gel changes the gelation time, mechanical strength and shear viscosity of the resulting gel, as well as time taken to release the lysozyme, and the overall amount released. Barzegar *et al.* showed that the addition of carbon black to a polyvinyl alcohol based gel vastly improved the energy density of a supercapacitor device in comparison to an aqueous electrolyte.[21] In this case, gels were initially postulated as a better material due to their high porosity causing a high energy density, however, their low conductivity and high viscosity created issues with their application. The addition of carbon black to the gel increased their conductivity and was shown to create a superior material for electric double layer capacitors.

1.2 Analysis of Gels

Analysis of the properties of gels has been conducted for decades across many different industries which has created many methods depending on the information required. The oldest and most crude gelation analysis is the vial inversion test. The gel is formed in a vial and if the gel remains in place upon inverting the vial then it is said to be a gel. If part of the gel remains liquid and falls to the "top"

of the vial then it is said to be a partial gel. This method is still used and widely reported today due to its ease of use. The dropping ball method is used to find the melting point of a gel, or the T_{gel}.[9] In this method, a gel is formed in a vial or measuring cylinder and a ball bearing placed on top of the gel. The gel is then heated until it reaches a temperature at which the ball falls through the gel as it liquefies, which is recorded as the gel melting point or T_{gel}.

1.2.1 Light and Spectroscopy Techniques

Gel formation in a bulk solution can often be easily observed using turbidity and light scattering. These methods are much cheaper than most microscopy visualisation techniques and therefore are more widely available. These methods detect the cloudiness of a sample or determine the amount of scattered or absorbed light. Figure 1.3 shows how light is emitted from a source and is detected as scattered light and/or transmitted light after passing through the sample. Some gels cannot be analysed using these methods, as the particle sizes are below the detection limit of the technique, which is normally in the range of 1-10 nm. Light scattering algorithms usually assume a spherical particle is seen which does not fit the solid structure of a gel as these are usually fibrous. This should then show a bimodal distribution showing diameter and length of the fibres, however, often the random orientation and aggregation of the fibres does not allow for accuracy in this method. Turbidity and light scattering have been used to follow gelation kinetics by tracking the formation of particles which reduce the transparency of the solvent.[24,25] However, this is difficult with many supramolecular gels which form transparent gels due to the negligible change in the turbidity of the sample when the gel is formed.[15,24,26]

Many other methods can be used to confirm gelation or self-assembly but they also do not give any information regarding the structure or assembly process. For example, Nuclear Magnetic Resonance (NMR) is often used to show the self-assembly of molecules by tracking peak broadening and an increase in peak intensity or height related to covalent bonds.[27] Peak shifts may also be tracked over

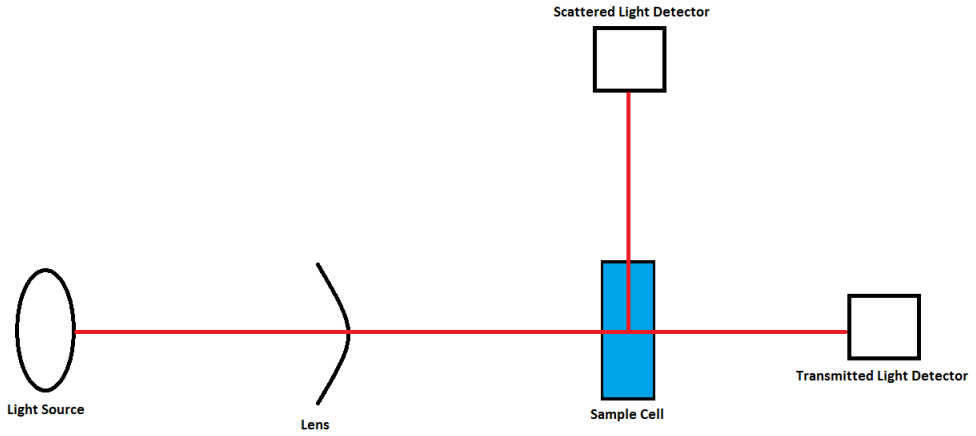

Figure 1.3: Schemtic showing the pathway of light detected in scattering techniques.

time to show the aggregation of the compound or a change in the overall chemical environment. However, NMR cannot give an indication of the physical structure that is formed. Other spectroscopy techniques, such as Fourier Transform Infrared (FTIR), can also show assembly by tracking peak broadening, or shifting of peak positions over time but they have the same limitations as NMR.[28]

1.2.2 Rheometry

Rheometry is arguably the most popular method for the analysis of gels. Rheometry allows for the study of the strength and breaking point of gels with only small volumes of the gel required.[29,30] One of the common techniques is the parallel plate technique which is conducted by placing the gel between two plates which then apply a shear or oscillatory stress to the gel and measure the response of the gel.[31] There are many different measurement geometries, such as Couette and cone and plate, which all come with various advantages and disadvantages.[32,33] However, none of these rheometry methods gives any indication of the structure of the solid portion of the gel which is thought to control many of the properties of gels.

To measure the strength of gels and their breaking points, two parameters can either be fixed or varied, i.e. the frequency and strain.[34] The strain may be kept constant while ramping the frequency at which the plates turn, which is known as

a frequency sweep.[35] Alternatively, in an amplitude sweep, the frequency is kept constant while the strain, or torque, is increased.[36] These sweeps are used to mimic different types of force applied to a material. Frequency sweeps simulate processes which are dependent on rate of flow, such as the flow through a tube. Amplitude sweeps simulate processes which are dependent on force, such as pushing materials out of a syringe. The storage modulus and loss modulus are then recorded during these measurements. Figure 1.4 shows the typical plot seen when storage modulus (G') and loss modulus (G") are plotted against strain to find the limit of the Linear Viscoelastic Region (LVER). This is the range during which the structure of the gel is not destroyed, and shows the breaking point of the gel. Frequency sweeps are used to gain understanding of the strength and long term stability of gels. To do this, the amplitude sweep is first performed to find the LVER and then the frequency sweep is performed within this region to ensure the gel remains intact.

Storage modulus is a measurement of the stored energy. This represents the elastic energy stored within the hydrogel upon deformation by the plates during testing, and it is what enables the hydrogel to restore to its original shape upon cessation of an external force. The loss modulus gives the viscosity of the hydrogel and represents the energy dissipated within the hydrogel upon application on an external load. When the force applied by the plates is greater than this stored energy then the gel will flow as the structure will be broken.[37] To compare these contributions and find where a gel is behaving elastically or viscously, the loss tangent is used which is defined by

$$tan\delta = G" / G'$$

Where tan δ is greater than one, the viscous component of the gel is the greater contributor and the gel is not seen to behave elastically.[38]

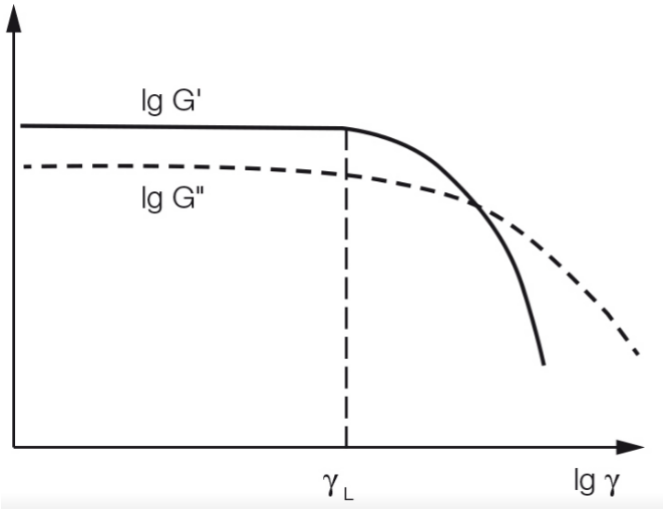

Figure 1.4: Amplitude sweep plot showing the storage modulus (G') and loss modulus (G") with change in strain. This is then used to find the limit of the linear viscoelastic region for gels.[36]

1.2.3 Microscopy Techniques

1.2.3.1 Electron Microscopy

As the solid structure of a gel can vary largely in size, several methods are often used to obtain a complete picture of the structure. The most common methods originally used to show the structure of gels were electron microscopy techniques.[26] Scanning Electron Microscopy (SEM) and Transmission Electron Microscopy (TEM) require the sample to be dried or frozen as it is conducted in a vacuum and it is unknown how this preparation may change the structure.[39–41] Freezing, in particular, may change the structure drastically as the solvent expands or contracts as it cools which will distort the solid portion of the gel.[42] The samples also need to be coated with either gold or carbon to create a conducting sample which could further alter the structure seen by the technique.

1.2.3.2 Confocal Laser Scanning Microscopy

Confocal Laser Scanning Microscopy (CLSM) can be used to image gels without significant sample preparation issues, however, the resolution is limited by the diffraction limit of the light used to image the sample. This means that many gel network structures are much too small to be visualised by this method. If the

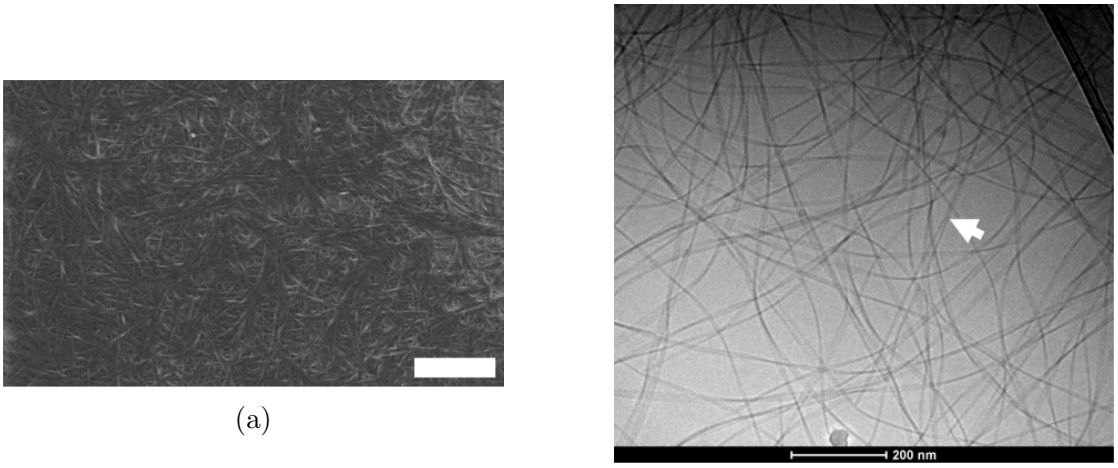

(a) (b)

Figure 1.5: (a) Scanning and (b) Transmission electron microscopy images of a LMW gel after drying.[41] The scale bar in image (a) represents 2 μm. The white arrow in image (b) indicates where two fibres are seen to form a helix structure. Reproduced from Ref. 41 with permission from The American Chemical Society.

fibres are large enough, this method can be used to image a gel in real time as the gel is assembled and disassembled by applying external stimuli such as heating and cooling. The laser light also applies heat in a concentrated area where the imaging is occurring and this may distort the image by melting the gel quickly.[43,44]

Recently, super-resolution microscopy has allowed the resolution of optical imaging methods to be vastly increased. This can be achieved by using Fluorescence Resonance Energy Transfer (FRET) to measure the energy transfer between molecules within the fibres and an added fluorophore. Using this in conjunction with CLSM, gels have been imaged with resolutions of 80 nm down to 20 nm.[45–47] However, this is still orders of magnitude too large to be able to image some gel networks.

Paterson *et al.* conducted a comparison of SEM and CLSM in the analysis of poly(2-hydroxyethyl methacrylate) based hydrogels to show the differences in the morphologies as well as the efficiency of the methods.[44] It was found that the morphology of the gel network changed significantly when the sample was freeze dried prior to analysis by SEM. Figure 1.7 shows that the structure seemed to have collapsed in the image captured by SEM. The CLSM method was also found to be quicker than the SEM method as little to no sample preparation was required and

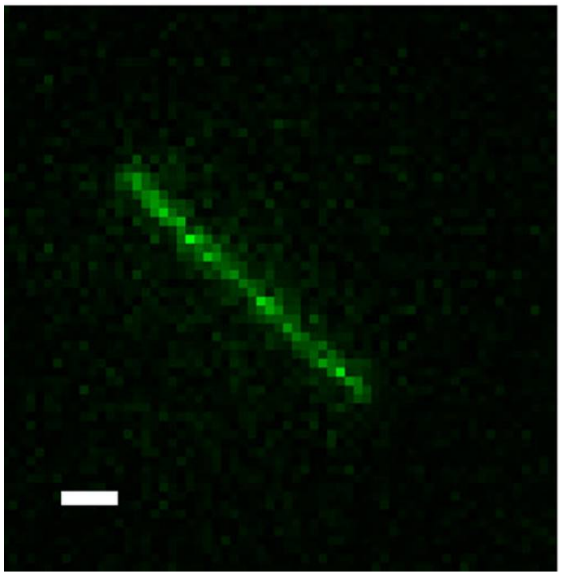

Figure 1.6: Super resolution microscopy image of a LMW gel fibre using fluorescent dyes and correlative image analysis to increase visibility. Scale bar is 1μm.[45]

the time to set up the instrument was shorter. This study conclusively pointed to *in situ* methods being required for the analysis of gels.

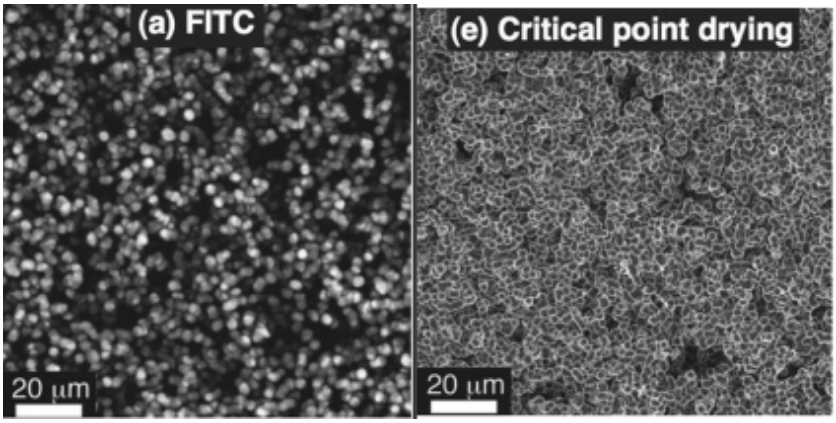

Figure 1.7: Comparison of the gel network of a poly(2-hydroxyethyl methacrylate) gel when imaged by CLSM (a) and SEM (e). This shows a significant difference in the networks seen by each method.[44] Reproduced from Ref. 44 with permission from John Wiley and Sons.

1.2.3.3 Scanning Near-Field Optical Microscopy

Scanning Near-field Optical Microscopy (SNOM) overcomes the diffraction limit and is a powerful technique for the imaging of small structures. In this technique only the light in the "near-field", or within one wavelength of the light, of the sample is recorded, i.e. before the light has undergone diffraction. This means the

resolution is only limited by the numerical aperture of the SNOM probe and not the diffraction limit of the light. This allows the resolution to be in the size range of many gel networks. Often the fluorescent nature of the fibres is used to facilitate visualisation of the structure which was buried within the gel.[48] If gels with fibres that did not exhibit fluorescence were analysed then their structure may not be able to be discerned by this technique.

1.2.3.4 Scanning Tunnelling Microscopy

Scanning Tunnelling Microscopy (STM) has been used to show self-assembly of molecules on a substrate. It is conducted by tunnelling a current from a probe, through the sample, to the instrument stage. This method can be used to show the gel network structure after the gel has formed. It is not possible to scan in electrically conductive liquids due to the potential that must be applied to create the tunnelling current. However, drying of the sample and the interaction with the substrate may change the structure and it is not possible to follow the assembly dynamically.[49] Samori *et al.* demonstrated the self-assembly of an ether phthalocyanine gel on graphite by STM.[50] Their study demonstrated the assembly of the sample into fibrous structures as well as lamellae, however, imaging was not performed with sufficiently high resolution to reveal the structure of the fibres.

1.2.3.5 Atomic Force Microscopy

Atomic Force Microscopy (AFM) is a relatively new form of imaging in which a probe interacts with the surface and these interactions are recorded as the topography of the surface.[51] It can also be used to show changes in properties of the surface based on how the probe interacts with the sample surface. Originally, the probe needed to be in constant contact with the surface which could damage the sample or create deformations which would be seen in the data. However, developments in the 1990s allow for an imaging mode in which the probe is intermittently brought into contact with the surface as it moves across the sample.[52] The cantilever that the probe is mounted on is oscillated near its resonant frequency and

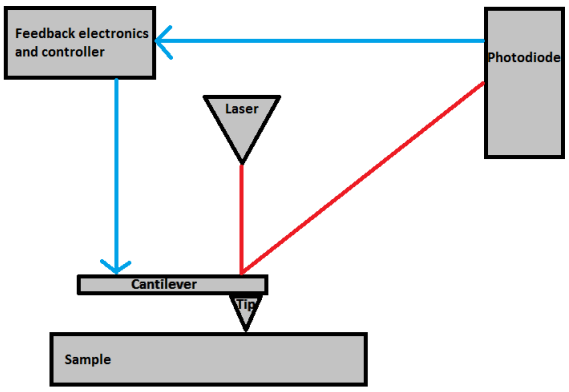

Figure 1.8: Schematic showing how an AFM uses a tip mounted on a cantilever to image the topography of a sample.

the tip then scanned across the surface. This greatly reduced the lateral forces applied to the sample and as such very soft samples like gels are now imaged widely using intermittent contact mode AFM.

Intermittent contact mode AFM is conducted by tapping a tip across the surface of a sample to record the topography. The tip is mounted on a cantilever which deflects when the sample surface changes height, allowing the instrument to record the change in topography. A laser is shone onto the back of the cantilever and reflected to a photodetector which records the deflection and creates a feedback loop, through the controller, to the scanner in which the cantilever is mounted.[52] Figure 1.8 shows a schematic of the basic elements of an AFM.

Studies of the physical structure of gels have been conducted extensively by AFM. To carry out this imaging technique, the gel is usually applied onto a substrate, dried and then imaged. While this gives information regarding the crosslinking and general network structure, it is difficult to draw further conclusions as it is unknown how the structure may change when the solvent is removed. The diameter of the fibres may shrink or expand and the fibres may also shorten or the entire structure may collapse during the drying process.[53–57]

Busch *et al.*[58] showed that polymer films could be imaged *in situ* by spin coating a thin film of the polymer and then imaging the film with tapping mode AFM. This can be conducted in tapping mode as long as the amplitude of the oscillation is kept lower than the film thickness, allowing the tip to remain within

the film during imaging. This showed very different results to a cross-sectional TEM experiment in which the sample was dried prior to analysis. The TEM results showed a surface lamellar structure which was not seen by AFM. This could be due to drying effects causing the structure to shrink in areas with a greater concentration of water.

In 2014, Schefer, Adamcik and Mezzenga used AFM to image a gel *in situ* for the first time and show its microscale structure.[59] They were able to show that anionic carrageenan polysaccharides form disordered coils which, upon the addition of the electrolyte sodium chloride, become a single helix structure. However, due to the specific instrument and mode used, the transition between these structures could not be imaged. The sample was set and imaged and then changed and imaged again which leaves the assembly process unseen. The images were also taken over 8 to 53 minutes which is far too slow given many gels form within a few minutes and can then quickly crystallise.[60]

PeakForce Tapping is a relatively recent AFM imaging mode in which the tip is driven at a frequency between 1 and 8 kHz, well below the cantilever's resonant frequency.[61] Each interaction with the sample is individually recorded rather than these interactions being smoothed and averaged across each oscillation. Previously, using tapping mode, a so-called phase image was acquired, however, this would filter out all deflection of the cantilever that was not at the resonant frequency and average all other forces. This made it impossible to know which properties were contributing to the change in phase. PeakForce tapping allows these properties to be individually visualised by analysing the full force curve.[62] In this force curve the tip will approach the sample, snap into contact with the sample due to attractive forces, apply a user-defined peak force and then be withdrawn from the sample. From this force curve, information regarding adhesion, stiffness, local modulus and numerous other physical qualities can be quantified. Figure 1.9 shows one full force curve and some of the properties that can be calculated from it. To quantify these values, the spring constant of the tip and deflection sensitivity of the sensor must be calibrated first.[63] Using a defined frequency at which to oscillate the tip means

changes in humidity and temperature can occur without the cantilever needing to be retuned, it also allows for imaging within a medium with changing viscosity. In tapping mode, these changes to the sample and sample environment would cause the resonant frequency of the cantilever to change. This would mean that as the changes occur, imaging would need to be stopped and the probe retuned, which does not allow for continuous imaging of dynamic processes.

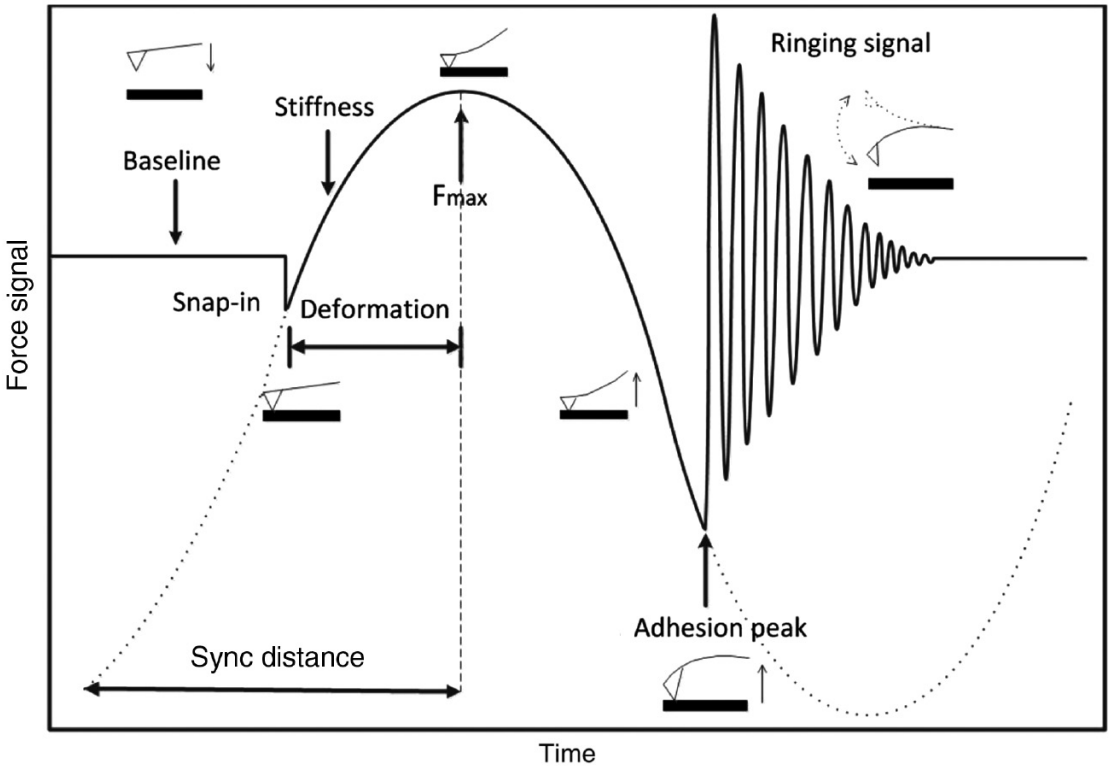

Figure 1.9: One full force curve from the interaction of an AFM tip with a sample during PeakForce tapping. Some of the properties which can be analysed by this method and the areas of the curve which are relevant to them are shown.[62]

The imaging mode was commercially distributed in 2010 which allowed it to be used in a vast number of research disciplines to image samples with a precise force to limit damage and gather information about physical properties.[64] In particular the ability to image at atomic resolution was increased as the tip can oscillate further from the sample without being disrupted by long range forces whereas tapping mode had to be conducted about 1 nm from the surface of the sample. This increased the likelihood of the tip sticking to the surface or being damaged by the surface. In tapping mode, the maximum force on the tip would also change drastically throughout the scan which could damage the tip. In PeakForce tapping

this is avoided as the feedback mechanism is the constant PeakForce rather than the dissipation. Due to these advancements, PeakForce tapping has been used to image monomers and polymers at the molecular level.[65–67]

As the forces experienced by the tip are captured in one fluid motion, it is difficult to separate the contributions to each of the physical properties, such as adhesion and stiffness or modulus. Several models have been proposed for the interaction of one body with another which define the forces exerted and experienced by each body during their interaction. The first model, known as the Hertzian model, was proposed in 1881 and defined the contact between two elastic bodies with no adhesion.[68] Later a model was proposed by Johnson, Kendall and Roberts (known as the JKR model) which included adhesion in the interaction of the bodies.[69] Another model which included adhesion was also given by Derjaguin, Muller and Toporov a few years later, this model became known as the DMT model.[70] Further research, pioneered by Tabor, built on the JKR and DMT models to define the interaction of specific materials and shapes.[71–73]

A study conducted by Prokopovich and Perni used AFM to study the adhesion between a polymer, polybutylene terephthalate (PBT) and silicone or glass.[74] The adhesion measured showed that the interaction between PBT and silicone agreed best with the simulated data from the JKR model. However, the adhesion recorded using AFM for PBT and glass agreed better with the DMT model. Currently, the Bruker Nanoscope software records modulus using the DMT model and does not allow for this to be easily recalculated using a different model. This study does appear to show that the interaction of an AFM tip with a gel fibre could be reasonably calculated using the DMT model.

In 2011, Young *et al.*[75] showed that PeakForce Mapping could be used to determine the stiffness of various polymers by mapping Young's modulus. This showed large differences in Young's moduli compared to the manufacturer reported values for the three probes tested. The results also correlated with existing methods for testing the stiffness of polymers.

In 2015, Barker *et al.* developed a method for imaging gels *in situ* by AFM

during the assembly and disassembly processes. This showed the reversible nature of the assembly and disassembly of the proline calix[4]arene gel with a $MgCl_2$ electrolyte.[76] Unfortunately, this method was only applicable to transparent gels as larger particles would scatter the laser following the probe and cause the instrument to stop imaging.

1.2.4 Small Angle Scattering

Small Angle X-ray Scattering (SAXS) and Small Angle Neutron Scattering (SANS) have been used extensively to study gelation. It is possible to conduct small angle scattering under almost any conditions with samples in any form but it only gives an overall picture of the structure. This means that any variation within the sample will be averaged across the whole sample and one structure is given, when in reality there may be many different structures within a sample. It is normally recommended to have some data on the structure of the gel before conducting small angle scattering in order to accurately fit models to the processed data. Similarly to CLSM, the beam applies a large amount of energy in a concentrated position which may change the structure of the gel in this area.

The effect of drying on the physical structure of a dipeptide Low Molecular Weight (LMW) gel was reported by Mears *et al.* using SANS, AFM, SEM and TEM. By comparing SANS data of the bulk and dried gels and the fibre diameters measured by all methods, the large effect of drying on the fibres could be shown.[41] It was observed that while the actual structure of the fibres and the network could be seen by SANS, after drying, the fibres bundled and it was impossible to image

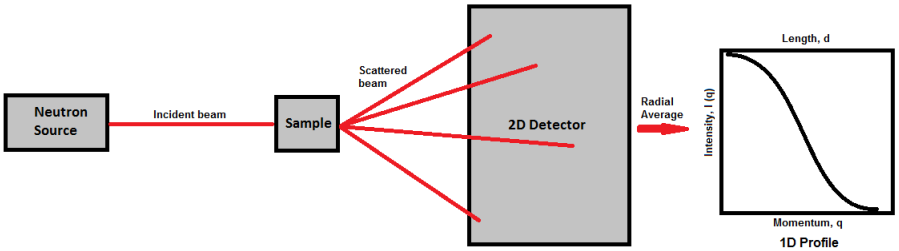

Figure 1.10: Schematic showing how small angle neutron scattering uses a neutron beam to give the structure of a gel.

them by either SEM or AFM while the TEM images only showed the individual fibres and not their interaction with each other within the bulk gel. However, an imaging method is necessary to complement SANS to ensure the correct model is used for the sample and so the correct sizes and distances are calculated. The accessibility of SANS is also much lower than the other techniques used in this experiment as beam time at a facility with a nuclear source is required.

The development of Time-of-Flight (TOF) SANS in the 1980s allowed for a greater range of samples to be analysed by SANS.[77] The TOF method follows each individual neutron from the source to the detector which allows the sample to be changing while data is being collected. If the sample were changing while data was being collected on an instrument with a monochromatic source, the data would all be averaged and one averaged value given after data analysis. Not only could the change in the sample not be seen, the data collected would be useless as it would not be from a monodisperse sample. Generally, data was originally collected on monochromatic sources by equilibrating the sample, setting the detector and collecting data and moving the detector. Only a single wavelength of neutrons is used as well. In TOF SANS, the detector is kept stationary and a wide range of neutron wavelengths are used. The neutron beam is in packets rather than a constant beam and this allows each neutron to be followed. Due to this, even if the sample is changing during analysis, the time at which each neutron interacts with the sample can be tracked and so this dynamic change can be followed. Initial instruments had a pulsed beam to create the packets of neutrons, however, more recent instruments have used rotating collimators to chop the beam into packets after it has left the source.[78,79] It is important that these packets do not overlap so the gap must be large enough for the high energy neutrons not to overtake the low energy neutrons during the path from the choppers to the sample.

1.3 Supramolecular Chemistry and Gels

Supramolecular chemistry is an area of chemistry which often falls between the bottom-up and top-down methods of building structures.[80] It deals with the self-

assembly of structures using intermolecular forces such as Van der Waals, hydrogen bonding and other electrostatic forces. The study of these structures has become more and more prevalent due to the reversible nature of the self-assembly process.[26]

Supramolecular gels have recently become popular in many industries due to their ability to be switched between a liquid and gel phase with outside stimuli.[81,82] These gels are comprised of small molecules which form intermolecular bonds to create the solid structure of the gel. These bonds are easily broken and reformed without damaging the gelator molecules so the gels can be assembled and disassembled continuously. This also means there are little to no degradation products which can make many other types of gels unsafe for use as they may become toxic as they degrade.[83] These gels are often referred to as LMW gels, however, there is not a widely accepted molecular weight at which a gel is no longer considered to be a LMW gel.

A major use of supramolecular gels in the biomedical research industry is as a biological scaffold for cell growth. In 2006, an N-hydroxysuccinimide gel was used to stop bleeding and is then used as a scaffold for the healing of tissue, breaking down into amino acids which will not be harmful to the body.[84] This allows for a fast method to stop bleeding without further damage to the area, unlike previous methods such as cauterisation. Supramolecular peptide gels have also been used for the successful culture of primary neurons. This is an important step in research for neuro-degenerative diseases such as dementia as neurons require a substrate to grow along as they do not simply split and proliferate like other cell types.[85] Hartgerink *et al.* used electron microscopy to show that a LMW peptide gel could serve as the extracellular matrix to grow hydroxyapatite to build bone tissue.[86]

The major difficulty to overcome with supramolecular gels is their strength which is normally quite weak in comparison to polymeric gels.[87] In 2013, Cornwell *et al.*, reported that a novel hydrogelator, a carboxylic acid derivative of Dibenzyldiene-D-Sorbitol (DBS-CO_2H), was able to assemble in the presence of a preformed polymer gel, agarose.[88] The agarose gel network still allowed the DBS-CO_2H gel to assemble and disassemble with changes in pH while the polymer

network remained stable. This method of mixing polymeric gels and supramolecular gels may allow very complex systems to be formed that will react to more than one stimulus to have multiple assembly and disassembly steps and also increase the strength of the gel.

Proline calix[4]arene is a gelator which was first reported in 2008 to gel water in the presence of certain electrolytes.[89] Figure 1.11 shows the gelator molecule is comprised of calix[4]arene with the proline amino acid functionalised onto the upper rim. The strength of the gels seemed to follow the Hofmeister series and the properties of the gels were linked to the selected cation. Gels which were more opaque (such as a gel triggered with lanthanum nitrate) formed networks which were more tangled and had fewer pores but many gels formed with this gelator were found to be transparent. The assembly of this LMW gel was seen to be based on supramolecular interactions as it was reversible with both temperature and pH.[56] The gel was shown to be stable at neutral to acidic pH and form upon cooling to temperatures below approximately 20 °C. Proline calix[4]arene is a chiral molecule and while both the D- and L- enantiomers formed gels, a racemic mixture was found to not form a gel.[9]

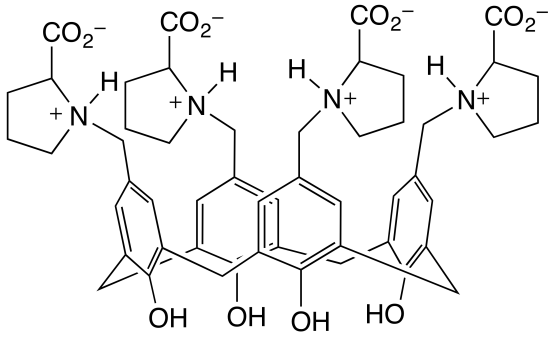

Figure 1.11: The proline functionalised calix[4]arene molecule which has been shown to form hydrogels in the presence of electrolytes and at low pH.[89] Reproduced from Ref. 89 with permission from The Royal Society of Chemistry.

NMR peak broadening showed that the fibres may self-assemble in the absence of an electrolyte when the gelator is at high enough concentrations, however, gelation was not seen, at least based on a vial inversion test. A crystal structure study revealed that a proline moiety can sit within the cavity of a neighbouring

calixarene cone. This hydrophobic interaction, along with some hydrogen bond interactions, is proposed to lead to the formation of elongated structures (Fig. 1.12a).[56] Figure 1.12b shows the intermolecular interaction in more detail. The initial *ex situ* AFM images showed the smallest fibres to be in the range of 7 nm in diameter which indicated that the fibres were much larger than one molecule, however, further *in situ* AFM imaging showed the individual fibres to be about 1 nm in diameter.[76]

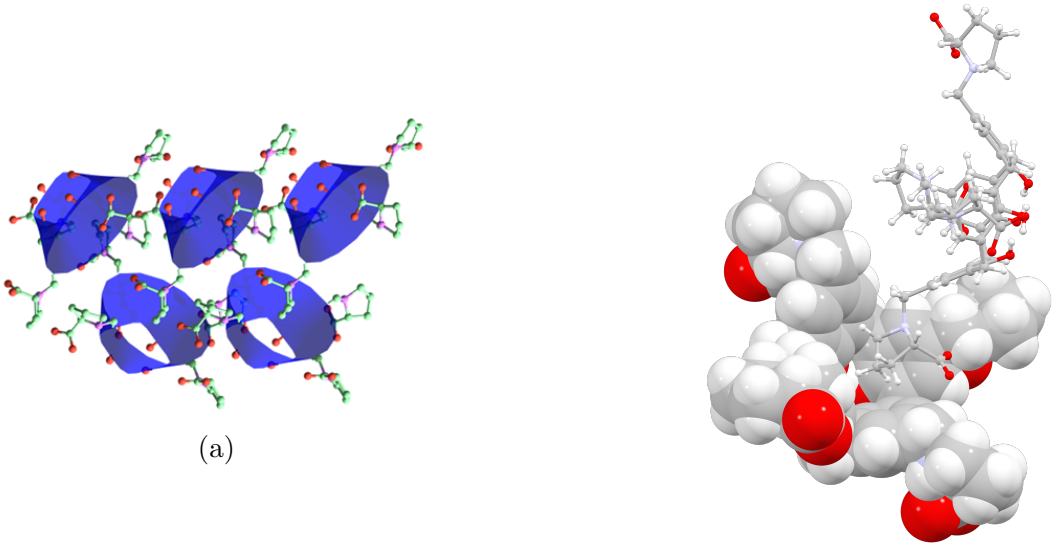

(a) (b)

Figure 1.12: Molecular structures and packing of proline calix[4]arene gelator forming a spiral structrue. This was deduced from a crystal structure study. (a) highlights the proline moiety within the calixarene cone and (b) shows the intermolecular interaction in more detail.[56] Reproduced from Ref. 56 with permission from The Royal Society of Chemistry.

Further research into the interaction of this gelator with modifiers showed that Tetrahydrofuran (THF) can inhibit the gelation and, at higher concentrations, stop gelation completely. This was proposed to be due to THF competing with the proline moiety for inclusion into the calixarene cavity.[9] A crystal structure for this interaction was obtained and can be seen in Figure 1.13a. Interactions with the metal cations present were also thought to cause the bundling of fibres. Figure 1.13b shows how a lanthanum ion interacts to link proline calix[4]arene molecular strands within a crystal structure.[56]

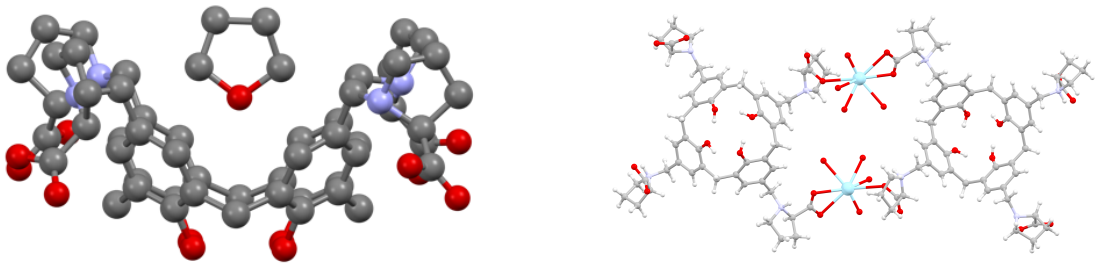

(a) (b)

Figure 1.13: Crystal structures of proline calix[4]arene showing (a) the interaction of the THF molecule with proline calix[4]arene to inhibit gelation and (b) the interaction of metal cations binding the proline calix[4]arene strands together.[9,56] Reproduced from Ref. 56 and 9 with permission from The Royal Society of Chemistry.

Gels are used extensively in cell culture due to their ability to mimic a cells natural extracellular matrix and support the cells during growth.[86,90,91] Hydrogels are particularly useful for 3D cell culturing as they have a very high water content and allow nutrients to move through the gel to feed the cells and move waste away.[85] Generally, it is best to use gelators comprised of molecule types that are found in the human body such as proteins, peptides and amino acids as they are more likely to be biocompatible, with less chance of eliciting an immune response.

There are many options for the synthesis of peptide gels as the gelator molecules are comprised of different amino acids blocks which are bonded in a set order within a chain. It is possible to hypothesise if a peptide will form a gel, however, the ability to predict properties of the subsequent gel, or even the conditions required for gelation is still poorly understood.[92] Often peptides are modified by changing one or two amino acids or changing the order of the amino acids slightly in an attempt to modify the gel which it forms.[93–95]

Recently, peptide gels have been studied for their potential use as carriers of bioactive components, such as drug compounds, vitamins and hormones.[96,97] These molecules can either be attached chemically to the gel molecule or, more commonly, incorporated physically during the formation of the gel.[98] The compounds are then released in a controlled manner either by diffusion or upon disassembly of the gel. Recently, Liu *et al.* reported the use of a peptide gel to release

hepatocyte growth factor (HGF) and heparin at the site of a cell transplant.[99] The HGF and heparin worked together to reduce inflammation and increase the success of the cell transplant. These cell transplants are used to treat diabetes mellitus which is a very common and often debilitating disease. The slow, controlled release of the bioactive compounds allowed for continued treatment of the site for 7 days which would greatly reduce the medical intervention required.

One of the major barriers to commercialisation of peptide gels as bioactive molecule carriers is the administration of the gel. For skin or surface applications, there has been great development, as the gel can simply be spread or poured over the area to be treated.[100,101] However, for uses within the body, the desired administration would be by injection. The difficulty here is that the gel generally needs to be formed to have the bioactive components encapsulated but a fully formed gel cannot be injected. A partially formed gel may be possible to inject, however, the shear stress applied to the gel upon injection may cause disassembly. Some peptide gels have been discovered which specifically solve this issue by forming upon the shear stress of injection so that the gel is formed at the site of injection.[102] The bioactive component can then be injected into the formed gel and diffuse out from this point.[103,104]

As cells need to be grown under physiological conditions it is difficult to find gels which can uniformly encapsulate cells. The gel needs to be a liquid at room temperature to allow a homogenous distribution of cells to be obtained throughout the gel network, but then set at a higher temperature (37 °C) for the incubation period. However, the majority of gels will either disassemble when heated as the added energy allows the intermolecular bonds to break or form at temperatures far below the 37 °C required for cell incubation. Gels with this reversed assembly process are known as Lower Critical Solution Temperature (LCST) gels.

The Fluorenylmethyloxycarbonyl-Gly-Phe-Phe-Arg-Gly-Asp (Fmoc-GFFRGD) gel was first reported by Wojciechowski *et al.* in 2017. Figure 1.14a shows the structure of the peptide which is comprised of an N-terminal capped peptide with the sequence Gly-Phe-Phe-Arg-Gly-Asp (GFFRGD). It was

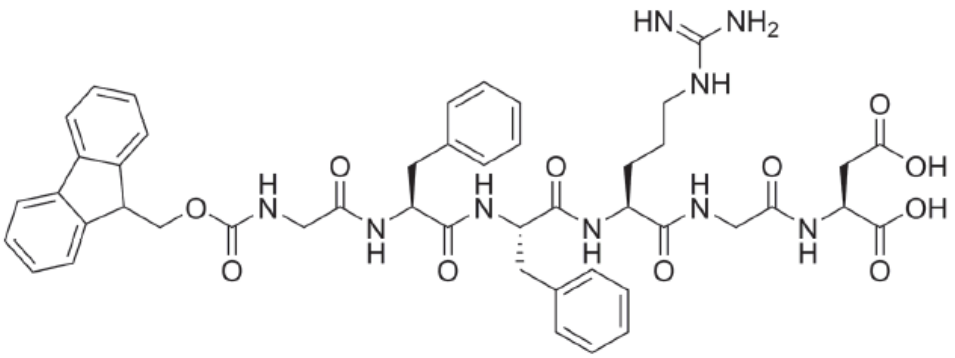

(a) Fmoc-GFFRGD molecular structure.

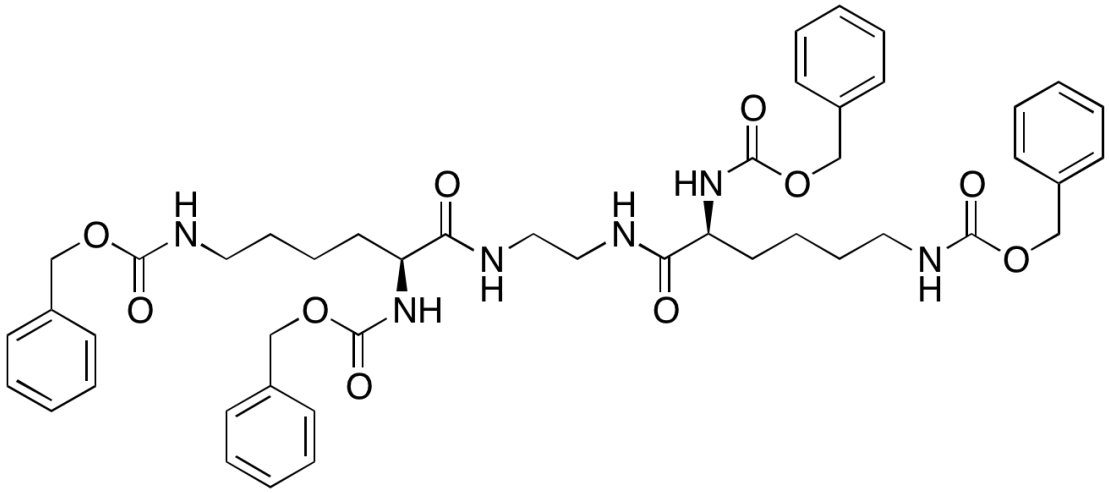

(b) N,N'-bis-[di-CBZ-L-Lyz]-ethylenediamine molecular structure.

Figure 1.14: Peptide gels analysed by *in situ* AFM in this study.

found to gel Dulbecco's Modified Eagle's Medium at 37 °C but remain liquid when left at 25 °C. The gelation was not reversible.[105]

A novel organogelator was synthesised by C. Duncan to investigate it as a treatment option for Human Papillomavirus and serendipitously found to gel chloroform.[106] While this gelator was unfortunately not found to gel non-toxic solvents, it presented the opportunity to test the AFM methods on an organogelator. This molecule had previously been synthesised by Schröder, Klieger and Gibian in 1961, however, the purity was quite low (56%). The properties of the compound were also not tested, likely due to the restriction of techniques at the time and this being outside the scope of the study. The structure of the peptide, N,N'-bis-[di-CBZ-L-Lys]-ethylenediamine, can be seen in Figure 1.14b.

1.4 Project Overview

It is well known that the wide range of applications of hydrogels - from catalysis, to cell culture materials, to food science - depends largely on their structure, inclusive of fibre diameter, pore size and cross-linking density. The overarching objective of this project was to characterise a subset of supramolecular hydrogels gels using newly developed AFM methods as this technique allowed for the analysis to be conducted with less change to the gel, so the real structure could be captured. Other techniques, like electron microscopy, need the gel to be dried in some way prior to imaging which may change the structure. While CLSM imaging can be conducted without drying, it does not have a high enough resolution to show the sizes of fibres that most supramolecular hydrogels form. SANS can also analyse the gels without drying but does not directly image the structure so only an average structure of the gel can be determined. The development of AFM to include PF QNM allowed for the *in situ* imaging of gels, during dynamic processes such as assembly, without drying or freezing the gel first. Chapter 2 gives a detailed overview of the methods developed during this project which were used to analyse gels. This method development was not a trivial task due to the relatively new development of AFM imaging capabilities such as PeakForce tapping. This work was built on research conducted at Curtin University from 2008 onwards on the characterisation of proline calix[4]arene gels.

Chapter 3 discusses further characterisation of proline calix[4]arene gels using AFM, SANS and rheometry techniques. These gels showed varying structures when formed with different electrolytes at different concentrations. Gels were analysed using AFM to show the structure of the gel networks and individual fibres, while rheometry showed the change in the strength of the gels over multiple assembly and disassembly cycles. SANS was then used to gain an overall understanding of the gel structure. The annealing process of the gel formed with magnesium chloride was investigated and showed a large change in the strength of the gel due to a structural change. Gels formed with lithium chloride indicated a helical structure which is due to the chiral nature of the molecule and was investigated

using AFM and SANS.

Further analysis of gels which was conducted is discussed in Chapter 4. As the AFM *in situ* method developed in 2015 at Curtin University did not allow for the analysis of opaque gels, attempts were made to develop a method to image gel assembly and disassembly within a thin film. This chapter also covers the analysis by AFM of novel peptide gels. To better understand the properties of gels during assembly and disassembly a MATLAB script was developed to analyse the change in physical properties of a gel network by imaging with PeakForce Quantitative Nanomechanical Mapping.

Chapter 2

Methods

The main analysis methods used to characterise the gels with regards to the structure of supramolecular gels and their assembly and disassembly were Atomic Force Microscopy (AFM) methods, namely *ex situ*, *in situ* (in droplet) and *in situ* (thin film) methods. AFM imaging progressed from *ex situ* to *in situ* to allow for imaging with minimal change to the gels prior to imaging. *In situ* thin film methods were attempted to be able to image opaque gels which could not be imaged by the initial *in situ* (in droplet) method. Rheometry and Small Angle Neutron Scattering (SANS) were also used as complementary methods.

2.1 Atomic Force Microscopy

Two methods were developed to characterise the gels, *in situ* and *ex situ*, by AFM. The gels were analysed on mica substrates. Environmental conditions were not controlled extensively, however, temperature and relative humidity did not vary widely during any experiment. Recordings of the temperature and humidity within the instrument hood across several hours did not show changes of greater than 5%.[107] Samples were analysed using the FastScan or Icon head on a Bruker Dimension Series AFM instrument which are shown in Figure 2.1. The FastScan head allows for very fast imaging of samples in tapping mode and PeakForce tapping mode without compromising the image quality. This head was also used

for *in situ* experiments by inserting the sample between a heater-cooler stage and the z-scanner (Fig. 2.2b) as the electrical components of the z-scanner are already isolated from the fluid. If the Icon head was used for these experiments, a specific probe holder for imaging in liquids is required and slower scan rates may have to be used which means that the faster processes are not captured. The vastly improved speed of this instrument, compared to previous instruments, allowed for the changes in the sample to be imaged dynamically. The instrument is encased within an insulated hood to reduce noise in the image and limit the effect of changes in the environment, such as temperature. The instrument is also vibrationally stabilised on a nitrogen pressurised table. A list of all AFM probe types used can be found in Table 2.1.

The mica substrate was mounted on a metal disc with epoxy glue and then rinsed with de-ionised water and treated with ultraviolet radiation in a UV-ozone cleaner (Bioforce Nanoscience, Inc. (USA), Model: UV.TC.220). Prior to preparing the sample, the substrates were cleaved with Scotch tape to create a clean, flat substrate. The substrates had a diameter of either 5 mm or 10 mm.

(a) (b)

Figure 2.1: Bruker Dimension instrument in both (a) FastScan and (b) Icon configurations.

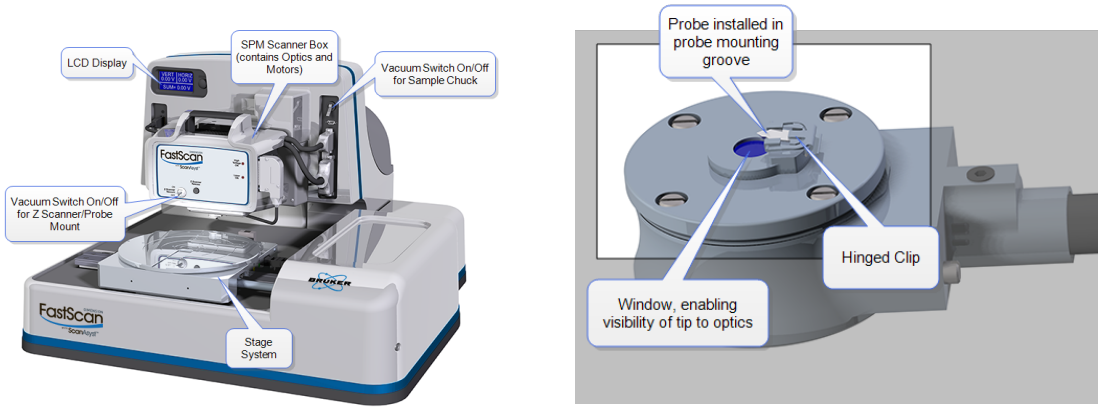

(a) Bruker FastScan AFM

(b) Z-scanner and probe holder of the Bruker FastScan AFM.

Figure 2.2: Bruker FastScan AFM used to image the gels both *ex situ* and *in situ*.[108]

Table 2.1: Probes used for Atomic Force Microscopy imaging.

Probe Type	*Tip Composition*	*Cantilever Composition*	*Nominal Spring Constant* (N/m)	*Nominal Tip Radius* (nm)
FastScan-A	Silicon	Silicon Nitride	18	5
FastScan-B	Silicon	Silicon Nitride	1.8	5
FastScan-C	Silicon	Silicon Nitride	0.8	5
TESPA	Silicon	Aluminium coated, antimony doped silicon	42	8
TESPA-V2	Silicon	Aluminium coated, antimony doped silicon	37	7
NHCV-A	Silicon	Aluminium coated, antimony doped silicon	40	8

2.1.1 *Ex situ* Atomic Force Microscopy Imaging

The gels were mixed immediately prior to imaging unless otherwise stated. The sample was smeared onto the substrate using a glass Pasteur pipette and left for approximately two minutes to dry. An alternative method was to spin coat the gels onto the substrate. Samples were spin coated at between 1000 rpm and 8000 rpm for durations of 30 seconds up to 10 minutes, depending on the viscosity of the gel.

To assemble and disassemble the gels, they were heated in the vials until above their melting temperature and cooled until they underwent gelation again.

Temperature cycles were achieved by placing the vials in a controlled temperature water bath for 10 minutes at 30 °C before being removed and the sample prepared. The gels were allowed to return to room temperature without temperature control, while the sample was analysed (approximately 1 hour). This process was then repeated for subsequent heat cycles. All samples were analysed using the Bruker Dimension FastScan instrument in either Tapping mode or PeakForce tapping mode. Silicon tips on silicon cantilevers were used to probe the sample (Bruker TESPA).

2.1.2 *In situ* (In Droplet) Atomic Force Microscopy

Samples were analysed using the FastScan head on the Bruker Dimension instrument. PeakForce tapping was used instead of tapping mode due to the continuous changes in viscosity upon temperature variations which would have prevented continuous imaging in Tapping Mode. The substrates were prepared as in section 2.1. Probes of type either FastScan B or FastScan C were used. After the tip was loaded into the instrument the substrate was scanned in air prior to the addition of the sample to verify the cleanliness of the substrate. The tip was then withdrawn and a glass Pasteur pipette was used to inject the gel (approximately 200 μL) between the substrate and the tip, ensuring the tip was submerged. Figure 2.3 shows how the tip, gel and substrate are set up with the heater/cooler sample stage underneath the substrate and the entire tip submerged by the droplet between the substrate and z-scanner. The gels were mixed and then immediately transferred to the stage using a Pasteur Pipette. Some self assembly of the gels was required prior to being injected onto the stage such that their structure would be visible however, a balance needed to be achieved as waiting too long would result in the formation of a fully formed gel, preventing transfer onto the mica substrate. This was determined to take approximately 30 seconds based on prior work completed in 2015.[76] The method required the gels to have a low enough viscosity that the force applied to the AFM tip to oscillate it

within the gel was low enough that it did not destroy the soft fibre network. The concentrations of the gel component solutions were adjusted until the viscosity allowed for a small enough peak force (0.75 - 2.5 nN) between probe and sample to be applied for imaging and the T_{gel} was within a range that the instrument allowed. The Bruker Dimension FastScan instrument can only be operated at temperatures between 0 °C and 40 °C without risking damage to the scan head. The optimum gel component concentrations were found by trial and error as it was not possible to adjust the concentrations of the gel components after they were injected onto the instrument stage. The concentrations would be adjusted and a new sample would be made and run.

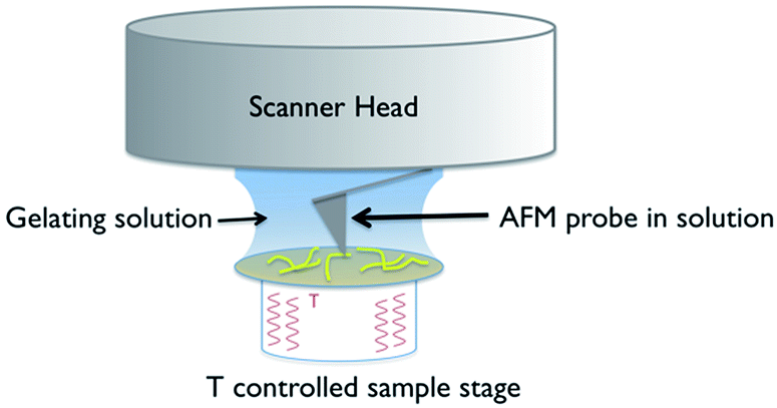

Figure 2.3: Depiction of the *in situ*, in droplet, set up used on the Bruker Dimension FastScan instrument.[76]

The probe was immediately engaged for scanning after the gel was injected. If fibres were imaged on the mica surface immediately, the sample was heated until the structure completely disassembled and the Z vs force plot appeared as shown in Figure 2.4, indicating that the viscosity was very low and the gel had become a liquid. The temperature was then reduced by 1-2 °C per image scan to facilitate the assembly of the gel and imaging was continued until the viscosity became too large for the applied peak force. The force was never increased further than 2.5 nN as higher forces could damage the soft structure of the gels. Typically, the force applied was 0.75 - 2.00 nN. As the sample was heated and cooled the viscosity changed and the force applied by the tip was required to be adjusted to

continue imaging the sample.

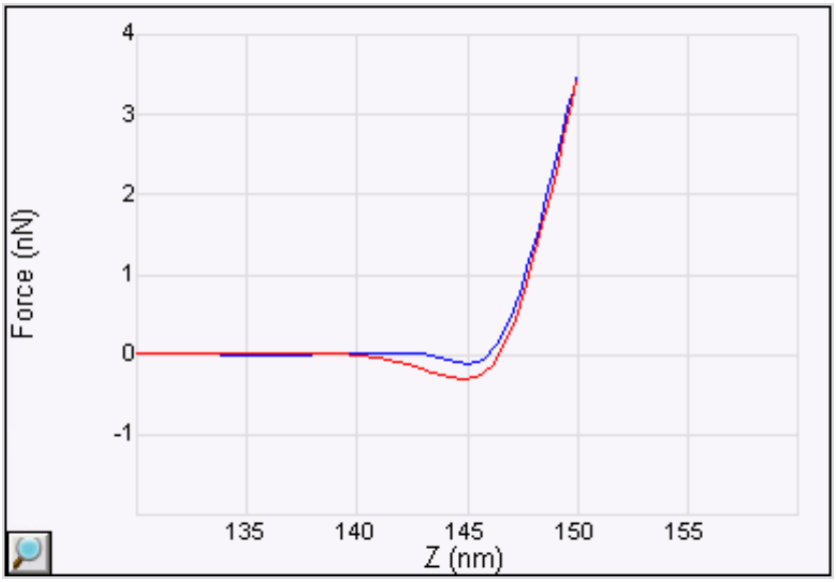

Figure 2.4: Force vs Z position plot from Bruker Nanoscope software showing the force on the cantilever during a full force curve. The curve shown is representative for the behaviour of an AFM probe in a gel with very low viscosity.[109]

2.1.3 *In situ* (Thin Film) Atomic Force Microscopy Method

Samples were analysed using the FastScan configuration on the Bruker Dimension instrument. PeakForce tapping was used instead of tapping mode due to the continuous changes in viscosity of the gels upon temperature variations. The substrates were prepared as in section 2.1. Either a FastScan B or FastScan C probe was loaded into the z-scanner. The gels were mixed and then immediately applied to a mica or Highly Ordered Pyrolytic Graphite (HOPG) substrate by smearing, spin coating or dip coating. The concentrations of the gel components were adjusted until the gel network was visible when imaging began at room temperature and the T_{gel} was within a range that the instrument allowed. After the tip was loaded into the z-scanner, and the sample surface focussed, the tip was allowed to approach the sample to determine if the film was too thick, which was assessed using the optical microscope of the instrument. The optics of the system would show if the back of the cantilever dipped under the surface of the

film. Provided the tip appeared to be remaining under the surface of the film and the cantilever remained in air, the sample was then imaged. The temperature was raised during imaging to disassemble the gel.

2.1.4 Image Processing

AFM images were analysed using Bruker Nanoscope Analysis 1.9. A first order plane fit was applied to remove tilt followed by a first order flattening to remove the difference between scan lines. Where required, a second order plane fit was applied to remove bowing. The z-scale of the image was adjusted to increase the visibility of the desired structures and to allow for comparison of certain images. Height measurements were performed using the Section function.

2.2 Rheometry

All rheometry measurements and data processing was performed by Dr. Adam Martin. Hydrogels were prepared by mixing solutions of proline calix[4]arene and either $MgCl_2$ or LiCl in equal volumes. The mixed gel (550 μL) was transferred to the lower plate of the Anton Paar MCR 302 Rheometer (Fig. 2.5a). The upper plate was lowered to a gap of 1 mm and the system was left at 10 °C for approximately 2 hours, to allow for gelation. During all measurements, to control the temperature and reduce evaporation of the solvent, a Peltier temperature control hood and a solvent trap were utilised.

Amplitude sweeps were conducted first to find the strain under which the gels transitioned from a viscoelastic solid to a viscoelastic fluid. This is termed the Linear Viscoelastic Region (LVER) and is essentially the strain that the gels can withstand before deforming significantly. These measurements were conducted at a constant frequency of 1 Hz over a log ramp strain of 0.1 - 100%. Frequency sweeps were then conducted at a strain within the LVER. These sweeps were performed with a constant strain of 0.2% across a log ramp frequency of 0.01 to

10 Hz. Data for storage and loss modulus were collected for all experiments.

Temperature sweeps were then conducted to show the temperature reversibility of the gels. The samples were heated over a period of 5 minutes and allowed to equilibrate at each temperature for 10 minutes with data being collected every 5 °C. These measurements were completed a minimum of 3 times with the final data averaged. Data for storage modulus was collected to determine the solution to gel transition temperature or T_{gel}.

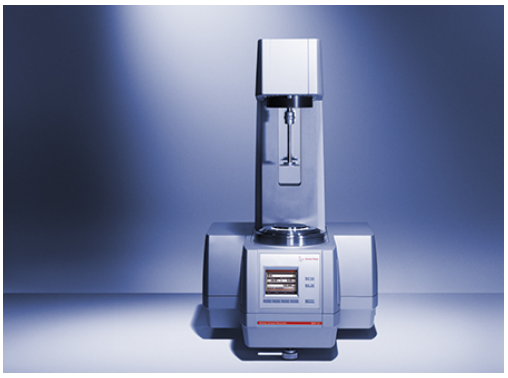

(a) Anton Paar MCR 302 rheometer used to analyse the flow properties of the gels.[110]

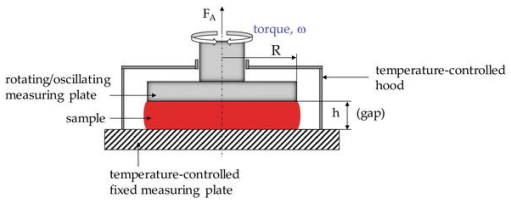

(b) Parallel plate geometry.[111]

Figure 2.5: Instrumentation for rheometry experiments.

2.3 Small Angle Neutron Scattering

Hydrogels were prepared by mixing solutions of proline calix[4]arene and either $MgCl_2$ or LiCl in equal volumes. The solutions were all prepared in D_2O. The mixed gels were immediately transferred to titanium demountable cells (Fig. 2.6a). The cells had a path length of 2 mm. These demountables were then cooled to 5 °C for approximately 4 hours before being transferred to a pre-cooled sample holder on the instrument (Fig. 2.6b) and allowed to equilibrate for a minimum of 30 minutes. Measurements were performed on the QUOKKA instrument at The Australian Nuclear Science and Technology Organisation (ANSTO). Data was collected at detector distances of 2 m and 14 m with a neutron wavelength of 5 Å and a 2θ scattering angle. The resulting q range was 0.005 - 0.35 $Å^{-1}$. Data were collected for the background solvent (D_2O), each of the gel components

individually (proline calix[4]arene and electrolytes), an empty cell and the empty beam. The data were reduced using IgorPro, with NIST macros specific to the QUOKKA instrument, normalised to an absolute intensity scale and then modelled with SASView.

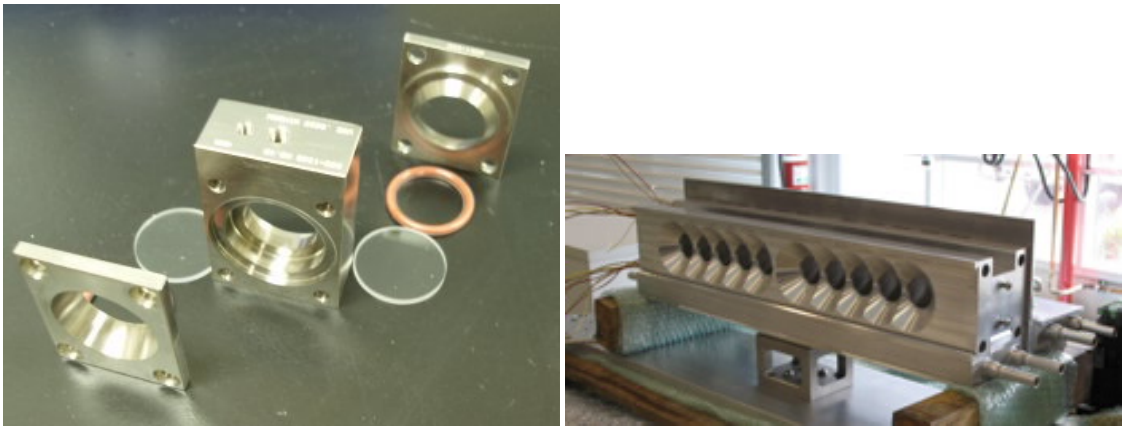

(a) (b)

Figure 2.6: (a) Titanium sample demountable and (b) sample changer used on the QUOKKA and BILBY instruments at ANSTO for SANS and Time-of-Flight (TOF) SANS measurements.

2.4 Time-of-Flight Small Angle Neutron Scattering

Hydrogels were prepared by mixing solutions of proline calix[4]arene and LiCl in equal volumes. The solutions were all prepared in D_2O as H_2O scatters quite strongly and will effectively hide scattering data from the sample. The mixed gels were immediately transferred to titanium demountable cells (Fig. 2.6a). The cells had a path length of 1 mm. The demountables were immediately placed in an oven at 30 °C after filling with the gel solution before being transferred to the sample holder on the instrument (Fig. 2.6b). Measurements were performed on the BILBY instrument at ANSTO. Data were collected at sample to detector distance of 7 m and a sample to last chopper distance of 17.884 m. Neutrons with wavelengths between 0 and 20 Å were used. The resulting q range was 0.001 - 0.11 $Å^{-1}$. Data were collected for the background solvent (D_2O), each of the

individual gel components solutions (proline calix[4]arene and LiCl), an empty cell and the empty beam. Data were reduced using MantidPlot, with NIST macros specific to the BILBY instrument, normalised to an absolute intensity scale and then modelled with SASView using a flexible cylinder model.

Chapter 3

Formation and Structures of Proline Calix[4]arene Gels

Part of the research in this chapter was previously published in

Emily C Barker, Adam D Martin, Christopher J Garvey, Ching Yong Goh, Franca Jones, Mauro Mocerino, Brian W Skelton, Mark I Ogden and Thomas Becker. Thermal annealing behaviour and gel to crystal transition of a low molecular weight hydrogelator. *Soft Matter*, 13(5):1006-1011, 2017.

A co-author attribution statement can be found in Appendix B.2.

3.1 Introduction

The proline calix[4]arene gelator had previously been tested across a large range of concentrations and found to gel most effectively at a concentration of 0.4 M when formed in the presence of lithium chloride (1.26 M).[89] Becker *et al.* imaged the fibrous structure formed by the gel by *ex situ* Atomic Force Microscopy (AFM). In 2015, Barker *et al.* showed that the assembly and disassembly of this gelator could be imaged *in situ* when formed with magnesium chloride.[76] This gelator

had been observed to yield gels with vastly different properties and structures when formed with different electrolytes.[56,89] Here, AFM, Small Angle Neutron Scattering (SANS) and rheometry were used to investigate the assembly process for gels of proline calix[4]arene when formed with different electrolytes.

3.2 Methodology

The materials used were: proline calix[4]arene (synthesised by Dr. Brendan Ennis), magnesium chloride hexahydrate (Sigma-Adrich, ≥99%) and lithium chloride (Sigma-Adrich, ≥99%). The materials were used as received without further purification.

The gels were analysed by *ex situ* and *in situ* AFM (section 2.1), rheometry (section 2.2) and SANS (section 2.3). AFM and SANS were used to probe the morphology of the fibres and the network while rheometry was used to study the flow properites of these gels during assembly and disassembly.

3.3 Results and Discussion

3.3.1 Annealing Behaviour of Proline Calix[4]arene Gel

3.3.1.1 Atomic Force Microscopy

Gels were imaged *in situ* according to the method detailed in section 2.1-*in situ*. The gels were imaged initially after loading onto the stage, then heated to disassemble and cooled to reassemble. This allowed multiple cycles of the assembly process to be imaged, *in situ*, and the change in the morphology to be assessed. Images were processed according to section 2.1-*Image Processing*. The high concentration initially used by Becker *et al.* (0.4 M) to image this gel was found to form a gel which was too viscous to be imaged *in situ* hence significantly lower concentrations were used (0.02 M - 0.25 M). While a fibrous structure was still seen on imaging, this rarely macroscopically formed a hard gel, even after several days.

Gels of proline calix[4]arene with lithium chloride as an electrolyte were imaged, *in situ*, using PeakForce tapping. PeakForce tapping allowed for continuous imaging while the viscosity of the gel changed (drastically) during the assembly and disassembly processes. Only small changes to the peak force (0.5 nN) applied by the probe to the structure, were required during imaging. Images took approximately 2.4 minutes to capture and the temperature was altered at 0.1 °C per scan. This was much slower than the usual 1 °C per scan as the assembly process of this gel was seen to be very fast compared to the previous gels that had been imaged. Varying concentrations of LiCl (between 500mM and 100mM) were tested, however, the fast assembly process of the gel was not affected by the concentration.

The images in Figure 3.1 show the fibre network seen after the first and second temperature cycle of this gel. No fibres were visible initially when this gel was loaded and it was slowly cooled, while continuing to scan, to form the gel. The gel began to form at 23 °C, however, it was only possible to completely scan one image as the gel became very viscous very quickly and imaging was halted until the gel was heated again and the viscosity reduced. This was done to reduce damage to the probe. Only a partial network was captured in this image (Fig. 3.1a). The gel was then heated to 28 °C to disassemble the gel and then cooled to reassemble the network a second time. The temperature was held at 24 °C as this was when fibres first became visible. Over several images, the structure continues to form (Fig. 3.1b) and was imaged until it became too viscous for the cantilever movement. The size of the fibres and the bundles was shown to be very similar for both assembly cycles, showing that this gel is temperature reversible. Histograms showing the heights of fibres observed on the mica surfaces can be seen in Figure 3.2. These images were generated using Bearing analysis function of the Bruker Nanoscope software and gave measurements with a skewed normal distribution centred around 14 nm.

As imaging the assembly of the proline calix[4]arene gel with LiCl *in situ* was shown to be very time consuming, due to the small temperature increments re-

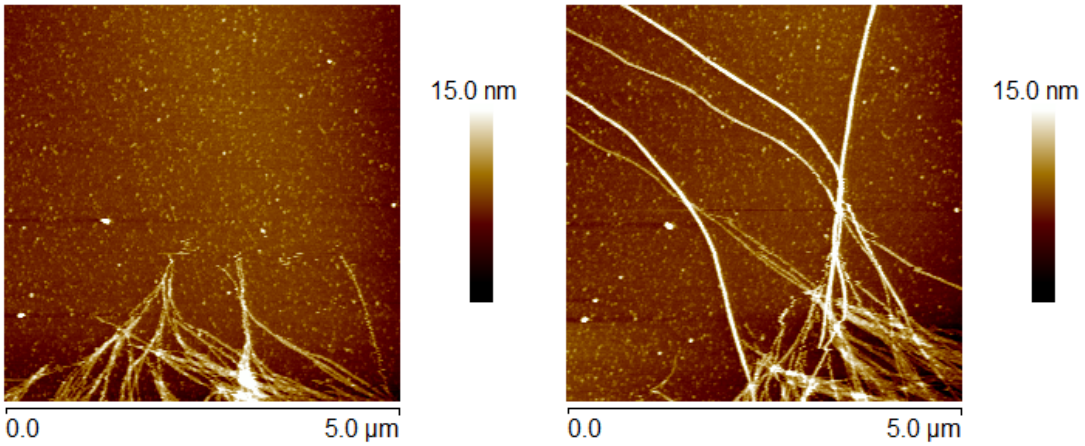

(a) First assembly, T = 23 °C. (b) Second assembly, T = 24 °C.

Figure 3.1: *In situ* AFM topography images of proline calix[4]arene (20 mM) gel fibres with LiCl (200 mM) electrolyte after the first and second assembly of the gel.

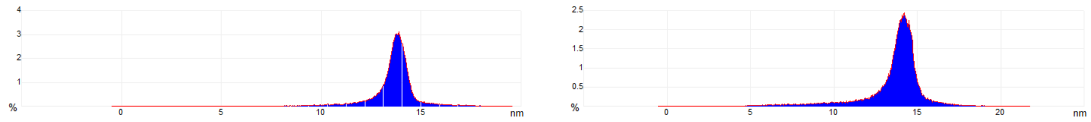

(a) (a) data measured from image in Figure 3.1a (b) (b) data measured from image in Figure 3.1b

Figure 3.2: Histograms showing the heights measured in the images shown in Figure 3.1. These heights would correspond to the diameters of the fibres due to their positioning on the surface.

quired, the gel was imaged *ex situ* before and after heat cycling. When run *in situ*, evaporation would become problematic, limiting the number of cycles which could be imaged. The samples were prepared and imaged according to section 2.1-*ex situ*. The concentration of the electrolyte was increased for this experiment to form a more complete network as the strength of the gel would not hinder imaging in this case.

Figure 3.3 shows the fibre structures seen after the same gel was allowed to form once and then heat cycled twice. Similar structures were seen in all images. This corroborates the results seen *in situ* and shows that this gel is temperature reversible as the network does not change between assembly cycles. The network was comprised of long (greater than 10 μm) curved fibres, with fibre bundles ranging from 1-10 nm in diameter. Some particulate structures in the size range of 20-30 nm were seen within the fibre networks, which are likely to be crystallised aggregates of LiCl due to drying of the gel during preparation.

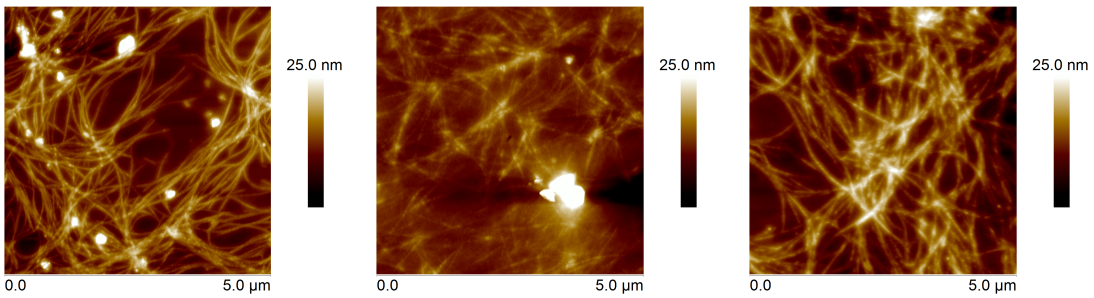

(a) Before heating. (b) After first heat cycle. (c) After second heat cycle.

Figure 3.3: *Ex situ* AFM topography images of proline calix[4]arene (20 mM) gel fibres with LiCl (1.30 M) electrolyte before heating and after two heat cycles.

The proline calix[4]arene gelator with magnesium chloride as an electrolyte was imaged, *in situ*, using PeakForce tapping. Images took approximately 2.4 minutes to capture and the temperature was changed by 1 °C per scan. This gel exhibited a much slower and more controlled assembly and disassembly compared to gels formed with lithium chloride as the electrolyte. The structure was visible initially, at 22 °C, immediately after the gel was loaded onto the stage. The sample was then heated to 31 °C to disassemble the network.

Figure 3.4 shows images of the fibres seen initially, during heating and at the

highest temperature imaged. The initial network was seen to be comprised of individual, mostly short, unbundled fibres, indicating that the gel was most likely still forming (Fig. 3.4a). These fibres had diameters of approximately 1-2 nm as seen in Figure 3.5. Upon heating the gel the fibres disappeared as the gel disassembled, however, a second structure began to form. This new structure was seen to be very straight with a much larger diameter (approximately 20 nm) than the structure that was initially imaged. Figure 3.4b shows both of these structures on the same image which gives a clear indication of the difference between the morphologies of these structures. Continued heating caused more of the larger structure to form after the initial structure had completely disappeared (Fig. 3.4c). When the sample was cooled again, the larger structure remained. It was not possible to cool the sample far enough to see the initial structure reassemble as the larger structure caused the sample to turn opaque, making further imaging impossible.

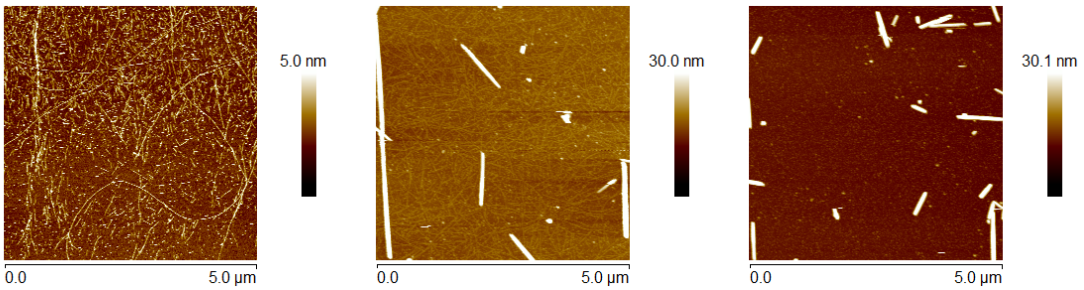

(a) First assembly - 22 °C. (b) During disassembly - 25 °C. (c) After disassembly - 31 °C.

Figure 3.4: *In situ* AFM topography images of proline calix[4]arene (20 mM) gel fibres with $MgCl_2$ (25 mM) electrolyte after the first and second assembly of the gel.

The proline calix[4]arene gelator with magnesium chloride electrolyte was further analysed by *ex situ* AFM to show the structures present after three heat cycles. This was done to allow structures to be imaged after further heat cycles which was not possible *in situ* due to the increasing opacity of the gel. Figure 3.6 shows the fibre structure imaged when the gel had initially been formed and after three heat cycles. While the initial structure was not as curved or long as in the lithium chloride electrolyte gel, it was seen to get shorter and straighter

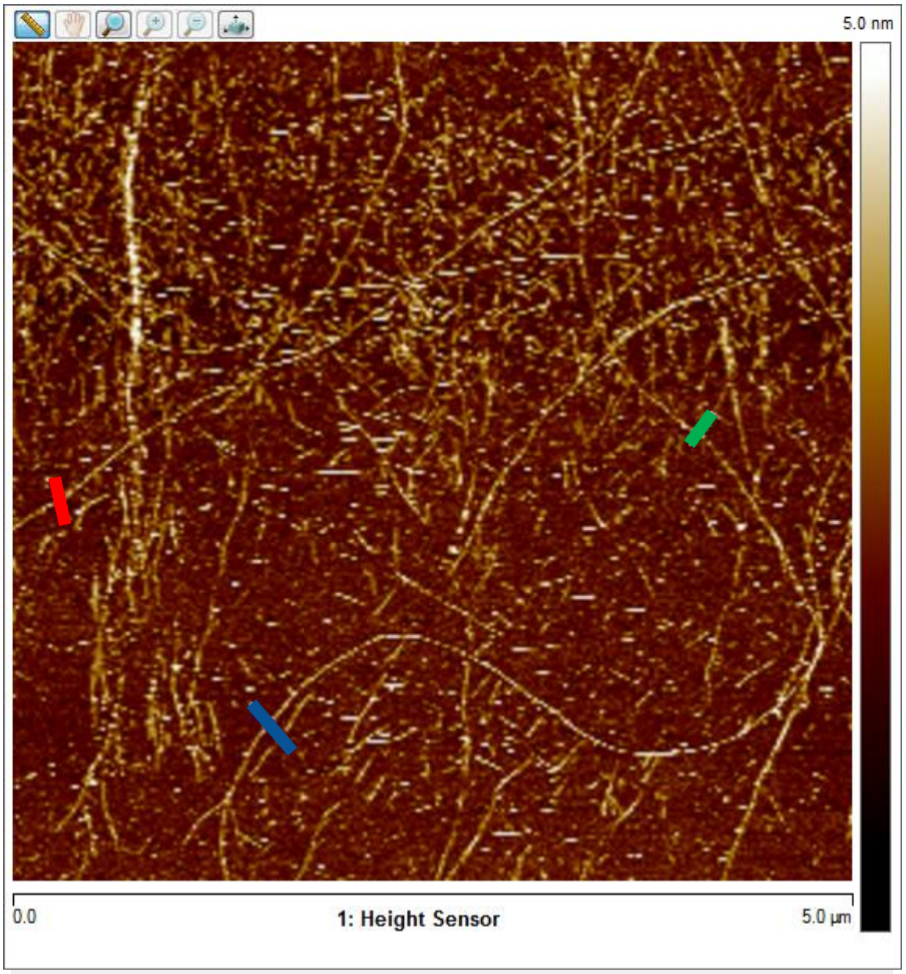

Pair	Horizontal Distance	Vertical Distance	Surface Distance
1	0.107 (µm)	1.339 (nm)	0.107 (µm)
2	0.040 (µm)	1.737 (nm)	0.040 (µm)
3	0.096 (µm)	1.897 (nm)	0.096 (µm)

Figure 3.5: Measurements of fibre diameters using Nanoscope Analysis v1.9 showing diameters of Proline calix[4]arene gel fibres formed with $MgCl_2$ to be between 1 and 2 nm.

over subsequent heat cycles. After three heat cycles, the fibres went from being greater than 4 μm in length to less than 1 μm in length. The initial structure was relatively straight compared to the other analysed gel, however, there was some curvature throughout the fibres which is not seen at all after three heat cycles. Non-fibrous, particulate structures were also seen to form after heat cycling.

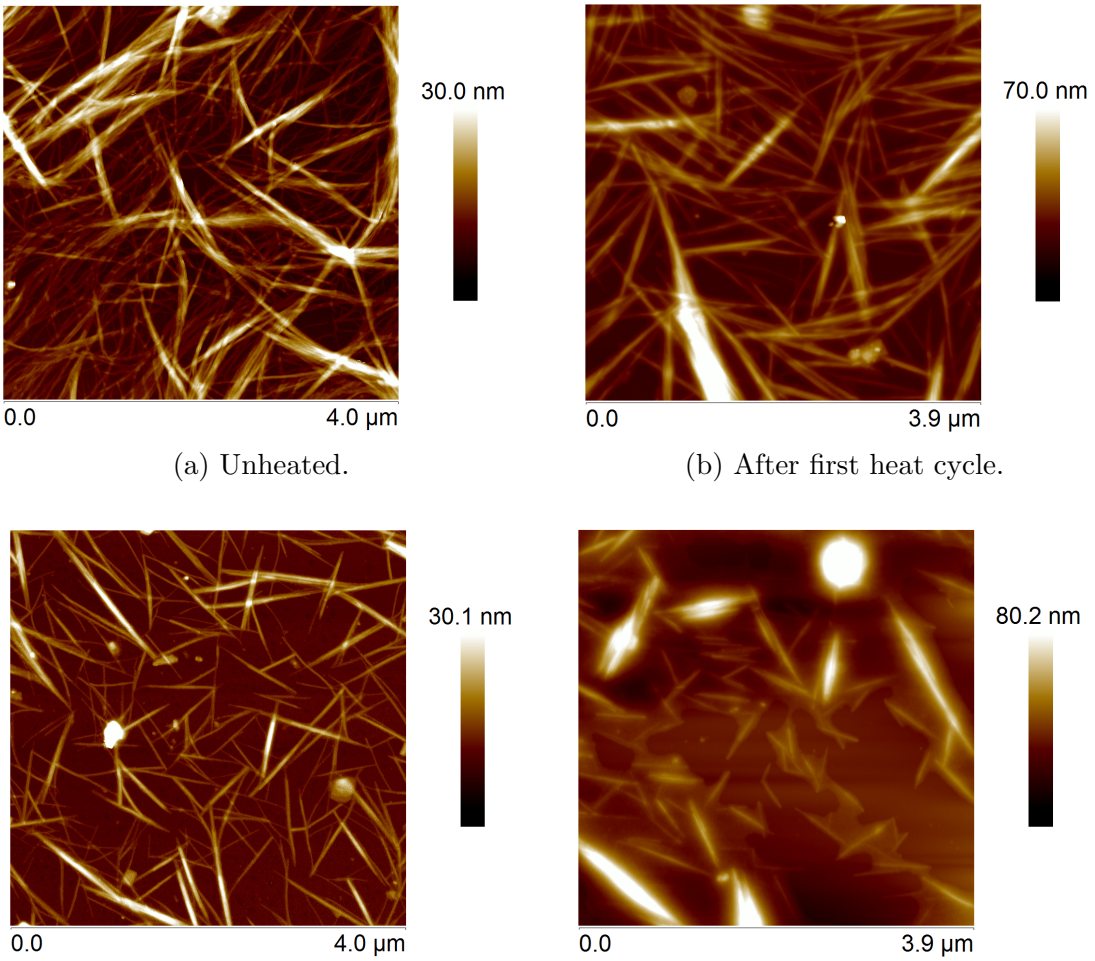

(a) Unheated.

(b) After first heat cycle.

(c) After second heat cycle.

(d) After third heat cycle.

Figure 3.6: AFM topography images of proline calix[4]arene (20 mM) gel fibres with $MgCl_2$ (25 mM) electrolyte before heating and after three heat cycles.

3.3.1.2 Rheometry

The flow properties of proline calix[4]arene hydrogels were analysed using rheometry according to the method detailed in section 2.2. Figures 3.7 - 3.8 show the frequency and amplitude sweeps for hydrogels of proline calix[4]arene with $MgCl_2$ or LiCl. The frequency sweeps showed that the $MgCl_2$ induced gel was two or-

ders of magnitude stiffer than the LiCl induced gel, even though the concentration of LiCl was much greater than that of $MgCl_2$. The amplitude sweeps, however, showed that while the $MgCl_2$ induced gel was stiffer, there was a deviation from the Linear Viscoelastic Region (LVER) for strains above 0.2% whereas this did not occur for the LiCl induced gel until strains above 3% were applied. The LVER indicates where the gel does not break from its structure, or flow. This suggests that while the $MgCl_2$ induced gel was much stronger, it was also more brittle. This shows that the choice of electrolyte used to induce gelation of proline calix[4]arene plays an important role in the physical properties of the resulting gel. This is not uncommon and it has been shown in other cation driven gelating systems that divalent cations trigger stiffer gels than their monovalent counterparts.[112]

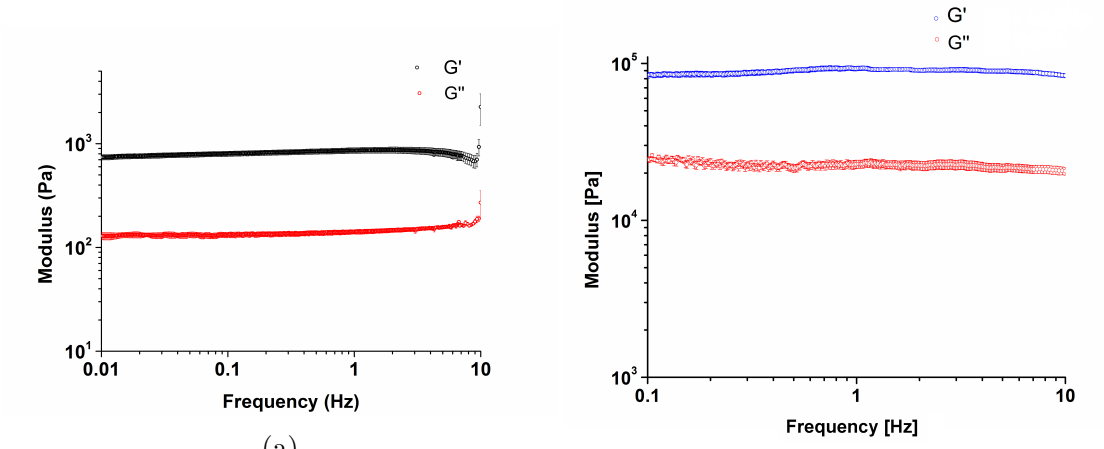

(a) (b)

Figure 3.7: Frequency sweeps of proline calix[4]arene (20 mM) with LiCl (250 mM) (a) and $MgCl_2$ (30 mM) (b) showing the LiCl induced gel to be two orders of magnitude weaker than the $MgCl_2$ induced gel. Error bars represent two standard deviations from the log-averaged mean. Data collected and processed by Dr. Adam Martin.

Temperature sweeps were then conducted to show the change in the strength of the gels across a temperature gradient. Figures 3.9a - 3.9b show temperature cycles from 10 °C to 30 °C for a LiCl induced gel and a $MgCl_2$ induced gel. This shows that while the LiCl induced gel appears to be temperature reversible, the $MgCl_2$ induced gel strengthened both when heated and when cooled. This result is unexpected for a hydrogel although it has been shown to occur for some polymer gels.[113] It also was not expected based on previous AFM imaging which

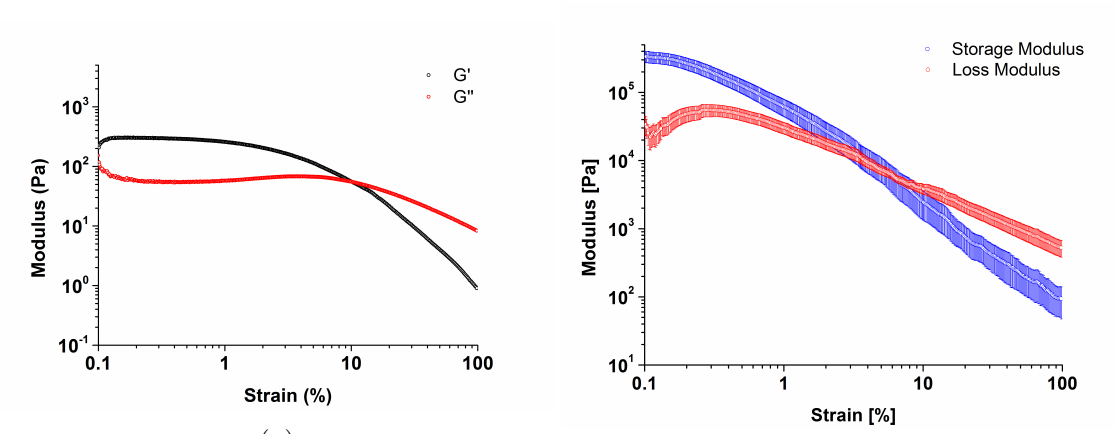

(a) (b)

Figure 3.8: Amplitude sweeps of proline calix[4]arene (20 mM) with LiCl (250 mM) (a) and $MgCl_2$ (30 mM) (b) showing the points at which the gels turn from a viscoelastic solid to a viscoelastic fluid, or the breaking point of the gels. Error bars represent two standard deviations from the log-averaged mean. Data collected and processed by Dr. Adam Martin.

showed the fibre structures disappearing upon heating. The strengthening during heating may be attributed to the larger structure which forms above 25 °C as can be seen in Figure 3.4 or it could be a continued assembly of the gel over time. Figure 3.9b shows the temperature sweeps for a $MgCl_2$ induced gel across ten temperature cycles. This shows that while the gel continues to strengthen across all of these cycles, both on heating and cooling, there is a maximum strength being approached.

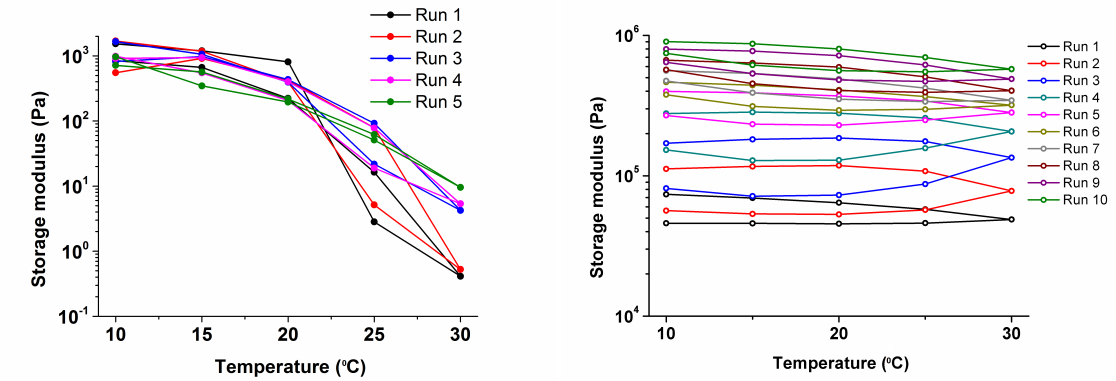

(a) (b)

Figure 3.9: Temperature sweeps of proline calix[4]arene (20mM) with (a) LiCl (250mM) and (b) $MgCl_2$ (30mM) showing the temperature reversibility of the gel with LiCl and the strengthening of the gel with $MgCl_2$. Data collected and processed by Dr. Adam Martin.

3.3.1.3 Small Angle Neutron Scattering

Hydrogels of proline calix[4]arene with $MgCl_2$ and LiCl were analysed by SANS over multiple temperature cycles to show the average change in morphology of the fibres and network over the assembly and disassembly of the gels. This was done to provide complementary information to that obtained from AFM as while both give information about the morphology of the gel, SANS allows for a much larger analysis area with an average structure given, compared to AFM which only allows for a very small region of the gel to be analysed. SANS has also been used for decades to analyse gels and the method for *in situ* analysis of gels by AFM is very recent so the use of SANS allows for confirmation of the morphology measured by AFM.

Modelling and fitting of the SANS data for these gels across the entire temperature range proved complicated. A flexible cylinder model was initially used as AFM imaging indicated that this was a physically realistic model for these systems. However, at higher temperatures, a flexible cylinder and power law model was used as this showed a better fit for the data (Fig. 3.10 - 3.11). This indicates a progression from a simple rod like structure to a more complex structure. This is consistent with AFM imaging seen in Figure 3.6.

Scattering profiles of both the LiCl and $MgCl_2$ induced gels showed a change in structure upon heating and a return to a similar structure when the gels were cooled again (Fig. 3.12). The LiCl gel had already changed structure at 20 °C, indicating that the gel had already begun to disassemble. The $MgCl_2$ gel showed a small drop in intensity at 20 °C but the scattering pattern did not significantly change until 30 °C was reached. This shows that the T_{gel} of the $MgCl_2$ gel is higher than that of the LiCl gel analysed, which is consistent with experiments conducted by rheometry seen in Figure 3.9. Both gels showed similar scattering patterns, indicating that they follow a similar trend of long flexible cylinders, followed by shortening when the gel is heated and lengthening when it is cooled. Both gels also showed a decrease in intensity in the second analysis at 10 °C. This is likely due to a shortened formation time in comparison to when the gels were

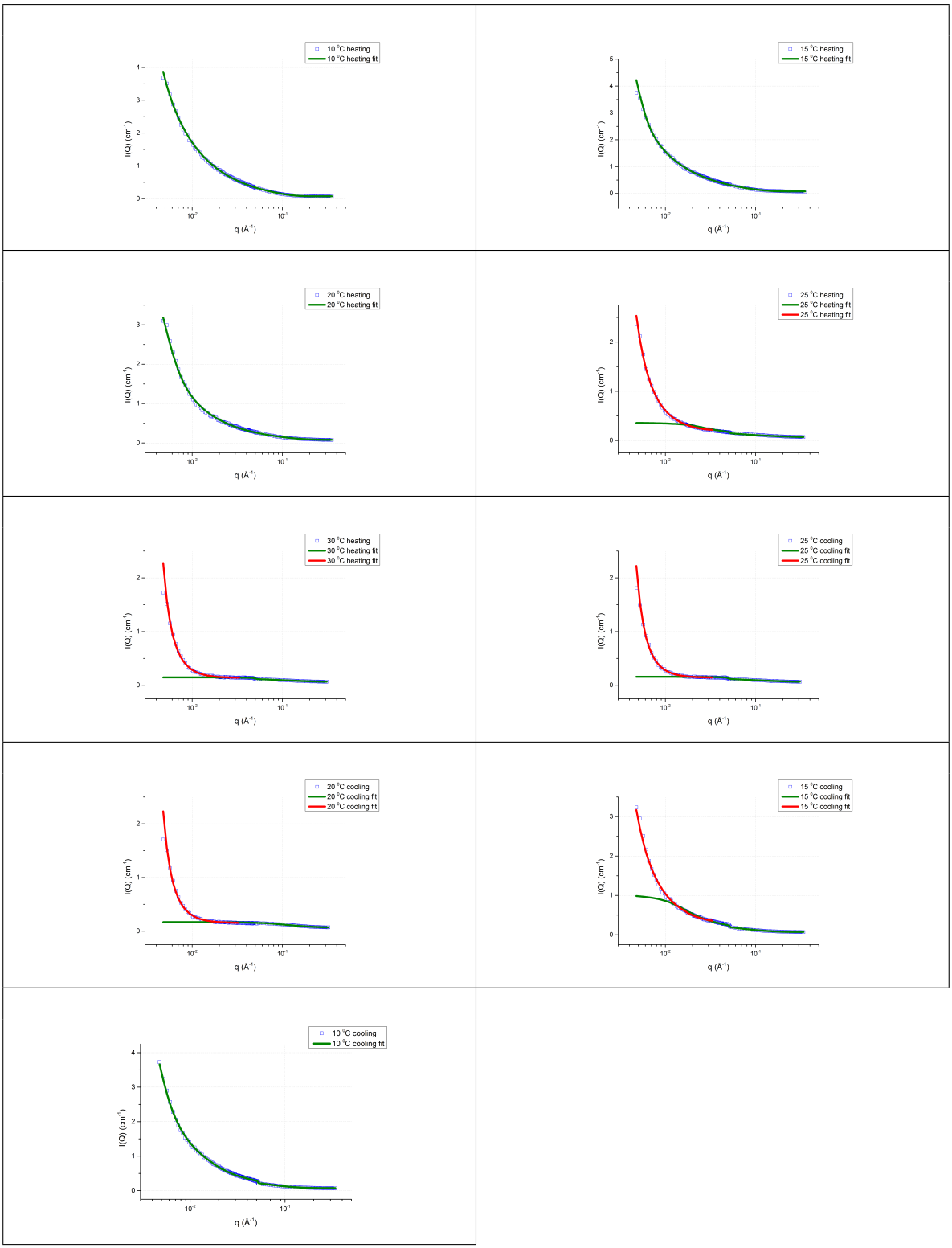

Figure 3.10: Model fitting for SANS data of $MgCl_2$ with proline calix[4]arene at various temperatures. Here, blue squares represent the scattering data, green lines the flexible cylinder model and red lines the power law model.[114]

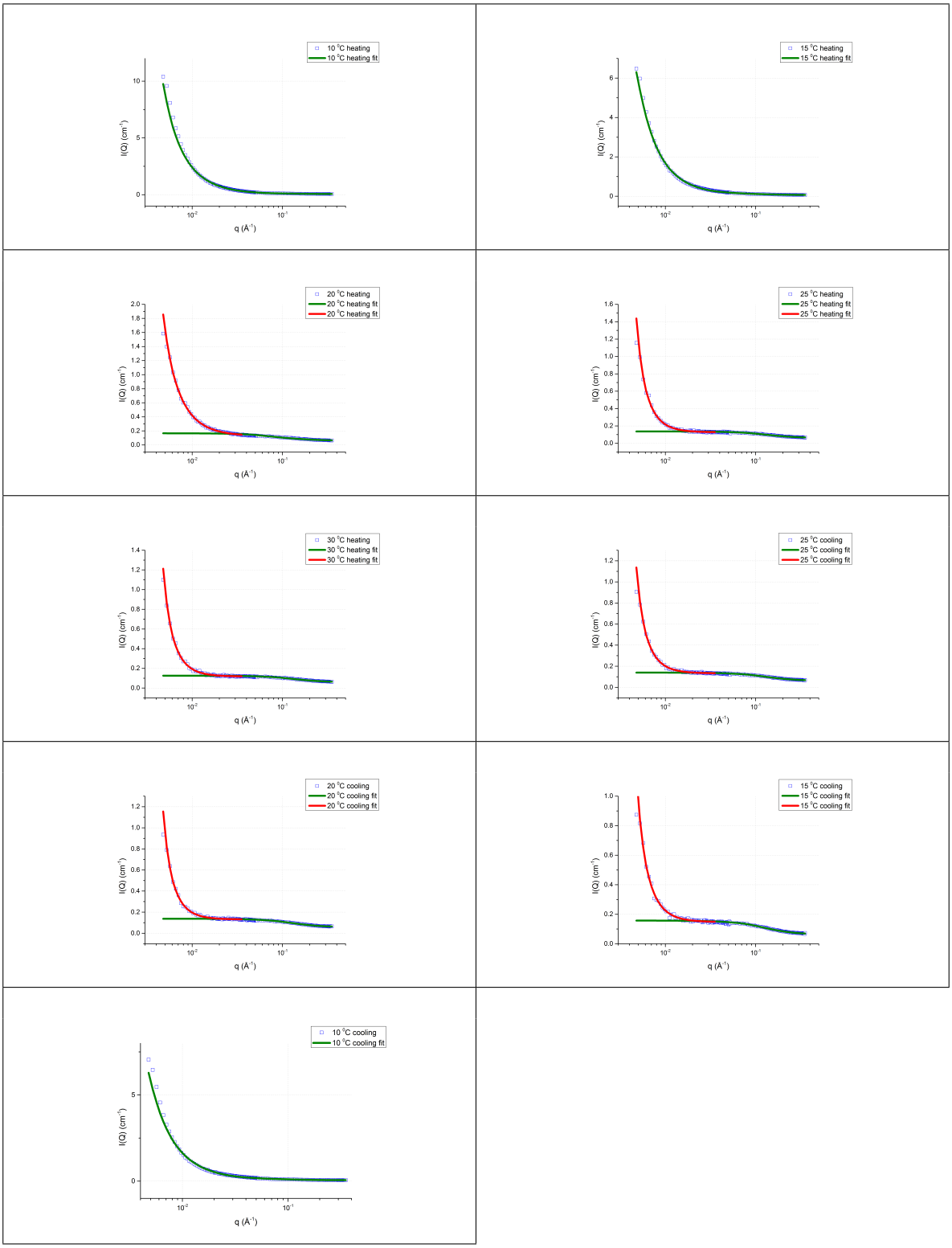

Figure 3.11: Model fitting for SANS data of LiCl with proline calix[4]arene at various temperatures. Here, blue squares represent the scattering data, green lines the flexible cylinder model and red lines the power law model.[114]

initially formed before analysis.

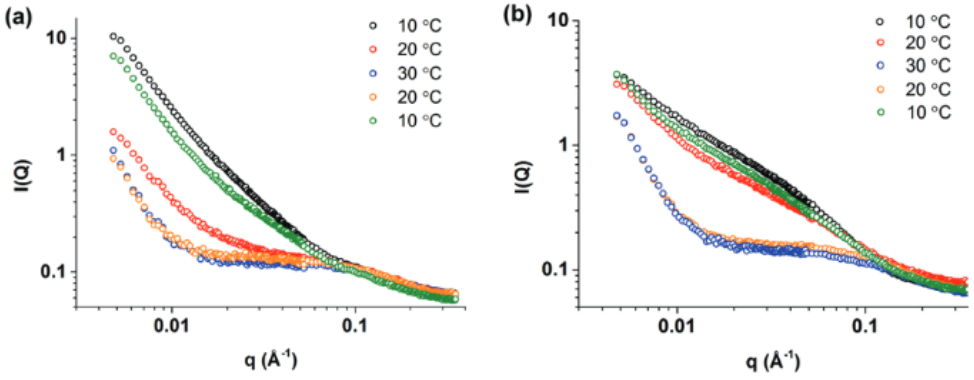

Figure 3.12: Scattering profiles obtained from SANS measurements for gels of and proline calix[4]arene with (a) LiCl and (b) $MgCl_2$ elctrolytes upon cycling the temperature from 10-30-10 °C. For these measurements, a calixarene concentration of 20 mM was used. Data is plotted on an absolute intensity scale (cm^{-1}).

Figures 3.13a and 3.13b show the average length of the fibres at each temperature. The values can be found in Appendix A.1. This showed that initially very long, curved, fibres were present, which shortened and became straight upon heating and lengthened again when the gels were cooled. This is confirmed by AFM imaging which shows the fibres disassembling at the curved sections first, leaving only short straight sections (Fig. 3.4). Kuhn length is a measure of the straightness of fibres and is the average distance along the fibres before a turn or curved section. For the LiCl-induced gel, restoration of the fibre network to its original, pre-annealed state is shown by recovery of fibre length and Kuhn length to their original values (large fibre length and small Kuhn length, indicating long, curved fibres). For the $MgCl_2$-induced gel, however, this did not occur, with the Kuhn length significantly increasing upon annealing, suggesting the transition from long, curved fibres pre-annealing to long, straight fibres upon annealing. This agrees with the AFM images observed in Figures 3.3 - 3.6. Based on the AFM and SANS data, coupled with the rheology measurements, it would appear as though the annealing of the fibre network in the $MgCl_2$ gels gives rise to straighter, larger fibres which in turn yields increased stiffness. It is known that stiffness is proportional to the square of the Kuhn length, thus explaining these observations.[115]

Figures 3.16a and 3.16b shows the average radius of the fibres at each tem-

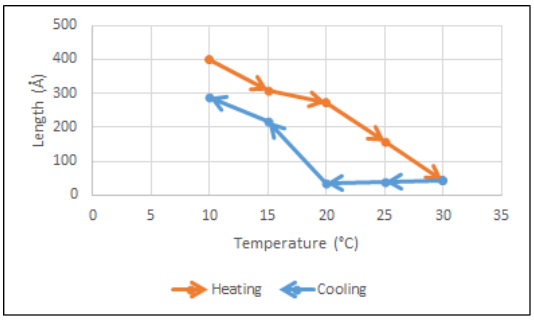

(a) $MgCl_2$

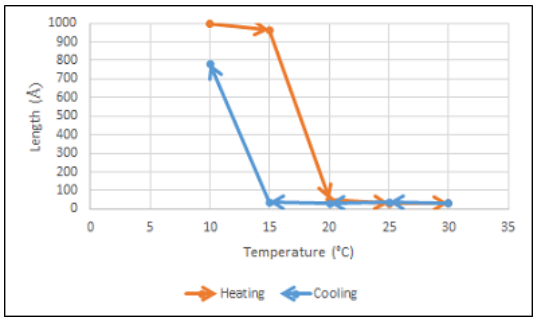

(b) LiCl

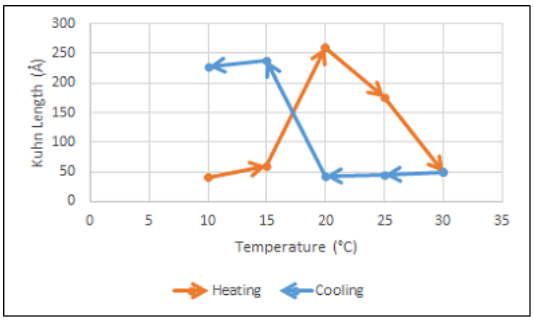

(c) $MgCl_2$

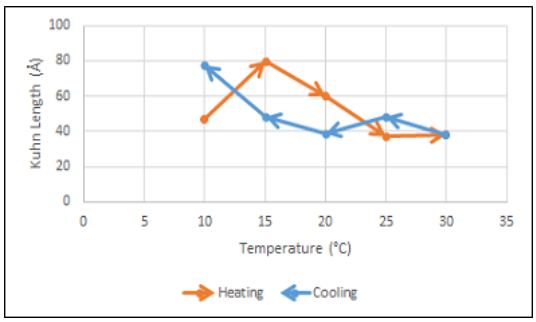

(d) LiCl

Figure 3.13: Graphs showing the change in length and Kuhn length with temperature of fibres formed by proline calix[4]arene with $MgCl_2$ and LiCl electrolytes. The analysis began at 10 °C, the samples were heated with measurements taken every 5 °C until 30 °C was reached. The samples were then cooled with measurements again taken every 5 °C.

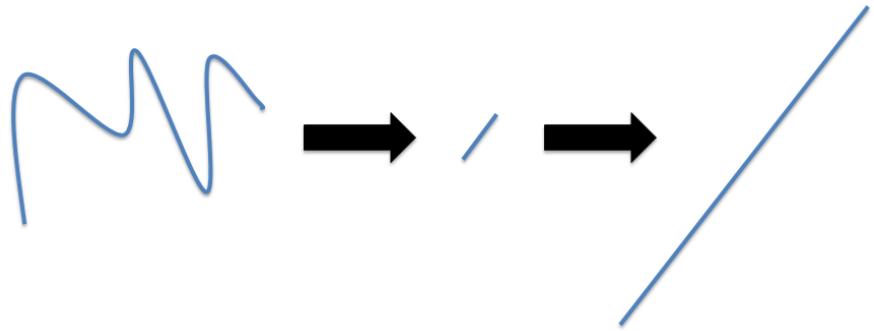

Figure 3.14: Graphical depiction of the structures observed by SANS across a full heat and cool cycle for the for the proline calix[4]arene, with $MgCl_2$ electrolyte, gel. This shows that the gel started with the same structure as the LiCl triggered gel and shortened in the same way during heating. However, upon cooling the $MgCl_2$ triggered gel formed long, straight fibres while the LiCl triggered gel returned to the initial structure.

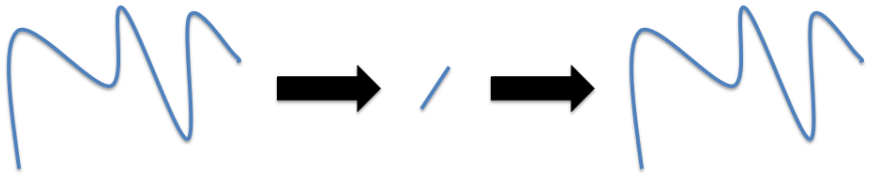

Figure 3.15: Graphical depiction of the structures observed by SANS across a full heat and cool cycle for the proline calix[4]arene, with LiCl electrolyte, gel. This shows that the gel started as long curved fibres, shortened upon heating and formed the initial structure when cooled.

perature analysed. The radius was seen to increase slightly when the gels were at lower temperatures which indicates bundling of the fibres. This is expected as more fibres are present in the gel. The radius seen is consistent with measurements made by AFM.

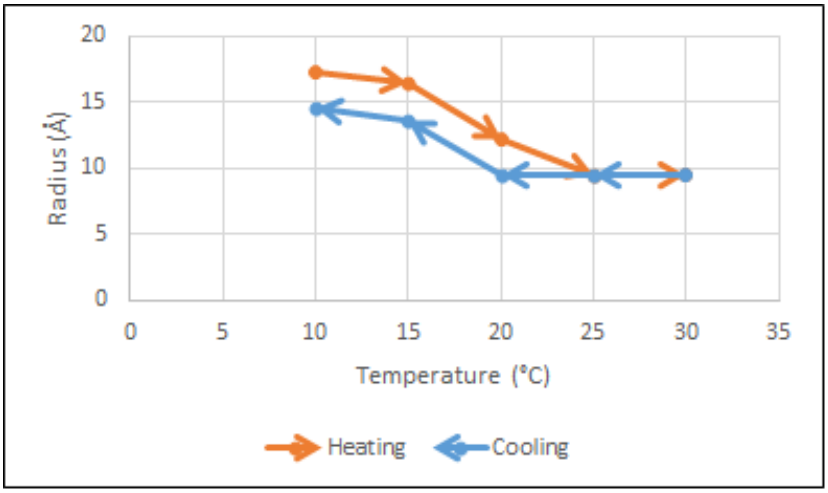

(a) $MgCl_2$

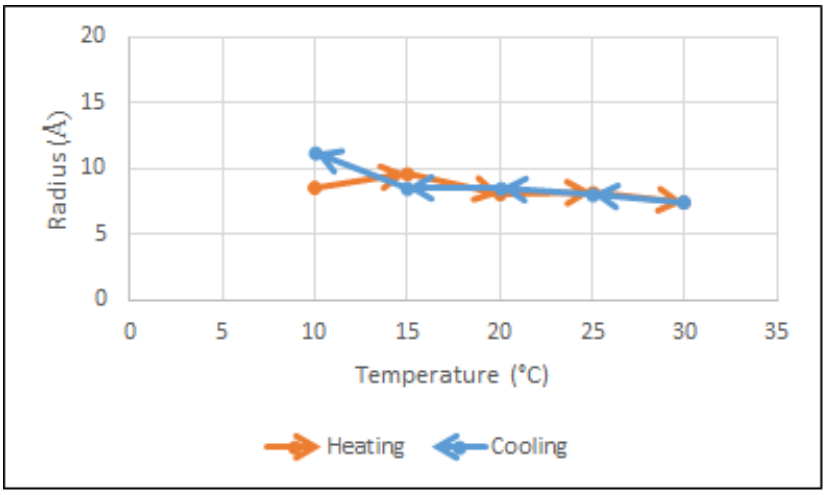

(b) LiCl

Figure 3.16: Graph showing the change in radius with temperature of fibres formed by (a) $MgCl_2$ and (b) LiCl electrolyte with proline calix[4]arene gels. The analysis began at 10 °C, the sample was heated with measurements taken every 5 °C until 30 °C was reached. The sample was then cooled with measurements again taken every 5 °C. The radius of the fibres is seen to be fairly consistent with some increase at the cooler temperatures, indicating bundling of the fibres.

3.3.2 Concentration Dependent Morphology of Lithium Chloride Triggered Proline Calix[4]arene Hydrogels

3.3.2.1 Atomic Force Microscopy

During *ex situ* imaging for section 3.3.1.1, the L-proline calixarene gel with LiCl was seen to form bundles of fibres in helices when the gelator was at higher concentrations (0.2 M). This had not been seen in any of the previous *in situ* or *ex situ* imaging which had always shown single fibres or disordered bundles when gels were made with concentrations of 0.02 M. Figure 3.17a shows the initial image of this high concentration gel depicting ordered helices which occur only in one direction. The opposing enantiomer of the gelator was synthesised and the corresponding gel imaged *ex situ* to investigate the structure further. It was found that the L-proline calixarene gelator (Fig. 3.17a) formed helices in the opposite direction to the D-proline calixarene gel (Fig. 3.17b).

Imaging was attempted *in situ* to study the assembly of this gel, however, as the structures have a larger radius than those observed for the gels formed at lower concentrations of the proline calix[4]arene, and crystallisation occurred, it was not possible to image with an in droplet method by AFM as opaque gels were formed. Due to this, it could not be investigated if the gel formed single fibres which then entangled or if the helices were built as the gel assembled. However, observation of the two directions of the fibres shows that the chirality of the molecule is important in the way they sit together to form fibres and assemble the gel.

3.3.2.2 Time-Of-Flight Small Angle Neutron Scattering

Hydrogels of proline calix[4]arene (L-proline calix[4]arene) with LiCl were analysed using Time-of-Flight (TOF) SANS to investigate the assembly of the helical structure seen by AFM. The TOF configuration allowed the samples to be continuously analysed over multiple temperature ramps to show time resolved changes in the structure. Previously, similar samples were investigated using SANS and samples were analysed at stabilised temperatures which could easily miss information in

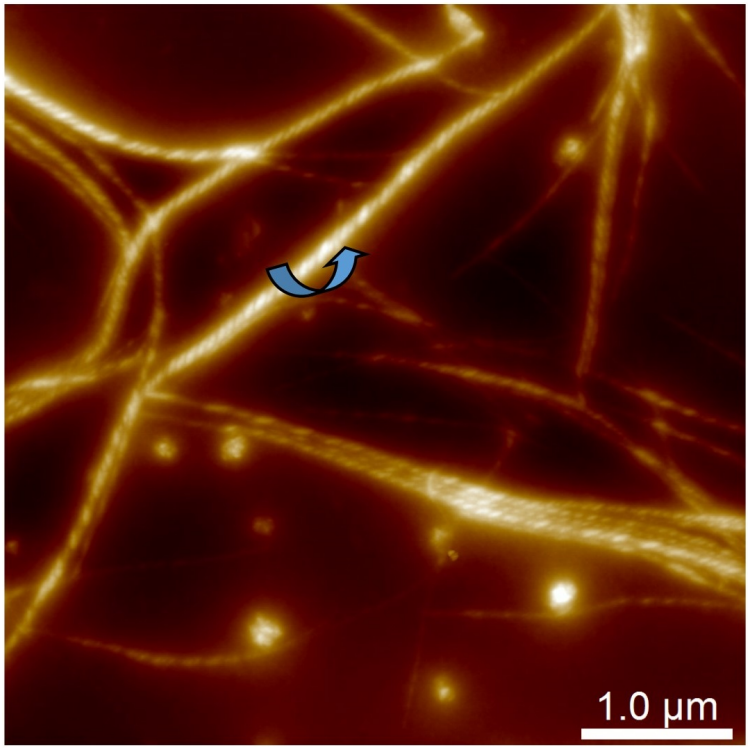

(a)

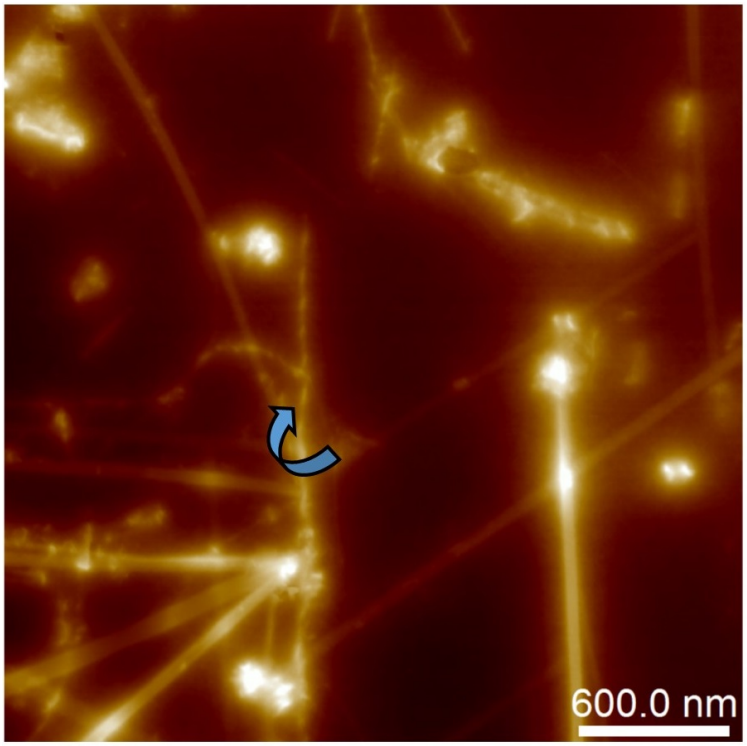

(b)

Figure 3.17: Proline calix[4]arene (0.2 M) with LiCl (0.13 M) gels imaged *ex situ*. Image (a) shows a right handed helical structure formed D-proline calix[4]arene. Image (b) shows a left handed helical structure formed with L-proline calix[4]arene.

the assembly process. These samples could not be analysed by *in situ* AFM due to the high concentration of the gel so while the final helical structure was shown by *ex situ* AFM imaging, it was impossible to see the assembly steps by AFM. The gels were analysed according to the method in section 2.4.

Modelling and fitting of the SANS data was complicated as the system was polydisperse. This presumably arose as the helices were entangled close enough to be seen as one structure with single fibres were also present. As a technique, SANS modelling and fitting will try to fit this as one structure and find an average, resulting in the modelling missing features in the fitting. A flexible cylinder model was used based on previous AFM imaging showing this to be the expected structure (Fig. 3.17a - 3.17b). Cross linking is also expected at these higher concentrations as more fibres will be within the same volume which will cause larger interactions between the fibres. This could result in other structures such as two dimensional sheets being seen.

The gel was seen to be temperature reversible with the length increasing on cooling and shortening again when heated. The radius was not seen to change greatly, varying between 7.7 Å and 11 Å. The first data point at which the length increases (where fibres begin to form), the radius was seen to be 7.7 Å, this then increased to 8.8 Å. This indicates that the system likely forms individual fibres which then intertwine into the helices. With further instrument time, this could be confirmed by running a slower temperature ramp across a smaller temperature range where the assembly has been seen to occur. As the radius was similar to that seen by SANS of the lower concentration gel (Fig. 3.16b), the system is confirmed to be a polydisperse system of single fibres and helices. Complete data from the SASView modelling can be found in Appendix A.2.

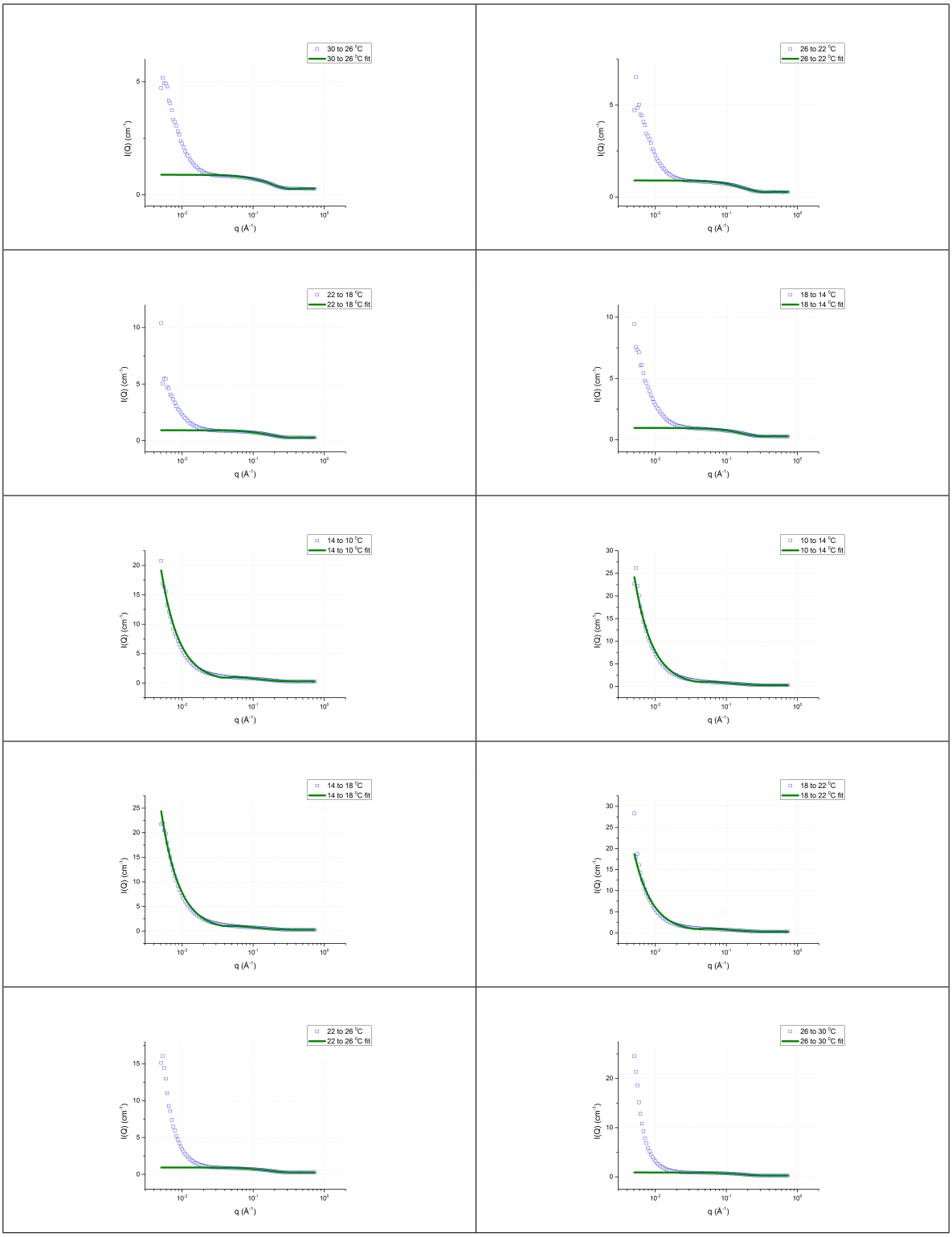

Figure 3.18: Model fitting for SANS data of LiCl electrolyte with proline calix[4]arene gel at various temperatures. Here, blue squares represent the scattering data and the green lines the flexible cylinder model.

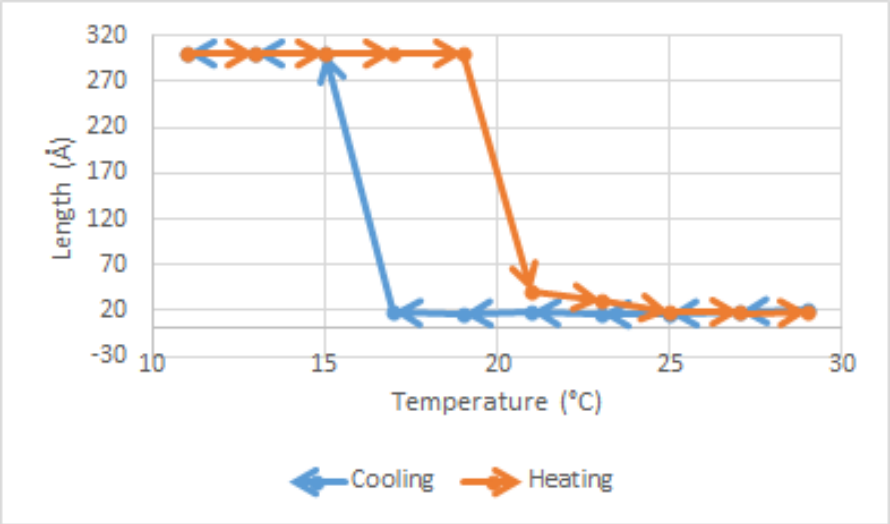

Figure 3.19: Graph showing the change in length with temperature of fibres formed by a high concentration LiCl electrolyte with proline calix[4]arene gel. The analysis began at 30 °C, the sample was then cooled to 10 °C and reheated to 30 °C with data captured throughout. The fibres are seen to lengthen when the gel is cooled and shorted again when the gel is heated.

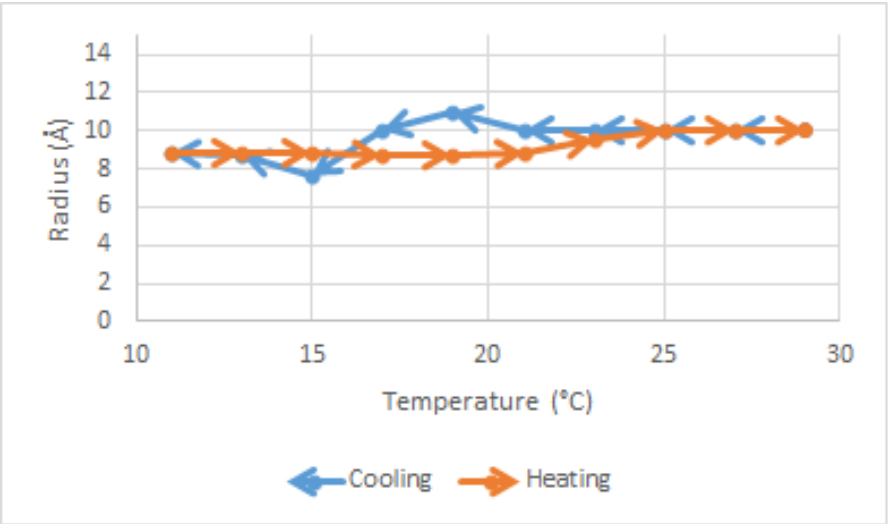

Figure 3.20: Graph showing the change in radius with temperature of fibres formed by a high concentration LiCl electrolyte with proline calix[4]arene gel. The analysis began at 30 °C, the sample was then cooled to 10 °C and reheated to 30 °C with data captured throughout. The radius is seen to remain at approximately 1 nm and then drop to 7.7 nm at 15 °C, corresponding with the temperature at which the fibres lengthen.

3.4 Conclusion

AFM imaging showed a change in fibre morphologies of the proline calix[4]arene gel with a $MgCl_2$ electrolyte when the gel was temperature cycled. It was also shown that a different structure formed when the gel was heated above approximately 25 °C. After each subsequent temperature cycle, the fibres became straighter and shorter on reassembly. Other rod like structures were also seen to form which had diameters orders of magnitude larger than the fibres. This was not seen with a proline calix[4]arene gel which was formed with LiCl. This gel was seen to be temperature reversible with a similar morphology forming after each temperature cycle. These observations were confirmed with SANS, showing the Kuhn length of the $MgCl_2$ induced gel increasing after temperature cycling while the LiCl induced gel returned to its original morphology, with no change in the length, Kuhn length or radius.

Rheometry of these gels shows that while the LiCl gel was temperature reversible in regards to its physical properties, the $MgCl_2$ gel continued to strengthen during each temperature cycle, upon both heating and cooling. This is quite rare for supramolecular gels, however, it has been previously reported for some polymeric gels. This strengthening could be due to the formation of the secondary structure or a continued formation and strengthening of this gel in longer time scales than the LiCl gel.

AFM of LiCl triggered proline calix[4]arene gels showed that at high temperatures, the fibres formed bundles in a helical structure. Imaging of gels formed with the D and L isomers showed that the helices formed in opposite directions depending on the enantiomer used. This is presumably due to the chirality of the proline calix[4]arene molecule forcing the fibres to wrap in only one direction. Helices were not seen in high concentration gels formed with $MgCl_2$.

Chapter 4

Further Investigations of Gelation by Atomic Force Microscopy

4.1 Thin Film Method for *in situ* Analysis of Gels

4.1.1 Introduction

In 2015, Barker *et al.* developed a method to analyse gels *in situ* during assembly and disassembly. This was a great leap in the ability to visualise gels and the assembly of gel networks without the risk of affecting the gel structure during the sample preparation (for example by freeze drying). However, the major limitation of this method is that it was only possible to image transparent gels. When imaging opaque gels, large particles may obstruct the feedback laser of the Atomic Force Microscopy (AFM) system which is used to detect the motion of the cantilever, causing the instrument to stop imaging. To further the analysis of gel self-assembly, it was hypothesised that imaging the gel in a thin film would allow the back of the cantilever to remain in air while the actual probe remained within the gel during imaging. A comparison of all the AFM configurations used is shown in Figure 4.1.

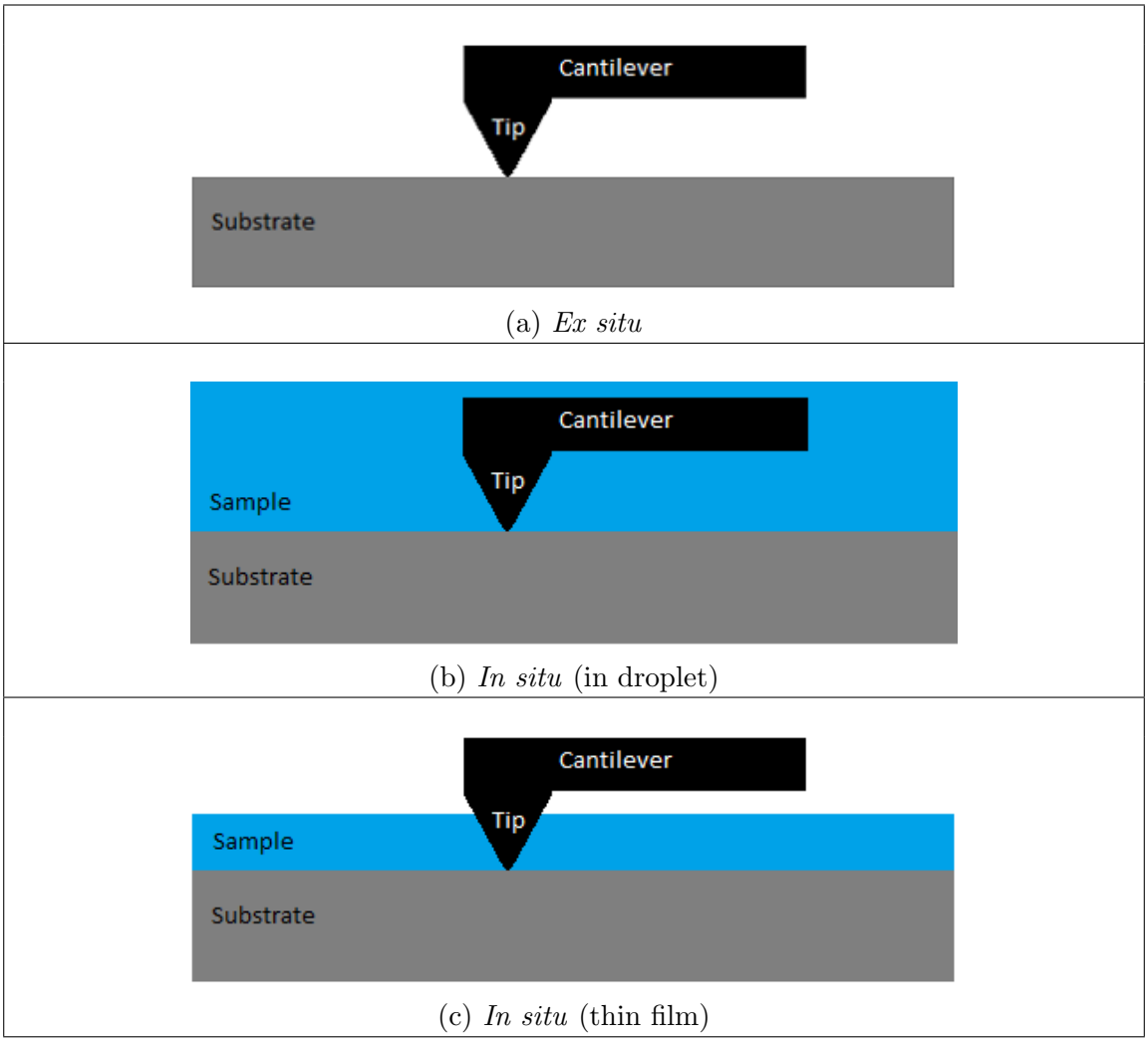

(a) *Ex situ*

(b) *In situ* (in droplet)

(c) *In situ* (thin film)

Figure 4.1: Schematics showing the set up of the AFM tip with the sample and substrate for the three AFM configurations used. The thin film configuration shown in (c) was used for this section.

4.1.2 Methodology

The materials used were: proline calix[4]arene (synthesised by Mr. Brendan Ennis), magnesium chloride hexahydrate (Sigma-Adrich, ≥99%) and lithium chloride (Sigma-Adrich, ≥99%). The materials were used as received without further purification.

The gels were analysed by *in situ* AFM within a thin film (section 2.1.3).

4.1.3 Results and Discussion

4.1.3.1 Proline Calix[4]arene with $La(NO_3)_3$ Electrolyte

To create the thin film, smearing the gel onto a mica surface was attempted, this had previously been shown to allow the imaging of the proline calix[4]arene gel *ex situ*. Care was taken to apply more gel to the surface, to create a thicker film, by starting with a larger droplet and applying less force when smearing the gel. A gel triggered through the addition of a lanthanum nitrate electrolyte (25 mM with 20 mM proline calix[4]arene) was tested, as this was previously too opaque to be imaged *in situ*. Initially, it was found that the fibre network was very thick which would hamper the ability to see the disassembly process of the individual fibres. As a thick film was still required so that the tip did not leave the film during its oscillation, the concentration of the gel was decreased significantly (17 mM $La(NO_3)_3$ and 13 mM proline calix[4]arene). This gel was suitable to be imaged using the thin film methodology, however, the sample did not disassemble by 45 °C which is the upper temperature limit of the Bruker Dimension FastScan instrument that was used. The difference in morphology between the initial gel and the heated gel can be seen in Figure 4.2.

This gel was seen to be a liquid in the vial after 1 hour but it still showed a very dense network in the AFM images. This may be because the network forms when it is applied to the substrate or it may have a network formed well before becoming a solid gel, which is not uncommon.[116,117] Finding a concentration that would be possible to clearly image the fibres within a thin film during assembly and

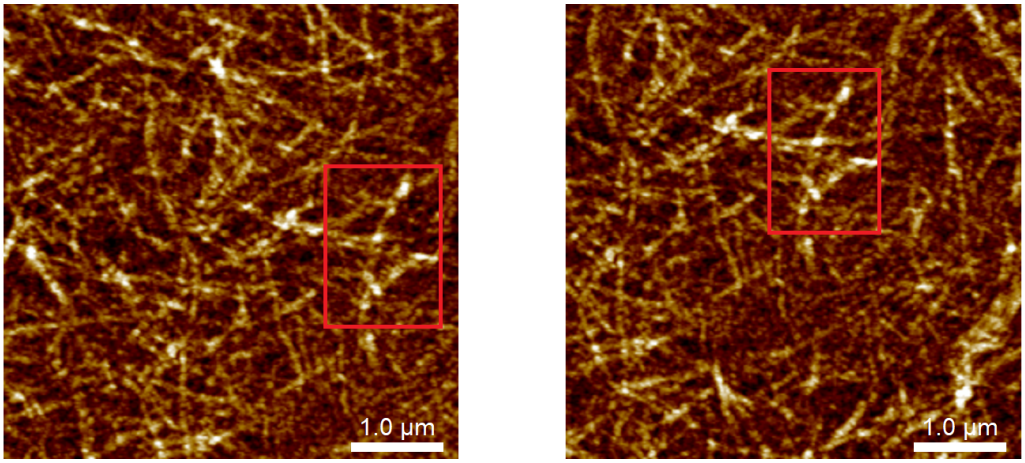

(a) Initial gel network, T = 24 °C. (b) Gel network after heating, T = 45 °C.

Figure 4.2: AFM topography images of proline calix[4]arene (13 mM) gel fibres with $La(NO_3)_3$ (17 mM) imaged *in situ*, in a thin film. The network was not seen to change across the heating cycle.

disassembly on the instrument would be very difficult with this gel as the opacity is a consequence of the large volume of fibres. This may be easier in samples where the opacity simply arises due to the size of the fibres rather than the density of fibres.

4.1.3.2 Proline Calix[4]arene with $MgCl_2$ Electrolyte

As a concentration which allowed for *in situ* imaging by the method outlined in 2.1.2 was already known for this gel, imaging in a thin film was attempted under these conditions (20 mM proline calix[4]arene, 25 mM $MgCl_2$). Here, the sample was prepared by spin coating at 1000 rpm for 1 minute. All samples showed fibres to be present both on the lighter (dried) and darker (wet) looking areas of the substrate which was determined using the optical microscope on the AFM. Wetter areas were chosen so imaging was performed in the thin film and not *ex situ*. Appendix Figure A.1 shows an image captured with the optical view of the Bruker Dimension FastScan instrument indicating the wetter and drier areas of a gel smeared on mica.

The network was again quite dense, which could make imaging gel disassembly difficult depending on how uniform the process was across the film. However, the network was seen not to change at all when heated from 25 °C to 38 °C. As the

T_{gel} for this gel at this concentration had been seen to be between 25 °C and 30 °C both macroscopically, in a vial, and by *in situ* AFM, this indicates that something different is occurring when the sample is prepared as a thin film. Figure 4.3 shows the gel network imaged initially and after heating. The network was seen to be significantly more densely packed than when imaged *in situ* in a droplet or when smeared, as shown in Section 3.3.1.1.

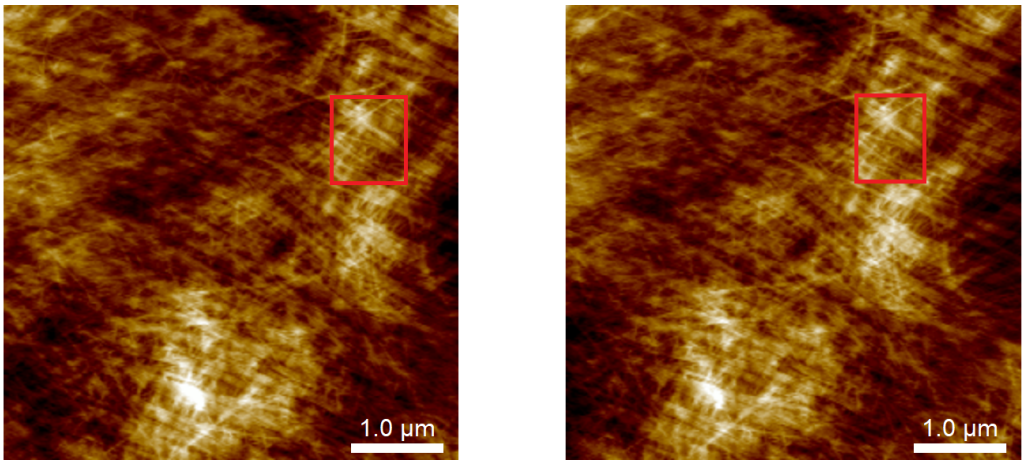

(a) Initial gel network, T = 25 °C. (b) Gel network after heating, T = 38 °C.

Figure 4.3: AFM topography images of proline calix[4]arene (20 mM) gel fibres with $MgCl_2$ (25 mM) imaged *in situ*, in a thin film. The thin film was prepared by spin coating the gel on a mica substrate at 1000 rpm to 1 minute. The network was not seen to change across the heating cycle.

To reduce the thickness of the gel network, the sample was spin coated faster, at 2000 rpm for 1 minute, to prepare the thin film. This did not seem to create a thinner film, nor was any change seen when the film was heated from 25 °C to 39 °C. A comparison of the initial film and the film after heating can be seen in Figure 4.4. As this was not successful, the sample was spin coated at 2000 rpm for 10 minutes to prepare the thin film. This did seem to be successful at creating a thinner film thickness, although fibres were still not as separated or sparse as in the *in situ* method. The fibre network was again not observed to change when heated from 25 °C to 43 °C as can be seen in Figure 4.5. The view with the optical microscope of the AFM allowed the observation that the sample appearance changed, potentially due to evaporation of the solvent, from approximately 40 °C. This indicated that a thicker film or an enclosed fluid cell

would be necessary to reduce evaporation during the analysis of this gel.

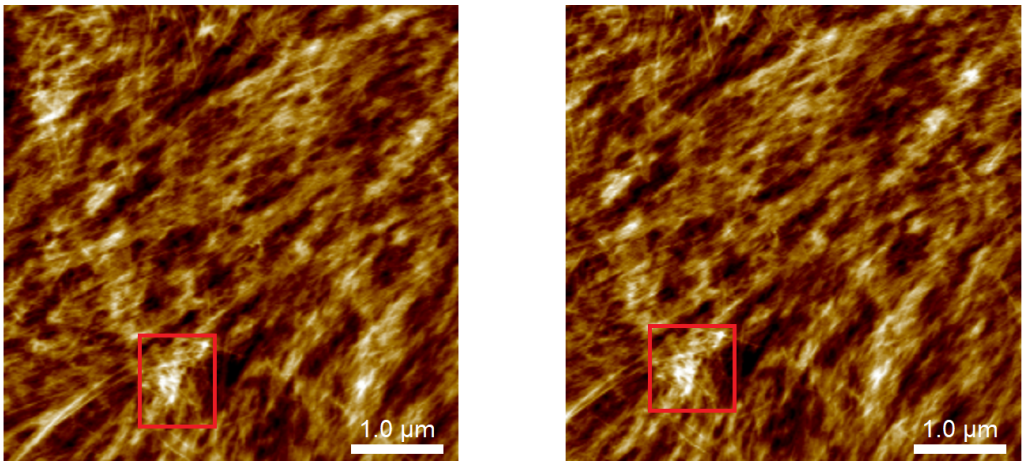

(a) Initial gel network, T = 25 °C. (b) Gel network after heating, T = 39 °C.

Figure 4.4: AFM topography images of proline calix[4]arene (20 mM) gel fibres with $MgCl_2$ (25 mM) imaged *in situ*, in a thin film. The thin film was prepared by spin coating the gel on a mica substrate at 2000 rpm to 1 minute. The network was not seen to change across the heating cycle.

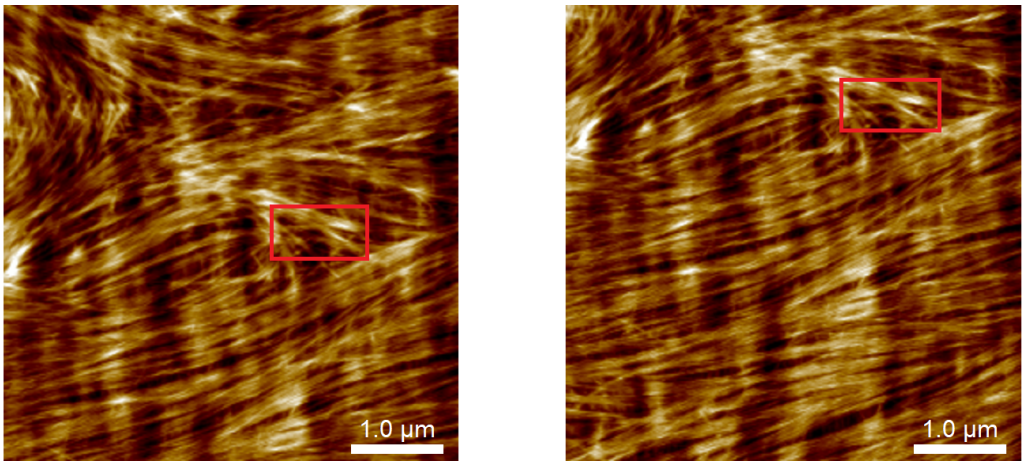

(a) Initial gel network, T = 25 °C. (b) Gel network after heating, T = 38 °C.

Figure 4.5: AFM topography images of proline calix[4]arene (20 mM) gel fibres with $MgCl_2$ (25 mM) imaged *in situ*, in a thin film. The thin film was prepared by spin coating the gel on a mica substrate at 2000 rpm to 10 minutes. The network was not seen to change across the heating cycle.

To produce a thicker film with fewer fibres, the proline calix[4]arene gel with magnesium chloride was made at a lower concentration (27 mM proline calix[4]arene and 17 mM $MgCl_2$) and spin coated at a slower speed (1000 rpm for 8 minutes). The slower speed was chosen as the lower concentration gel was less loaded with fibres and 2000 rpm was seen to leave no fibres on the surface.

A longer time period was used as this was successful in creating a film with the desired thickness, as shown in Figure 4.5. This gel again did not disassemble between 25 °C and 36 °C. A roughness calculation conducted in Nanoscope Analysis on comparable areas of the image showed that the image had smoothed from a roughness average of 5.5 nm to 5.0 nm. These images can be seen in Figure 4.6. This could indicate that some of the gel has disassembled, making the film thinner and flatter than previously. However, it is more likely that some evaporation occurred which shrunk the film and created a smoother surface. Also, given the small change, the temperature needed to fully disassemble the gel in this film would likely result in evaporation of the solvent before disassembly was seen.

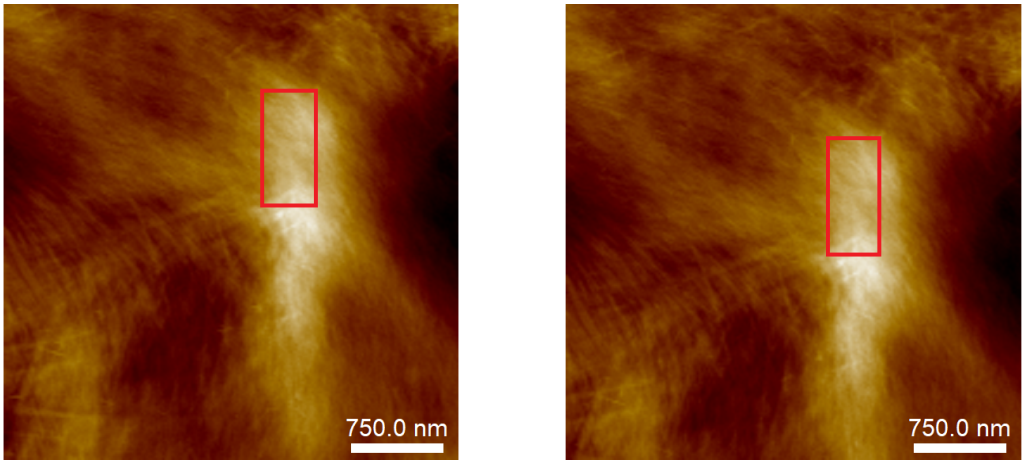

(a) Initial gel network, T = 25 °C. (b) Gel network after heating, T = 36 °C.

Figure 4.6: AFM topography images of proline calix[4]arene (27 mM) gel fibres with $MgCl_2$ (17 mM) imaged *in situ*, in a thin film. The network was not seen to change across the heating cycle. However, roughness calculations across the images show the average roughness decreasing from 5.5 nm to 5.0 nm.

The same gel was spin coated onto a Highly Ordered Pyrolytic Graphite (HOPG) hydrophobic substrate at various speeds for varying time periods to attempt to form a thinner gel network. An optimal coating was formed at 3500 rpm for 2 minutes. While the film showed fibres individually separated which would allow the observation of disassembly of individual fibres easily, the gel network did not disassemble between 25 °C and 50 °C (Fig. 4.7). This is most likely because the liquid phase evaporated before the network disassembled due to the hydrophobic nature of the HOPG substrate. A closed cell would be required to stop this

evaporation and allow the assembly and disassembly to occur. It is therefore not useful to image using this substrate as a closed cell would solve the same issues when using a mica substrate which allows for better imaging of this gel due to its hydrophilicity. The hydrophilicity of the mica substrate causes the fibres to lay down on the substrate so that they are then properly scanned as the tip moves across the substrate. The hydrophobic HOPG substrate can cause the proline calix[4]arene gel fibres to be repelled and sit slightly above the substrate, in the gel.

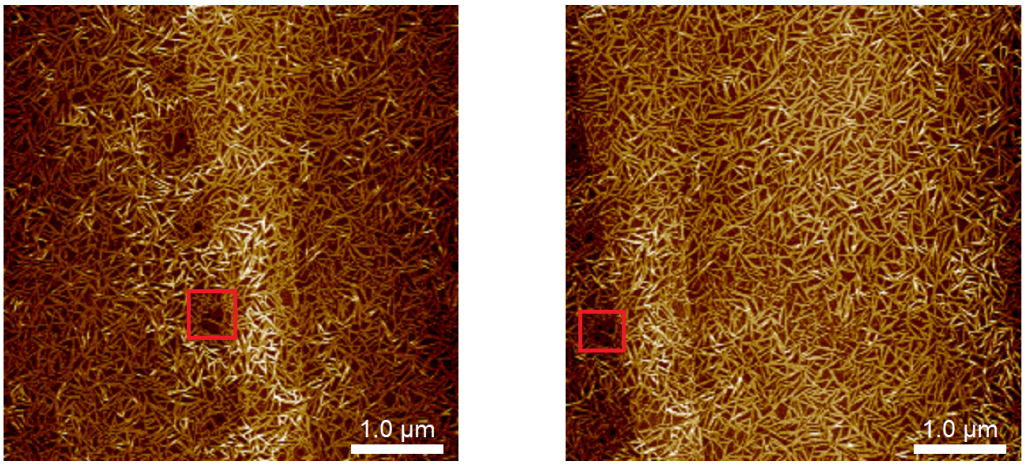

(a) Initial gel network, T = 25 °C. (b) Gel network after heating, T = 50 °C.

Figure 4.7: AFM topography images of proline calix[4]arene (27 mM) gel fibres with $MgCl_2$ (17 mM), spin coated on an HOPG substrate and imaged *in situ*, in a thin film. The network was not seen to change across the heating cycle even though the network was seen to be thinner on the surface than when mica was used as a substrate.

As spin coating and smearing had been shown to form thin films which did not have sufficient liquid phase to disassemble the gel network when heated, dip coating was used to prepare the thin films on mica and HOPG. When mica was used, the gel network prepared was extremely thick and did not disassemble on heating. However, when HOPG was used, a film was not formed at all due to the hydrophobic surface. AFM images showing the HOPG surface after dip coating can be seen in Figure 4.8. Droplets can be seen on the HOPG surface which is due to the water repelling the hydrophobic surface. Given the size of the droplets (less than 500 nm), it is unlikely there was significant assembly within them although inside the droplets was not scanned.

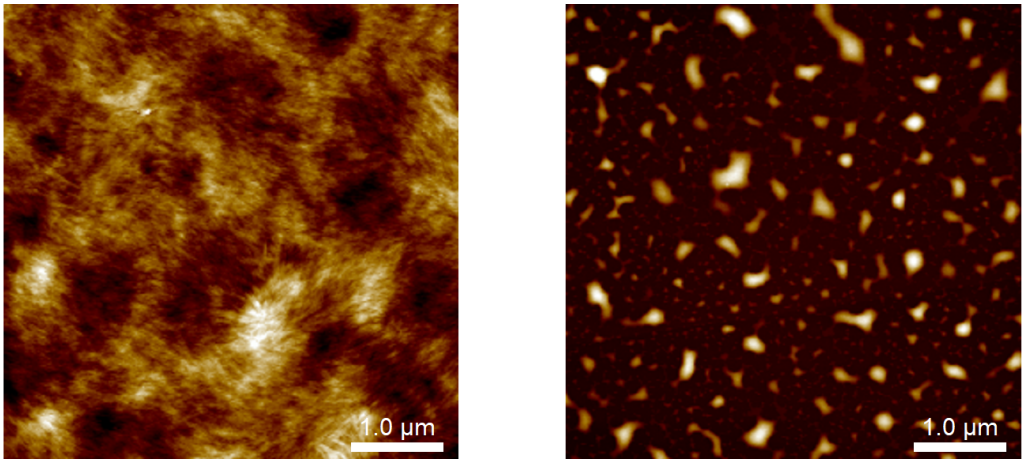

(a) (b)

Figure 4.8: AFM topography images of proline calix[4]arene gel fibres with $MgCl_2$ (17 mM), dip coated on (a) mica and (b) HOPG. The network was too thick when prepared on mica and did not form on HOPG.

4.1.4 Conclusion

Thin films of the required thickness were successfully prepared and imaged *in situ* (thin film) by smearing, spin coating and dip coating. Spin coating proved to be the most robust method in terms of consistently producing films with an even coating in which imaging was possible. However, the solvent appears to evaporate quickly upon heating which stops the gel network from disassembling. This method may be successful if it is conducted in a small enclosed cell to reduce the evaporation, such as is available on the Bruker Multimode AFM. This was not conducted due to not having access to an AFM with a closed liquid cell, and time restraints. Other improvised attempts at reducing evaporation, such as humidifying the area around the sample by placing a wet Kimwipe around the sample, were unsuccessful and are potentially harmful to the electronics of the AFM scanner.

This method may be successful with other gels where the fibres disassemble at temperatures closer to where the gel is seen to melt macroscopically, as in a vial inversion method. This gel has shown a difference of approximately 5 - 10 °C between when the gel is seen to melt in a vial and when the fibres are seen to disassemble by *in situ* AFM imaging.[76] As the gel melts, it is more likely to allow the solvent to evaporate before the fibres are seen to disassemble. This is likely to be a phenomenon seen with most supramolecular gels as the interactions between

the fibres will be broken by heating well before the interactions within the fibres.

4.2 Imaging of Peptide Gels by Atomic Force Microscopy

4.2.1 Introduction

Peptide gels have been studied extensively due to the vast range with an even greater range of properties.[92] Two novel peptide gels, Fmoc-GFFRGD and N,N'-bis-[di-CBZ-L-Lys]-ethylenediamine, were recently reported and used in this research. These gels show the duality of the industry with the former being designed and created purposefully and the latter being a serendipitous discovery.

4.2.2 Methodology

The materials used were: N,N'-bis-[di-CBZ-L-Lys]-ethylenediamine (synthesised by C. Duncan), Fmoc-GFFRGD (synthesised by Dr. Jonathon Wojciechowski), sodium hydroxide (Sigma-Adrich, $\geq$98%) and Dulbecco's Modified Eagle's Medium (DMEM) (Sigma-Adrich, $\geq$99%). The materials were used as received without further purification.

To form the gel, Fmoc-GFFRGD (0.01g) was dissolved in a solution of ultrapure water (1.78 mL) and 0.1 M NaOH (0.22 mL). This was then mixed with DMEM at a 1:1 ratio. The resulting solution remained liquid at room temperature and was a bright pink colour due to the phenol red present in the DMEM cell culture media. This formed a gel of concentration 0.25% w/v.

To form the N,N'-bis-[di-CBZ-L-Lys]-ethylenediamine gel, the peptide (5.0 mg) was dissolved in chloroform (0.500 mL) and left at room temperature for several minutes. A hard, transparent gel was seen to form with a concentration of 1% w/v.

The gels were analysed by *ex situ* and *in situ* AFM (sections 2.1.1 and 2.1.2).

4.2.3 Results and Discussion

4.2.3.1 Fmoc-GFFRGD gel

The Fmoc-GFFRGD gel was imaged *in situ* according to the method in section 2.1-*in situ*. This method requires a transparent gel to allow the detection of the cantilever motion with the AFM feedback laser during imaging. The pink colour of the gel (Fig. 4.9) did not present any issues during imaging. Images were processed according to section 2.1-*Image Processing*.

Figure 4.9: Fmoc-GFFRGD gel in vial used for imaging.

While the gel was a liquid when imaging was started at 25 °C, the tip appeared to be experiencing large damping forces and adhesion to the substrate surface during imaging. This is likely due to the large amount of ions present in the DMEM cell culture media which may have bonded to the mica surface and caused the tip to adhere to the surface. No AFM images were captured due to these issues during imaging.

4.2.3.2 N,N'-bis-[di-CBZ-L-Lys]-ethylenediamine gel

The gel was initially imaged *ex situ* according to the method in section 2.1-*ex situ* (as it was a novel system and the structure was entirely unknown). The first gel which was imaged was formed with chloroform as solvent. As this gel appeared to take several hours to form, it was imaged after approximately 24 hours. Prior to preparing the sample for AFM, the gel was heated to 40 °C and allowed to cool to room temperature to reform. This formed a stiff, transparent gel within minutes.

The physical structure was seen to be comprised of short fibres which had

formed small bundles (Fig. 4.10). As the gel was recently formed and clear, and the structures are curved, it is unlikely that the structures seen are crystals. Measurements of the structures show diameters of approximately 3 nm with bundles of over 40 nm. The fibres are quite short with all fibres appearing to be less than a micrometre in length.

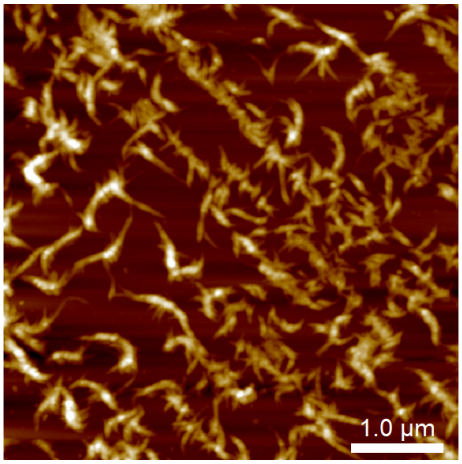

Figure 4.10: AFM image of N,N'-bis-[di-CBZ-L-Lyz]-ethylenediamine (2 % w/v) with chloroform solvent.

This gelator was a good candidate for *in situ* imaging as it was temperature reversible within a range compatible with the capabilities of the instrument, and it formed a clear gel. However, the solvent initially used, chloroform, was too volatile to allow for imaging in a droplet as the sample chamber is not sealed and the solvent would evaporate as the gel was heated to disassemble. Several solvents were tested to find a gel which was still clear but with a less volatile solvent, however, only very hazardous solvents (bromoform, toluene and tetrachloroethane) were found to gel and the kinetics were very slow. The gels formed between 24 and 48 hours after mixing the solution although they stayed stable and clear for over a week and were still temperature reversible after this time. The gels were found to have a T_{gel} of approximately 40 °C.

As it would be too hazardous to heat this sample and run it for several hours outside of a fume hood (as in the droplet method in section 2.1.2), *ex situ* heat cycles were run to test the temperature reversibility of the gel according to the method in section 2.1-*ex situ*. The gel was heated to 45 °C instead of 30 °C during

each cycle, as it was seen to have a higher T_{gel}. Due to the very slow kinetics of this gel, it remained liquid during the entire process. However, a physical structure was seen by AFM after each heat cycle.

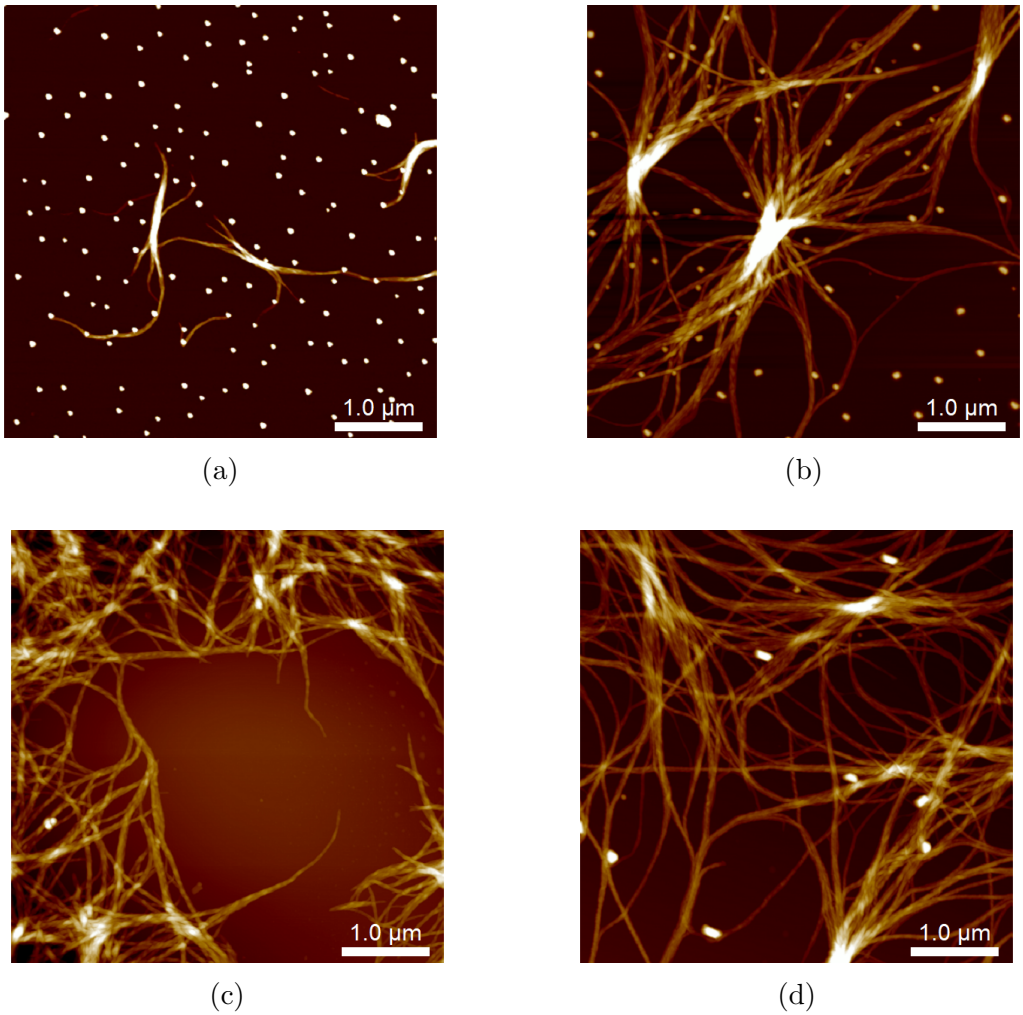

(a) (b)

(c) (d)

Figure 4.11: AFM topography images of N,N'-bis-[di-CBZ-L-Lyz]-ethylenediamine (1 % w/v) formed in the presence of bromoform as solvent after the first (a and b) second (c and d) heat cycle to disassemble the gel. Fibre assembly is observed in both heat cycles with the addition of small structures which are likely crystallisation of the gelator. The round structures seen are likely residual solvent which has formed droplets on the hydrophilic mica substrate.

The gel network was not seen to change after three heat cycles as can be seen in Figures 4.11 to 4.12. The fibres were always seen to be longer than 5 μm and highly curved with little to no cross-linking or branching. The bundles ranged in diameter from approximately 10 nm to 80 nm and the smallest fibres measured were 4 nm, however, these may not be a single fibre.

An ordered structure was seen in some of the bundles which might suggest a

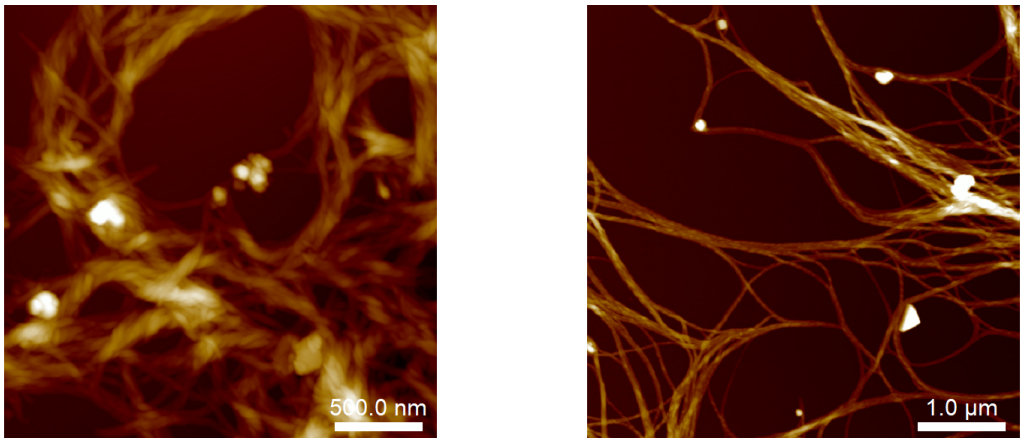

(a) (b)

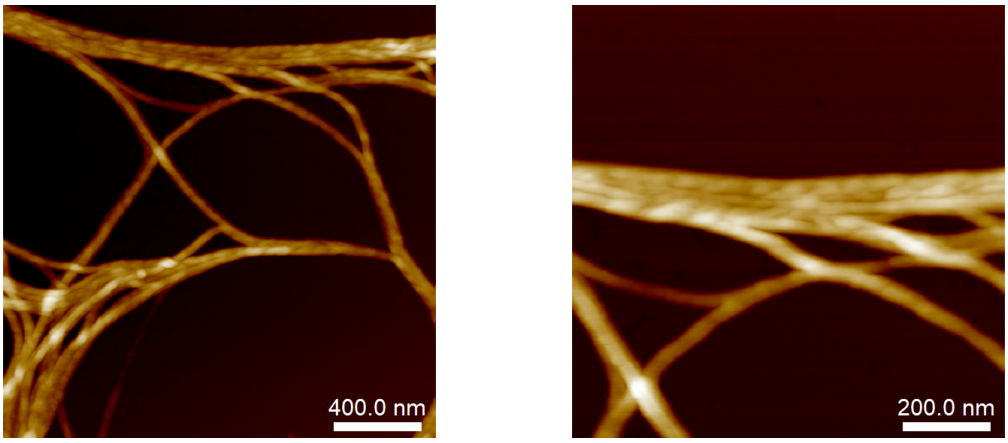

(c) (d)

Figure 4.12: AFM topography images of N,N'-bis-[di-CBZ-L-Lyz]-ethylenediamine (1 % w/v) formed in the presence of bromoform as solvent after the third heat cycle to disassemble the gel. Fibre assembly is still observed with the addition of small structures which are likely crystallisation of the gelator. Figures (c) and (d) show sections of the fibres with an ordered bundling structure.

helical bundling of fibres. This was further investigated by reducing the scan size to 2 μm and then 1 μm, these images are shown in Figure 4.12c and 4.12d. The height difference between the structures seen was measured to be approximately 1.2 - 2 nm which could indicate the individual fibres have diameters in this range. A fibre diameter in this range is to be expected as the gel is clear and so it does not have particles large enough to scatter light. The helices do appear to all be in a right handed direction which is consistent with the chiral nature of the molecule.

4.2.4 Conclusion

The Fmoc-GFFRGD gel was initially seen as a promising candidate for the *in situ* AFM method. However, the buffer exerted large adhesion forces on the tip, which were too large to image through. It may be possible to image the assembly of this gel if the solvent used was water with a buffer and $CaCl_2$ which has been shown to form a gel.

The N,N'-bis-[di-CBZ-L-Lys]-ethylenediamine gel was imaged *ex situ* after three heat cycles showing a similar fibrous structure was observed after each cycle. The gel was not seen to form macroscopically (by vial inversion) after each heat cycle, however, this was expected as it had been observed to have very slow kinetics. This temperature reversibility could be taken advantage of to image the gel's assembly and disassembly *in situ*. However, this was not conducted as a non-hazardous solvent would need to be found or an AFM with a closed liquid cell used to reduce the hazards in conducting the experiments. Further imaging is required to investigate the ordered bundling of the fibres which may be forming helical structures.

4.3 Characterisation of Gel Assembly by PeakForce Quantitative Nanomechanical Mapping

4.3.1 Introduction

Gel properties are often analysed using rheometry to show the strength and breaking point of the gel, as discussed in section 1.2. However, this technique does not allow for imaging of the gel network during the process which makes it impossible to link a change in the properties with a change in the gel structure. The ability to show the change in these properties simultaneously may allow for a greater understanding of gelation and the ability to target make gels.

PeakForce Quantitative Nanomechanical Mapping (PeakForce QNM) is an AFM mode similar to intermittent contact mode. In this mode, the tip approaches the sample, snaps into contact, presses down to a user defined peak force and then pulls off the sample. It then continues this motion on each data point on the sample. Figure 4.13 shows one full cycle of the AFM tip in this mode. A major positive factor in the use of this mode for the imaging of gels is the ability for the user to control the force applied to the sample. As gel networks are very soft structures, particularly during the initial stages of assembly, very low forces can be used so as not to damage the sample. These forces are generally less than a nanonewton.

Provided the physical properties of the AFM tip (i.e. cantilever spring constant, cantilever deflection sensitivity and tip radius) are known, the repulsion or attraction of the tip during different parts of this cycle allows the instrument to quantitatively measure nanomechanical properties. The AFM tip is quantified prior to imaging by measuring it's spring constant and the radius and shape of the tip. Then the interactions with the sample can be quantitatively measured. Some of the properties it is capable of measuring are adhesion, modulus and deformation. These properties are recorded for each data point across an image and can

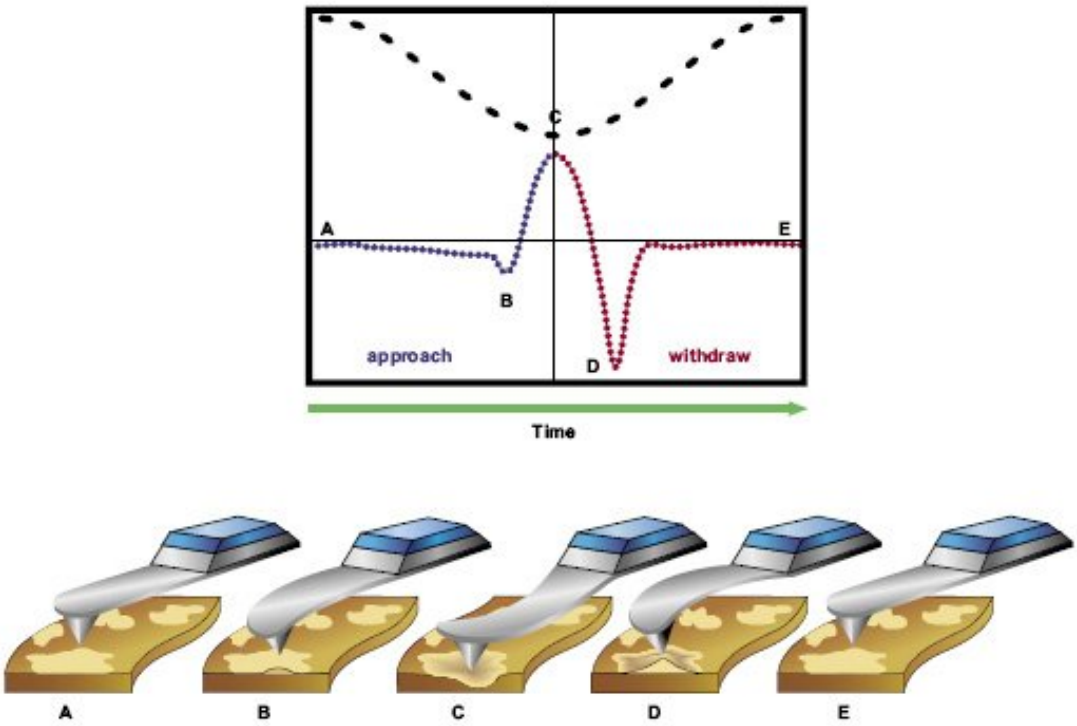

Figure 4.13: Schematic of the force applied to an AFM tip across one full data point in PeakForce Quantitative Nanomechanical Mapping mode.

then be viewed as a colour scale image or extracted as numerical values.

There is a large difference to be considered in comparing the modulus measured by rheometry and by AFM which is the directionality. In these AFM measurements, the transverse modulus is likely to dominate the measurements. This has previously been studied by Choy et al with drawn polyethelene mats using laser-generated ultrasonic pulses.[118] In these modern materials, strips of gel are patterned on to a surface with high aspect ratios to form "tapes" which give different properties to surface completely covered in the gel, such as high strength in one direction. In addition, the method captures qualitative data showing the strength of the gel across its assembly and disassembly process.

Imaging the assembly of a gel, in PeakForce QNM mode, during assembly could show the changes in the properties of the fibres as the network grows. However, it is only possible to follow this while the gel has at least partially formed as fibres would need to be present to be imaged. It has previously been shown that many gels have fibres present while they are still liquid so this could follow quite a large

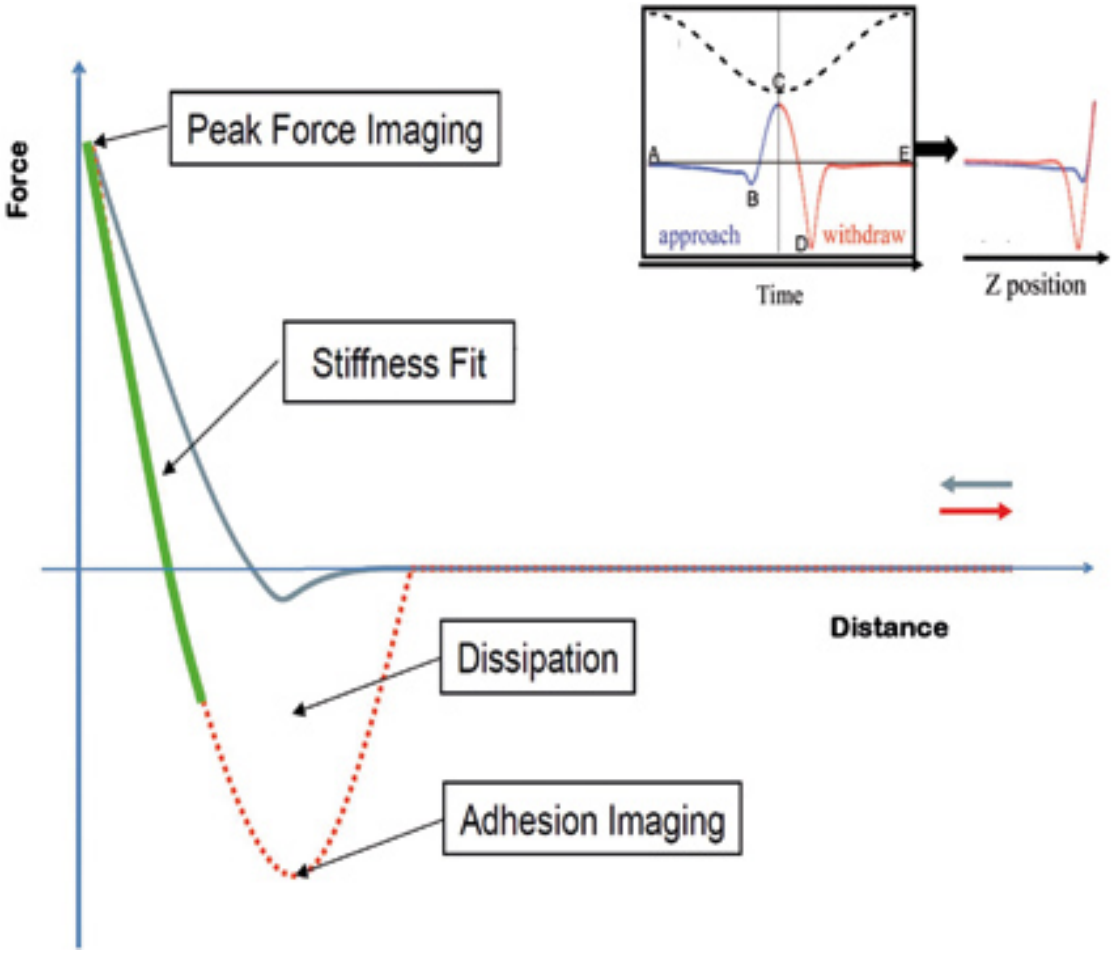

Figure 4.14: Schematic showing the force applied by an AFM tip during one full cycle and how this relates to the nanomechanical properties that can be analysed.

range of the stages of assembly of the gel. It is also important only to take the data points which are on the fibres and not the substrate as if an average was taken across an entire image, the data points on the substrate would skew the results.

4.3.2 Methodology

First, a MATLAB code was written to process the results collected from the *in situ* imaging of the samples. This code was written to allow the user to pick which data points were on fibres by choosing only points above a certain height and selecting them in a matrix which corresponds to the image. Then, when analysing channels relating to the properties of the sample, only these data points would be used and an average would be calculated across these points. This allows the user to quickly calculate an average value for properties such as deformation without needing to individually measure points on the images.

The code would then run this for all images within a run and export these values to a table. The measurements across one image could be thousands of data points so this makes this method possible where it previously would have been too time consuming or only a few data points could be taken.

The samples would be run according to the method reported in section 2.1.2.

4.3.3 Results and Discussion

Initially, the proline calix[4]arene (27 mM) gel with $MgCl_2$ (17 mM) was analysed as the parameters to image this gel *in situ* by this method were already known. Previously, this gel had been imaged at 3.92 Hz and 256 points per line across a 5 µm image with the temperature being raised one degree per image. This allowed for images to be captured within a few minutes which allowed the assembly to be analysed fully without missing stages. However, when the data was first analysed using the MATLAB code, it was found that this resolution was too low. The standard deviation of the data points used was very high in comparison to the values calculated. This is most likely because the data points were falling partly on the fibres and partly on the substrate so while the height might have been large

enough to include the data point, the other measurements made were not only of the fibres. The Derjaguin-Muller-Toporov (DMT) moduli recorded for the fibres across the initial assembly and a heat and cool cycle are shown in tables 4.1 - 4.2 for two separate experiments.

While a large difference was seen in the moduli recorded between the different experiments, they both show the same trend. The modulus increases as the temperature increases and does not return to a lower value when the gel is cooled. This matches previous data recorded for this gel by rheometry which showed the gel strengthening across multiple heat and cool cycles, as discussed in section 3.3.1.2. This increase in modulus can be seen in Figures 4.15 and 4.16. The deformation was also seen to decrease with heating which corresponds with the fibres becoming stiffer. The data recorded for height, adhesion and deformation can be found in Appendix A.4.

Table 4.1: Moduli of gel fibres calculated using the Nanoscope MATLAB Utility toolbox from Bruker for a gel of proline calix[4]arene and (27mM) $MgCl_2$ (17mM) over a single heat and cool cycle. Measured using the PeakForce Quantitative Nanomechanical Mapping mode of Atomic Force Microscopy

T (°C)	DMT Modulus (MPa)	Standard Deviation (MPa)
19.0	12.1936	2.5007
20.6	11.3462	1.4746
22.9	4.2854	1.2414
24.6	4.4955	1.0036
26.7	3.7001	1.4459
27.0	17.1698	4.4153
27.0	18.9187	4.8893
27.8	15.1924	5.3797
28.8	18.3400	5.5375
29.8	21.1520	3.0111
30.8 - 31.9 - 27.2	no fibres observed	
26.2	31.8444	4.4585
25.2	32.6142	2.6117
24.2	31.2079	3.0394
23.3	31.3296	3.5479
21.9	30.9752	3.5598
21.2	25.1457	4.8450
20.3	16.9639	4.2992

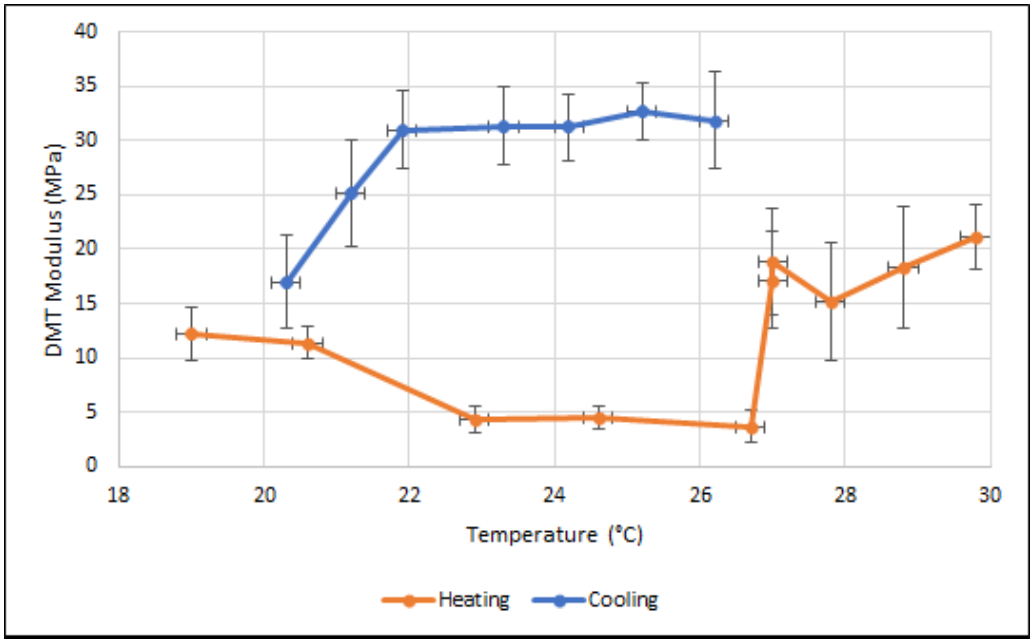

Figure 4.15: Plot of the data in Table 4.1 showing the change in DMT modulus with temperature over a single heat and cool cycle of a proline calix[4]arene (27mM) $MgCl_2$ (17mM) gel.

Table 4.2: Moduli of gel fibres calculated using the Nanoscope MATLAB Utility toolbox from Bruker for a gel of proline calix[4]arene and $MgCl_2$ (17mM) over a single heat and cool cycle. Measured using the PeakForce Quantitative Nanomechanical Mapping mode of Atomic Force Microscopy

T (°C)	DMT Modulus (MPa)	Standard Deviation (MPa)
22.3	0.4472	0.1053
21.4	0.5811	0.1585
20.6	0.4506	0.1369
20.8	0.2984	0.1050
23.7	0.5962	0.1179
24.7	0.6423	0.0963
25.7 - 30 - 23.3	no fibres observed	
22.1	1.9827	0.2067
21.3	1.5132	0.5702
20.4	1.4612	0.2711

To combat the high standard deviation of values, the resolution needed to be increased. As the fibres had been shown to be approximately 0.7 nm in diameter and the pixel size captured (or resolution) in this initial test was 20 nm, it is easy to see that the resolution was not in the range required. The points per line would need to be increased to at least 1024, which would still give a pixel size of 4.9

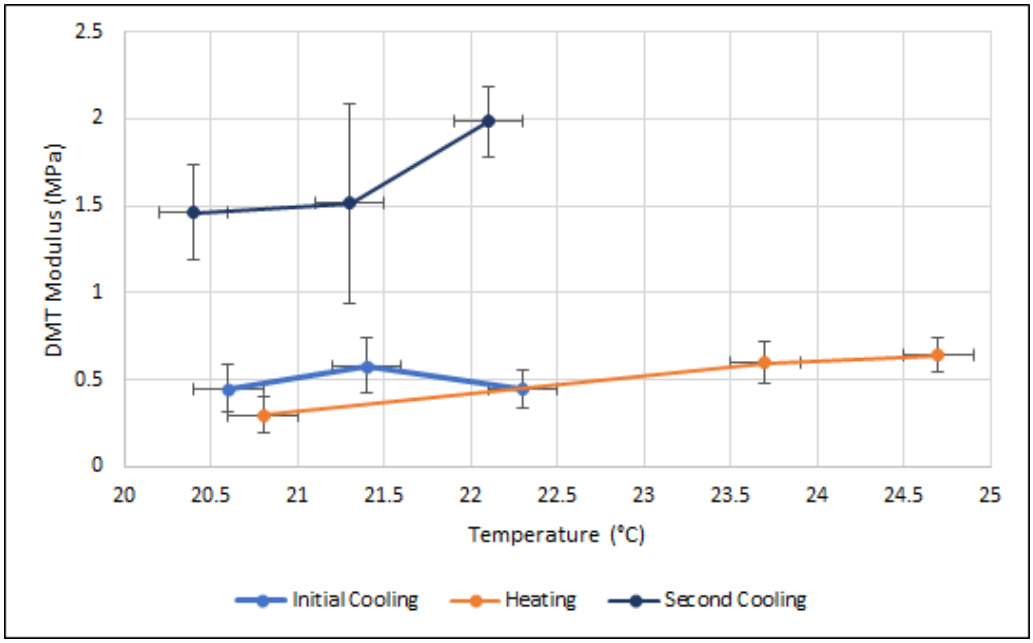

Figure 4.16: Plot of the data in Table 4.2 showing the change in DMT modulus with temperature over a single heat and cool cycle of a proline calix[4]arene (27mM) $MgCl_2$ (17mM) gel.

nm. However, the method is also limited by the scan speed as the instrument may duplicate data points if the scan speed and number of points per line are too high. However, reducing the scan speed and increasing the points per line would greatly increase the time taken to capture an image which may miss stages of the assembly so this would need to be balanced to allow the correct data to be captured. The method may also be limited by the radius of the tip as it may not be able to interact with a small enough area to only record data from the fibres and not the substrate.

While these large standard deviation values were seen, the average values calculated for the points on the fibres were seen to be in agreement with what was measured in Nanoscope Analysis using the Particle Analysis function. A typical image showing the four channels analysed can be seen in Figure 4.17, showing topography, DMT modulus, deformation and adhesion. The histograms of the points on the fibres for these channels is shown in Figure 4.18 for the corresponding image in the previous figure. The red dotted line/peak on the histograms shows the value calculated by the MATLAB toolbox for this image which falls towards the centre of the histogram, indicating a reasonable value has been found.

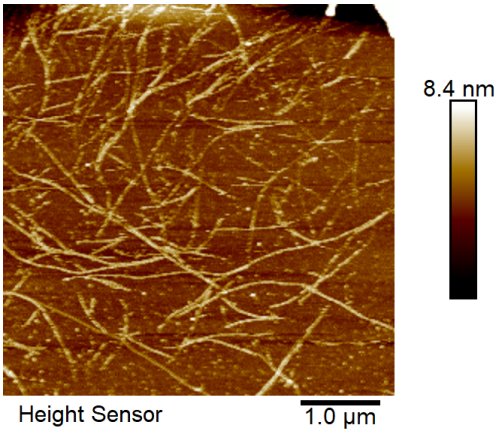

(a) Topography

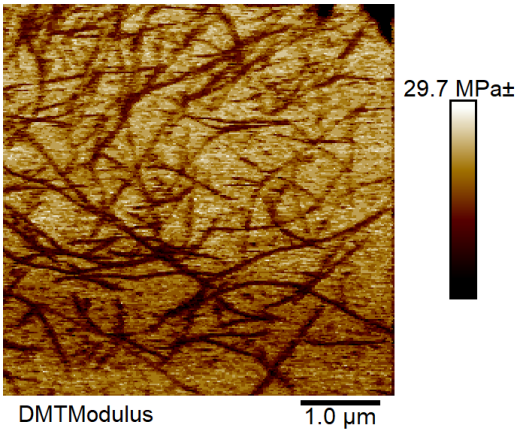

(b) DMT Modulus

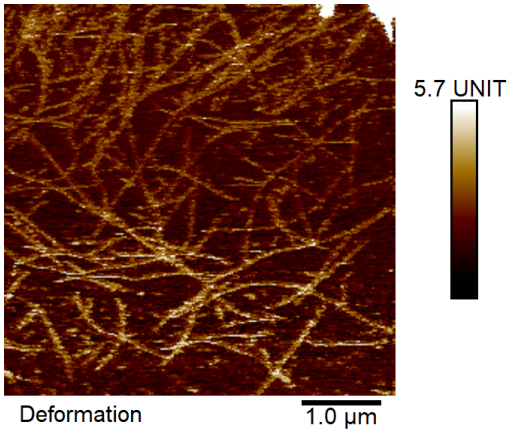

(c) Deformation

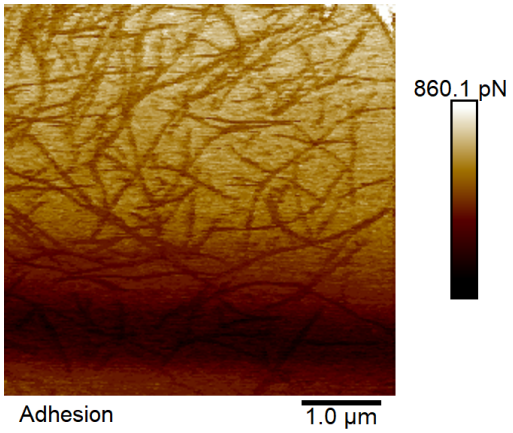

(d) Adhesion

Figure 4.17: AFM images from the four channels of proline calix[4]arene (27 mM) gel fibres with $MgCl_2$ (17 mM) electrolyte at 21.2 °C.

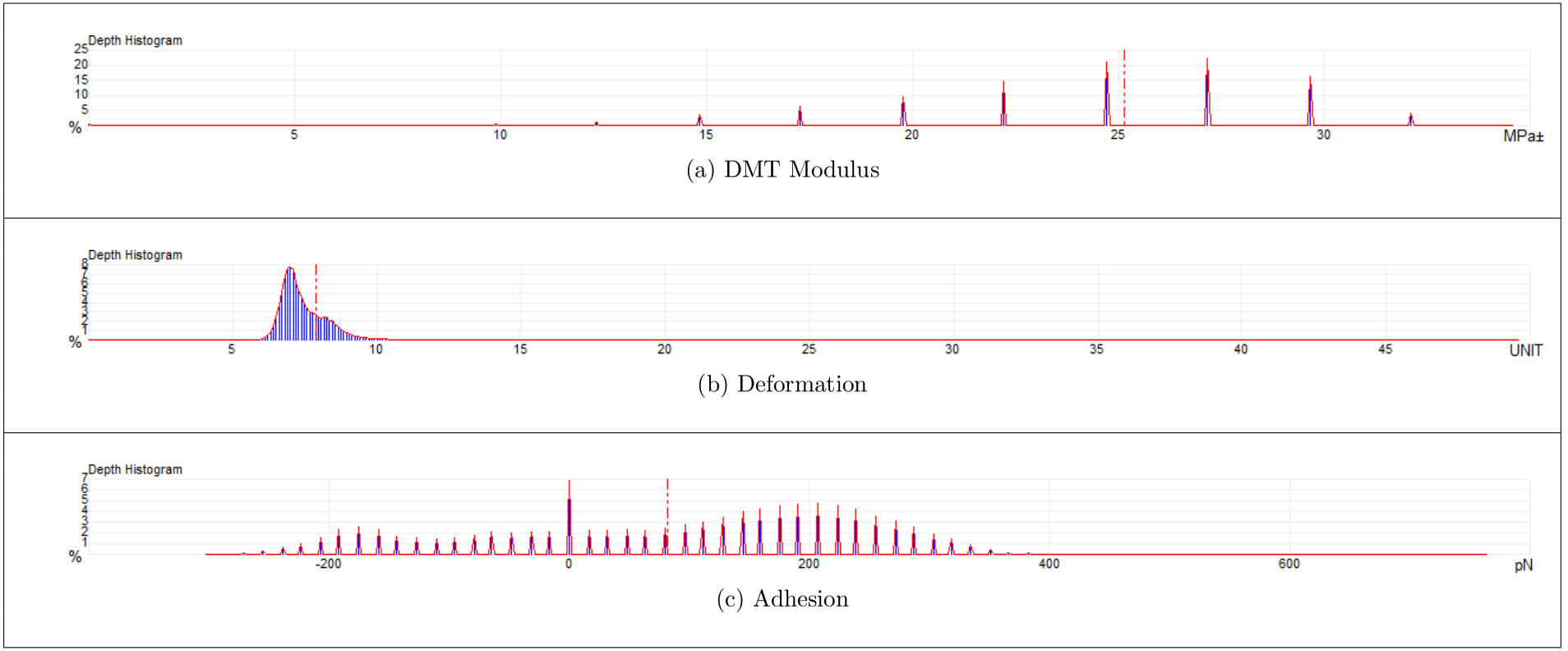

(a) DMT Modulus

(b) Deformation

(c) Adhesion

Figure 4.18: Histograms from the Particle Analysis feature of NanoScope Analysis for DMT modulus, deformation and adhesion corresponding to the images in Figure 4.17. The red dotted line indicates the value calculated the physical properties for this image using the Nanoscope MATLAB Utility Toolbox.

4.3.4 Conclusion

Imaging the assembly and disassembly process of proline calix[4]arene by PeakForce QNM was possible, however, the resolution used was found to be too low for the properties of the gel fibres to be analysed as the data was convoluted by that of the substrate. While the standard deviation was very high in comparison to the values calculated, the DMT modulus showed a trend which had been recorded for this gel by rheometry. The deformation also showed a decrease across the experiment which corresponds to the increase in modulus. The resolution is easily increased by increasing the points per line on each image but this will slow down the imaging and may result in the assembly being missed. The temperature increments per image could be reduced to try to slow the assembly down but it is likely that the assembly is triggered at a certain temperature and will occur quite quickly after this temperature is reached.

Chapter 5

Conclusions and Future Work

5.1 Conclusions

The objective of this project was to further characterise gelation through the use of AFM. This was achieved by building on prior work at Curtin University in the development of an *in situ* AFM method. This method was used to analyse the annealing of proline calix[4]arene gels with magnesium chloride along with complementary methods, rheometry, Small Angle Neutron Scattering (SANS) and *ex situ* AFM. The AFM imaging showed the straightening of fibres with each assembly and disassembly cycle of the gel network as well as the production of larger structures which were likely crystallisation of the gelator or bundles of fibres. The rheometry showed the gel continued to strengthen and become more brittle with each cycle and the SANS analysis showed the fibres disassembling and reassembling with the same length and radius but a much longer Kuhn length which indicates the straightening of the fibres. None of this could be seen macroscopically, in a vial, when this gel was heated and cooled. The gel was seen to melt and reform as a transparent gel each time. In comparison, a proline calix[4]arene gel made in the presence of lithium chloride was seen to be completely reversible by all three methods with similar results being observed after each heating and cooling cycle.

Increasing the concentration of the proline calix[4]arene gel to concentrations used in the initial experiments with these gels in 2008 showed the formation of

helical structures by *ex situ* AFM when formed with the lithium chloride electrolyte. These structures could not be analysed using the *in situ* method as the gel was too strong to allow imaging within the droplet due to the forces on the tip cantilever. To gain a better understanding of these structures, the gel was made with the opposite enantiomer (D-proline calix[4]arene instead of L-proline calix[4]arene) and shown to form left handed instead of right handed helical structures. This gel was further analysed using Time-of-Flight (TOF) SANS to observe the building of these structures in the bulk of the gel as it was not possible by *in situ* AFM. A polydisperse system was seen and this indicates that fibres are assembling individually before entwining to form the helices.

As the developed *in situ* AFM method was only applicable to clear gels, attempts were made to image the assembly process of gels in a thin film so that opaque gels could also be studied. The disassembly was never successfully imaged as the solvent would evaporate when the gel was heated. The gels were often imaged *in situ* which would reduce the artefacts of drying a gel, however, the assembly process could not be imaged.

Two novel peptide gels, Fluorenylmethyloxycarbonyl-Gly-Phe-Phe-Arg-Gly-Asp (GFFRGD) and N,N'-bis-[di-CBZ-L-Lys]-ethylenediamine were imaged by *ex situ* AFM. It was found that the Fmoc GFFRGD gel could not be imaged *in situ* when formed in Dulbecco's Modified Eagle Media (DMEM) as the solvent was too viscous to allow the AFM cantilever to oscillate easily. This meant large peak forces were necessary which would damage the fibre network. The N,N'-bis-[di-CBZ-L-Lys]-ethylenediamine gels were imaged for the first time, possibly showing a helical structure. This gel was not imaged *in situ* due to the hazardous solvents which it was found to gel and the open set up of the experiments.

A MATLAB script was developed to analyse the average physical properties of the gel network during assembly and disassembly. These properties were collected during *in situ* AFM imaging in PeakForce Quantitative Nanomechanical Mapping mode. The script would analyse only the points on the fibres and collate the data to find an average value for properties like Young's Modulus within a single image.

These values were found to have a large uncertainty when collated from previous experiments. This is likely due to either the resolution of the imaging, allowing contribution to the data points from the substrate, or the experiment being run too quickly, with fibres of varying properties being present at each time period.

5.2 Further Work

Several parts of this research could be extended with the use of an Atomic Force Microscope that is equipped with a closed cell for experiments. This may make the thin film work possible as the film is unlikely to evaporate during heating. These experiments may also be possible if a solvent with a much higher boiling point than the T_{gel} were used. The experiments in this work used gels with a T_{gel} with the range of 30 to 40 °C in water so the difference between these values would need to be very large. There was also seen to be a large hysteresis between the proline calix[4]arene gels macroscopically melting and the gel fibres disassembling which indicates the film is no longer a hard gel when fibres are still being imaged. Gels which have a large difference (100 °C and over) between the T_{gel} and the solvent boiling point and show a similar disassembly temperature in a vial as when imaged by AFM are more likely to be amenable to this method. These experiments may also be possible if stimuli other than temperature was used.

Imaging of the N,N'-bis-[di-CBZ-L-Lys]-ethylenediamine would also benefit from the use of a closed cell instrument. This would allow the *in situ* imaging of this gel by AFM in the solvents it has already been found to gel. Further investigation into this novel gel may also reveal solvents which are less hazardous and allow the experiment to be run in the open lab. With more time, the helical structure of this gel could also be investigated. At the time of this work, the other enantiomer of the molecule had not been studied and time was not taken to image the structures during the initial imaging of the gels. Understanding of this structure may lead to conclusions regarding the slow formation time of this gel. Further imaging of the helical structure formed by the proline calix[4]arene gel with lithium chloride could also be conducted to show in greater detail how these

fibres interact to entwine. Decreasing the scan size and increasing the resolution of the scans could in theory show the molecular structure of the fibres and how they interact with each other.

With more time the Fmoc GFFRGD gel could possibly be imaged by the current *in situ* method when formed in water with a buffer and a calcium chloride electrolyte. This will show the assembly process of this gel, however, this gel is mostly applied in cell culture which requires the use of the DMEM solvent and this may change the structure of the gel network.

Further imaging is required to test the usefulness of the MATLAB script in defining a gel by the nanoscale physical properties of its gel network. The *in situ* AFM experiments should be run with a higher resolution to ensure the values recorded are only for the fibres. The experiments used to test the script used a resolution of approximately 20 nm which is much too large given the diameter of the fibres is less than 1 nm. The resolution would need to be increased to be in line with the diameter of the fibres and the temperature gradient slowed to allow the entire assembly process to be imaged. In previous experiments, 2 °C per scan was used, this would likely need to be decreased in direct correlation with the increase in resolution of the image, or the scan time.

While the method to analyse the physical properties by PeakForce Quantitative Nanomechanical Mapping did show agreement with the rheology data, the results were not consistent quantitatively from experiment to experiment. Further testing of this method is required to ensure the results collated are correct. While the measurements agreed with what was seen in Nanoscope Analysis, a large standard deviation was recorded for all measurements (10 % to 400 % of the values). Imaging with a higher resolution is likely to solve this as the data recorded will only be from the fibre and not from the surrounding area or the substrate.

References

[1] P J Flory. Introductory lecture. *Faraday Discussions of the Chemical Society*, 57:7–18, 1974.

[2] M Brückner-Gühmann, M Banovic, and S Drusch. Towards an increased plant protein intake: Rheological properties, sensory perception and consumer acceptability of lactic acid fermented, oat-based gels. *Food Hydrocolloids*, 96(11):201–208, 2019.

[3] J Chen, T Mu, D Goffin, C Blecker, G Richard, A Richel, and E Haubruge. Application of soy protein isolate and hydrocolloids based mixtures as promising food material in 3D food printing. *Journal of Food Engineering*, 261(11):76–86, 2019.

[4] K E Uhrich, S M Cannizzaro, R S Langer, and K M Shakesheff. Polymeric systems for controlled drug release. *Chemical Reviews*, 99(11):3181–98, 1999.

[5] C C Peng and A Chauhan. Ion transport in silicone hydrogel contact lenses. *Journal of Membrane Science*, 399-400:95–105, 2012.

[6] B Hu, Q Chen, Q Cai, Y Fan, P J Wilde, Z Rong, and X Zeng. Gelation of soybean protein and polysaccharides delays digestion. *Food Chemistry*, 221:1598–1605, 2017.

[7] H Tian, C Buckley, M Paskevicius, and D Sheppard. Acetic acid catalysed carbon xerogels derived from resorcinolfurfural for hydrogen storage. *International Journal of Hydrogen Energy*, 36(1):671–679, 2011.

[8] T Graham. Liquid Diffusion Applied to Analysis. *Philosophical Transactions of the Royal Society of London*, 151:183–224, 1861.

[9] C Y Goh. *Amino acid functionalised calixarenes: crystal growth modifiers and low molecular weight gelators*. PhD thesis, Curtin University, 2012.

[10] R G Weiss and P Terech. *Molecular gels: Materials with self-assembled fibrillar networks*. Springer, Netherlands, 2006.

[11] R C Huber, A S Ferreira, J C Aguirre, D Kilbride, D B Toso, K Mayoral, Z H Zhou, N Kopidakis, Y Rubin, B J Schwartz, T G Mason, and S H Tolbert. Structure and Conductivity of Semiconducting Polymer Hydrogels. *Journal of Physical Chemistry B*, 120(26):6215–6224, 2016.

[12] P R A Chivers and D K Smith. Shaping and structuring supramolecular gels. *Nature Reviews Materials*, 4(7):463–478, 2019.

[13] M Itoh, M Kuroda, Y Okawa, H Kobayashi, T Ohno, T Tani, and H Haruta. The Effect of Thermal History on the Gelation of Gelatin Solutions. *The Journal of Photographic Science*, 40(5-6):184–186, 2016.

[14] T Funami, M Hiroe, S Noda, I Asai, S Ikeda, and K Nishinari. Influence of molecular structure imaged with atomic force microscopy on the rheological behavior of carrageenan aqueous systems in the presence or absence of cations. *Food Hydrocolloids*, 21(4):617–629, 2007.

[15] E R Draper and D J Adams. Low-Molecular-Weight Gels: The State of the Art. *Chem*, 3(3):390–410, 2017.

[16] D R Griffin, W M Weaver, P O Scumpia, D Di Carlo, and T Segura. Accelerated wound healing by injectable microporous gel scaffolds assembled from annealed building blocks. *Nature Materials*, 14(7):737–744, 2015.

[17] C M Rubert Perez, L A Rank, and J Chmielewski. Tuning the thermosensitive properties of hybrid collagen peptide-polymer hydrogels. *Chemical Communications*, 50(60):8174–8176, 2014.

[18] Y Onuki, N Hasegawa, C Kida, Y Obata, and K Takayama. Study of the Contribution of the State of Water to the Gel Properties of a Photocrosslinked Polyacrylic Acid Hydrogel using Magnetic Resonance Imaging. *Journal of Pharmaceutical Sciences*, 103(11):3532–3541, 2014.

[19] T Nakanishi. *Supramolecular soft matter : applications in materials and organic electronics*. Wiley, Hoboken, N.J, 2011.

[20] J L Figueiredo. Carbon gels with tuned properties for catalysis and energy storage. *Journal of Sol-Gel Science and Technology*, 89(1):12–20, 2018.

[21] F Barzegar, J K Dangbegnon, A Bello, D Y Momodu, A T C Johnson, and N Manyala. Effect of conductive additives to gel electrolytes on activated carbon-based supercapacitors. *AIP Advances*, 5(9):097171–097179, 2015.

[22] J A Foster, R M Edkins, G J Cameron, N Colgin, K Fucke, S Ridgeway, A G Crawford, T B Marder, A Beeby, S L Cobb, and J W Steed. Blending gelators to tune gel structure and probe anion-induced disassembly. *Chemistry - A European Journal*, 20(1):279–291, 2014.

[23] D Ma, L M Zhang, X Xie, T Liu, and M Q Xie. Tunable supramolecular hydrogel for in situ encapsulation and sustained release of bioactive lysozyme. *Journal of Colloid and Interface Science*, 359(2):399–406, 2011.

[24] P Terech and R G Weiss. Low Molecular Mass Gelators of Organic Liquids and the Properties of Their Gels. *Chemical Reviews*, 97(97):3133–3160, 1997.

[25] H Asai, K Nishi, T Hiroi, K Fujii, T Sakai, and M Shibayama. Gelation process of Tetra-PEG ion-gel investigated by time-resolved dynamic light scattering. *Polymer*, 54(3):1160–1166, 2013.

[26] J W Steed. Supramolecular gel chemistry: developments over the last decade. *Chemical communications*, 47(5):1379–1383, 2011.

[27] Å Östlund, D Bernin, L Nordstierna, and M Nydén. Chemical shift imaging NMR to track gel formation. *Journal of Colloid and Interface Science*, 344(1):238–240, 2010.

[28] O Daniela, W Lizhe, B André, M Edmond, and M A E Auty. Characterization β-lactoglobulin fibrillar assembly using atomic force microscopy polyacrylamide gel electrophoresis, and in situ fourier transform infrared spectroscopy. *Journal of Agricultural and Food Chemistry*, 58(6):3667–3673, 2010.

[29] A V Zhukhovitskiy, M Zhong, E G Keeler, V K Michaelis, J E P Sun, M J A Hore, D J Pochan, R G Griffin, A P Willard, and J A Johnson. Highly branched and loop-rich gels via formation of metal–organic cages linked by polymers. *Nature Chemistry*, 8(1):33–41, 2015.

[30] J Aalaie, E Vasheghani-Farahani, A Rahmatpour, and M A Semsarzadeh. Gelation rheology and water absorption behavior of semi-interpenetrating polymer networks of polyacrylamide and carboxymethyl cellulose. *Journal of Macromolecular Science, Part B: Physics*, 52(4):604–613, 2013.

[31] J Aalaie and M Youssefi. Study on the dynamic rheometry and swelling properties of the polyacrylamide/laponite nanocomposite hydrogels in electrolyte media. *Journal of Macromolecular Science, Part B: Physics*, 51(6):1027–1040, 2012.

[32] P J Cullen, C P O'Donnell, and M Houška. Rotational rheometry using complex geometries - A review. *Journal of Texture Studies*, 34(1):1–20, 2003.

[33] A J Davies. Loading errors in cone-plate rheometry. *Measurement Science and Technology*, 26(12):127001, 2015.

[34] Anton Paar GmbH. Basics of rheology. https://wiki.anton-paar.com/au-en/basics-of-rheology/ Last Accessed: 2020-08-21, 2020.

[35] Anton Paar GmbH. Frequency sweeps. https://wiki.anton-paar.com/en/frequency-sweeps/ Last Accessed: 2020-08-21, 2020.

[36] Anton Paar GmbH. Amplitude sweeps. https://wiki.anton-paar.com/en/amplitude-sweeps/ Last Accessed: 2020-08-21, 2020.

[37] A Franck. Viscoelasticity and dynamic mechanical testing. Technical report, TA Instruments, Germany.

[38] Iker Agirre-Olabide, Joanes Berasategui, Maria J. Elejabarrieta, and M. Mounir Bou-Ali. Characterization of the linear viscoelastic region of magnetorheological elastomers. *Journal of Intelligent Material Systems and Structures*, 2014.

[39] Y Wu, D Zhu, Z Guo, and Y Feng. Rheology and phase behavior of thermoreversible pentablock terpolymer hydrogel. *Journal of Polymer Science, Part B: Polymer Physics*, 51(18):1335–1342, 2013.

[40] A Nakagawa, F Steiniger, W Richter, A Koschella, T Heinze, and H Kamitakahara. Thermoresponsive hydrogel of diblock methylcellulose: Formation of ribbonlike supramolecular nanostructures by self-assembly. *Langmuir*, 28(34):12609–12618, 2012.

[41] L L E Mears, E R Draper, A M Castilla, H Su, Zhuola, B Dietrich, M C Nolan, G N Smith, J Doutch, S Rogers, R Akhtar, H Cui, and D J Adams. Drying Affects the Fiber Network in Low Molecular Weight Hydrogels. *Biomacromolecules*, 18(11):3531–3540, 2017.

[42] K Kozłowicz and F Kluza. Gel products properties influenced by freezing in different conditions. *International Journal of Refrigeration*, 35(6):1715–1721, 2012.

[43] L Ong, R R Dagastine, S E Kentish, and S L Gras. The Effect of Milk Processing on the Microstructure of the Milk Fat Globule and Rennet Induced Gel Observed Using Confocal Laser Scanning Microscopy. *Journal of Food Science*, 75(3):E135–E145, 2010.

[44] S Paterson, Y Casadio, D Brown, J Shaw, T Chirila, and M Baker. Laser Scanning Confocal Microscopy Versus Scanning Electron Microscopy for Characterization of Polymer Morphology: Sample Preparation Drastically Distorts

Morphologies of Poly(2-hydroxyethyl methacrylate)-Based Hydrogels. *Journal of Applied Polymer Science*, 127(6):4296–4304, 2013.

[45] R M P Da Silva, D Van Der Zwaag, L Albertazzi, S S Lee, E W Meijer, and S I Stupp. Super-resolution microscopy reveals structural diversity in molecular exchange among peptide amphiphile nanofibres. *Nature Communications*, 7(1):1–10, 2016.

[46] S Onogi, H Shigemitsu, T Yoshii, T Tanida, M Ikeda, R Kubota, and I Hamachi. In situ real-time imaging of self-sorted supramolecular nanofibres. *Nature Chemistry*, 8(8):743–752, 2016.

[47] H Cox, P Georgiades, H Xu, T A Waigh, and J R Lu. Self-Assembly of Mesoscopic Peptide Surfactant Fibrils Investigated by STORM Super-Resolution Fluorescence Microscopy. *Biomacromolecules*, 18(11):3481–3491, 2017.

[48] D A Higgins, J Kerimo, D A Vanden Bout, and P F Barbara. A molecular yarn: Near-field optical studies of self-assembled, flexible, fluorescent fibers. *Journal of the American Chemical Society*, 118(17):4049–4058, 1996.

[49] K S Birdi. Application of Scanning Tunnelling Microscopy [STM] & Atomic Force Microscopy [AFM] in Colloid & Surface Chemistry (Nanotechnology). *Journal of Dispersion Science and Technology*, 20(1-2):795–837, 1999.

[50] P Samorí, H Engelkamp, P De Witte, A E Rowan, R J M Nolte, and J P Rabe. Self-assembly and manipulation of crown ether phthalocyanines at the gel-graphite interface. *Angewandte Chemie - International Edition*, 40(12):2348–2350, 2001.

[51] G Binnig, C F Quate, and C Gerber. Atomic force microscope. *Physical Review Letters*, 56(9):930–933, 1986.

[52] Q Zhong, D Inniss, K Kjoller, and V B Elings. Fractured polymer/silica fiber surface studied by tapping mode atomic force microscopy. *Surface Science*, 290(1):L688–L692, 1993.

[53] A C Knall, S F Hoefler, M Hollauf, F Thaler, S Noesberger, I Hanzu, H Ehmann, M Hobisch, S Spirk, S Wen, R Yang, T Rath, and G Trimmel. Synthesis of a tetrazine–quaterthiophene copolymer and its optical, structural and photovoltaic properties. *Journal of Materials Science*, 54(13):10065–10076, 2019.

[54] W Wang, P Lu, Y Fan, L Tian, S Niu, J Zhao, and L Ren. A facile antifogging/frost-resistant coating with self-healing ability. *Chemical Engineering Journal*, 378(12):122173, 2019.

[55] T M Radić, V Svetličić, V Žutić, and B Boulgaropoulos. Seawater at the nanoscale: Marine gel imaged by atomic force microscopy. *Journal of Molecular Recognition*, 24(3):397–405, 2011.

[56] C Y Goh, T Becker, D H Brown, B W Skelton, F Jones, M Mocerino, and M I Ogden. Self-inclusion of proline-functionalised calix[4]arene leads to hydrogelation. *Chemical Communications*, 47(21):6057–6059, 2011.

[57] P H J Kouwer, M Koepf, V A A Le Sage, M Jaspers, A M van Buul, Z H Eksteen-Akeroyd, T Woltinge, E Schwartz, H J Kitto, R Hoogenboom, S J Picken, R J M Nolte, E Mendes, and A E Rowan. Responsive biomimetic networks from polyisocyanopeptide hydrogels. *Nature*, 493(7434):651–655, 2013.

[58] P Busch, D Posselt, D Smilgies, B Rheinländer, and F Kremer. Lamellar Diblock Copolymer Thin Films Investigated by Tapping Mode Atomic Force Microscopy: Molar-Mass Dependence of Surface Ordering. *Macromolecules*, 36(23):8717–8727, 2003.

[59] L Schefer, J Adamcik, and R Mezzenga. Unravelling secondary structure changes on individual anionic polysaccharide chains by atomic force microscopy. *Angewandte Chemie - International Edition*, 53(21):5376–5379, 2014.

[60] E R Draper, T O McDonald, and D J Adams. A low molecular weight hydrogel with unusual gel aging. *Chemical Communications*, 51(30):6595–6597, 2015.

[61] A M Gigler. *Dynamic Investigation of Polymeric Materials - Reproducible Data Aquisition and Profound Mechanical Analysis*. PhD thesis, Universität Ulm, 2006.

[62] K Xu, W Sun, Y Shao, F Wei, X Zhang, W Wang, and P Li. Recent development of PeakForce Tapping mode atomic force microscopy and its applications on nanoscience. *Nanotechnology Reviews*, 7(6):605–621, 2018.

[63] B Pittenger. PeakForce Tapping and ScanAsyst. https://www.bruker.com/service/education-training/webinars/afm.html Last Accessed: 2017-06-08, 2013.

[64] B Pittenger. Atomic Imaging with PeakForce Tapping. https://www.bruker.com/service/education-training/webinars/afm.html Last Accessed: 2017-06-08, 2012.

[65] F Rico, C Su, and S Scheuring. Mechanical mapping of single membrane proteins at submolecular resolution. *Nano Letters*, 11(9):3983–3986, 2011.

[66] I Medalsy, U Hensen, and D J Muller. Imaging and quantifying chemical and physical properties of native proteins at molecular resolution by force-volume AFM. *Angewandte Chemie - International Edition*, 50(50):12103–12108, 2011.

[67] V V Korolkov, S Allen, C J Roberts, and S J B Tendler. Green chemistry approach to surface decoration: Trimesic acid self-assembly on HOPG. *Journal of Physical Chemistry C*, 116(21):11519–11525, 2012.

[68] Heinrich Hertz. Über die Berüehrung fester elastischer Körper (On the Contact of Solid Elastic Bodies). *Journal für die reine und angewandte Mathematik (Journal for the pure and applied mathematics)*, 1881.

[69] K L Johnson, K Kendall, and A D Roberts. Surface energy and the contact of elastic solids. *Proceedings of the Royal Society of London. A. Mathematical and Physical Sciences*, 1971.

[70] B V Derjaguin, V M Muller, and Yu P Toporov. Effect of contact deformations on the adhesion of particles. *Journal of Colloid And Interface Science*, 1975.

[71] D Tabor. Surface forces and surface interactions. *Journal of Colloid And Interface Science*, 1977.

[72] D Maugis. Adhesion of spheres: The JKR-DMT transition using a dugdale model. *Journal of Colloid And Interface Science*, 1992.

[73] J F Waters, S Lee, and P R Guduru. Mechanics of axisymmetric wavy surface adhesion: JKR-DMT transition solution. *International Journal of Solids and Structures*, 2009.

[74] P Prokopovich and S Perni. Comparison of JKR- and DMT-based multi-asperity adhesion model: Theory and experiment. *Colloids and Surfaces A: Physicochemical and Engineering Aspects*, 2011.

[75] T J Young, M A Monclus, T L Burnett, W R Broughton, S L Ogin, and P A Smith. The use of the PeakForceTM quantitative nanomechanical mapping AFM-based method for high-resolution Young's modulus measurement of polymers. *Measurement Science and Technology*, 22(12):125703, 2011.

[76] E C Barker, C Y Goh, F Jones, M Mocerino, B W Skelton, T Becker, and M I Ogden. Investigating hydrogel formation using in situ variable-temperature scanning probe microscopy. *Chemical Science*, 6(11):6133–6138, 2015.

[77] P A Seeger and R P Hjelm. Small-angle neutron scattering at pulsed spallation sources. *Journal of Applied Crystallography*, 24(5):467–478, 1991.

[78] C D Dewhurst, I Grillo, D Honecker, M Bonnaud, M Jacques, C Amrouni, A Perillo-Marcone, G Manzin, and R Cubitt. The small-angle neutron scattering instrument D33 at the Institut Laue-Langevin. *Journal of Applied Crystallography*, 49(1):1–14, 2016.

[79] A Sokolova, A E Whitten, L De Campo, J Christoforidis, A Eltobaji, J Barnes, F Darmann, and A Berry. Performance and characteristics of the bilby timeof-

flight small-angle neutron scattering instrument. *Journal of Applied Crystallography*, 52(1):1–12, 2019.

[80] J W Steed. *Core concepts in supramolecular chemistry and nanochemistry*. Wiley, Chichester, England ; Hoboken, NJ, 2007.

[81] J A Sáez, B Escuder, and J F Miravet. Selective catechol- triggered supramolecular gel disassembly. *Chemical Communications*, 46(42):7996–7998, 2010.

[82] J Zhang, D S Guo, L H Wang, Z Wang, and Y Liu. Supramolecular binary hydrogels from calixarenes and amino acids and their entrapment-release of model dye molecules. *Soft Matter*, 7(5):1756–1762, 2011.

[83] J A Foster, M M Piepenbrock, G O Lloyd, N Clarke, J A K Howard, and J W Steed. Anion- switchable supramolecular gels for controlling pharmaceutical crystal growth. *Nature Chemistry*, 2(12):1037–1043, 2010.

[84] R G. Ellis-Behnke, Y X Liang, D K C Tay, P W F Kau, G E Schneider, S Zhang, W Wu, and W F So. Nano hemostat solution: immediate hemostasis at the nanoscale. *Nanomedicine*, 2(4):207–215, 2006.

[85] A D Martin, S W Chua, C G Au, H Stefen, M Przybyla, Y Lin, J Bertz, P Thordarson, T Fath, Y . Ke, and L M Ittner. Peptide Nanofiber Substrates for Long-Term Culturing of Primary Neurons. *ACS Applied Materials and Interfaces*, 10(30):25127–25134, 2018.

[86] J D Hartgerink, E Beniash, and S I Stupp. Self-assembly and mineralization of peptide-amphiphile nanofibers. *Science*, 294(5547):1684–1688, 2001.

[87] D K Smith. Supramolecular gels: Building bridges. *Nature Chemistry*, 2(3):162, 2010.

[88] D J Cornwell, B O Okesola, and D K Smith. Hybrid polymer and low molecular weight gels – dynamic two-component soft materials with both responsive and robust nanoscale networks. *Soft Matter*, 9(36):8730–8736, 2013.

[89] T Becker, C Y Goh, F Jones, M McIldowie, M Mocerino, and M Ogden. Proline-Functionalised Calix[4]arene: An Anion-Triggered Hydrogelator. *Chemical Communications*, 33:3900–3902, 2008.

[90] V Jayawarna, M Ali, T A Jowitt, A F Miller, A Saiani, J E Gough, and R V Ulijn. Nanostructured hydrogels for three-dimensional cell culture through self-assembly of fluorenylmethoxycarbonyl-dipeptides. *Advanced Materials*, 18(5):611–614, 2006.

[91] C Diaferia, M Ghosh, T Sibillano, E Gallo, M Stornaiuolo, C Giannini, G Morelli, L Adler-Abramovich, and A Accardo. Fmoc-FF and hexapeptide-based multicomponent hydrogels as scaffold materials. *Soft Matter*, 15(3):487–496, 2019.

[92] J K Gupta, D J Adams, and N G Berry. Will it gel? Successful computational prediction of peptide gelators using physicochemical properties and molecular fingerprints. *Chemical Science*, 7(7):4713–4719, 2016.

[93] A D Martin, J P Wojciechowski, E Y Du, A Rawal, H Stefen, C G Au, L Hou, C G Cranfield, T Fath, L M Ittner, and P Thordarson. Decoupling the effects of hydrophilic and hydrophobic moieties at the neuron-nanofibre interface. *Chemical Science*, 11(5):1375–1382, 2020.

[94] X Du, J Zhou, J Shi, and B Xu. Supramolecular Hydrogelators and Hydrogels: From Soft Matter to Molecular Biomaterials. *Chemical Reviews*, 115(24):13165–13307, 2015.

[95] A M Garcia, D Iglesias, E Parisi, K E Styan, L J Waddington, C Deganutti, R De Zorzi, M Grassi, M Melchionna, A V Vargiu, and S Marchesan. Chirality Effects on Peptide Self-Assembly Unraveled from Molecules to Materials. *Chem*, 4(8):1862–1876, 2018.

[96] K Basu, A Baral, S Basak, A Dehsorkhi, J Nanda, D Bhunia, S Ghosh, V Castelletto, I W Hamley, and A Banerjee. Peptide based hydrogels for cancer drug

release: Modulation of stiffness, drug release and proteolytic stability of hydrogels by incorporating d-amino acid residue(s). *Chemical Communications*, 52(28):5045–5048, 2016.

[97] J Mayr, C Saldías, and D Díaz Díaz. Release of small bioactive molecules from physical gels. *Chemical Society Reviews*, 47(4):1484–1515, 2018.

[98] A G Cheetham, R W Chakroun, W Ma, and H Cui. Self-assembling prodrugs. *Chemical Society Reviews*, 46(21):6638–6663, 2017.

[99] S Liu, L Zhang, J Cheng, Y Lu, and J Liu. Sustained release of hepatocyte growth factor by cationic self-assembling peptide/heparin hybrid hydrogel improves β-cell survival and function through modulating inflammatory response. *International Journal of Nanomedicine*, 11:4875–4890, 2016.

[100] R Roy and P Dastidar. Supramolecular Synthon Approach in Developing Anti-Inflammatory Topical Gels for In Vivo Self-Delivery. *Chemistry - A European Journal*, 23(62):15623–15627, 2017.

[101] R Parveen and P Dastidar. Supramolecular Gels by Design: Towards the Development of Topical Gels for Self-Delivery Application. *Chemistry - A European Journal*, 22(27):9257–9266, 2016.

[102] S Sathaye, A Mbi, C Sonmez, Y Chen, D L Blair, J P Schneider, and D J Pochan. Rheology of peptide- and protein-based physical hydrogels: Are everyday measurements just scratching the surface? *Wiley Interdisciplinary Reviews: Nanomedicine and Nanobiotechnology*, 7(1):34–68, 2015.

[103] D R Nisbet, T Y Wang, K F Bruggeman, J C Niclis, F A Somaa, V Penna, C P J Hunt, Y Wang, J A Kauhausen, R J Williams, L H Thompson, and C L Parish. Shear Containment of BDNF within Molecular Hydrogels Promotes Human Stem Cell Engraftment and Postinfarction Remodeling in Stroke. *Advanced Biosystems*, 2(9):1800113, 2018.

[104] F L Maclean, G M Ims, M K Horne, R J Williams, and D R Nisbet. A Programmed Anti-Inflammatory Nanoscaffold (PAIN) as a 3D Tool to Understand the Brain Injury Response. *Advanced Materials*, 30(50):1805209, 2018.

[105] J P Wojciechowski, A D Martin, E Y Du, C J Garvey, R E Nordon, and P Thordarson. Non-reversible heat-induced gelation of a biocompatible Fmoc-hexapeptide in water. *Nanoscale*, 12(15):8262–8267, 2020.

[106] Caitlin Duncan. Gelation of N,N'-bis-[di-CBZ-L-Lys]-ethylenediamine. Manuscript in preparation, 2019.

[107] B N Dorakumbura. *Fundamental Studies into the Chemical and Physical Properties of Latent Fingermarks*. PhD thesis, Curtin University, 2017.

[108] J Jiang and X Zhou. Bruker Dimension Icon AFM. https://mmrc.caltech.edu/AFM Dimension Icon/Icon-AFM Users Manual old.pdf Last Accessed: 2020-07-21, 2014.

[109] B Pittenger. Latest Innovations in PeakForce QNM and Other Advanced Force Spectroscopy Techniques. https://www.nanophys.kth.se/nanolab/afm/peak-force-calibr.pdf Last Accessed: 2020-07-21, 2015.

[110] Anton Paar GmbH. Modular Compact Rheometer: MCR 102/302/502. https://www.anton-paar.com/au-en/products/details/rheometer-mcr-102-302-502/ Last Accessed: 2020-08-28, 2020.

[111] C Kukla, I Duretek, J Gonzalez-Gutierrez, and C Holzer. Rheology of Highly Filled Polymers. In *Polymer Rheology*. IntechOpen, 2018.

[112] H Mcewen, E Y Du, J P Mata, P Thordarson, and A D Martin. Tuning hydrogels through metal-based gelation triggers. *Journal of Materials Chemistry B*, 5(47):9412–9417, 2017.

[113] N Osaka and K Hamamoto. Simultaneous stiffening, strengthening and toughening of poly(vinylidene fluoride)/propylene carbonate gels by thermal annealing near peak melting temperature. *Polymer*, 141:132–142, 2018.

[114] E C Barker, A D Martin, C J Garvey, C Y Goh, F Jones, M Mocerino, B W Skeleton, M I Ogden, and T Becker. Thermal annealing behaviour and gel to crystal transition of a low molecular weight hydrogelator. *Soft Matter*, 13(5):1006–1011, 2017.

[115] M Jaspers, M Dennison, M F J Mabesoone, F C MacKintosh, A E Rowan, and P H J Kouwer. Ultra-responsive soft matter from strain-stiffening hydrogels. *Nature Communications*, 5(1):5808, 2014.

[116] L Chen, T O McDonald, and D J Adams. Salt-induced hydrogels from functionalised-dipeptides. *RSC Advances*, 3(23):8714–8720, 2013.

[117] A D Martin, J P Wojciechowski, A B Robinson, C Heu, C J Garvey, J Ratcliffe, L J Waddington, J Gardiner, and P Thordarson. Controlling self-assembly of diphenylalanine peptides at high pH using heterocyclic capping groups. *Scientific Reports*, 7(1):43947, 2017.

[118] C. L. Choy, Y. W. Wong, G. W. Yang, and Tetsuo Kanamoto. Elastic modulus and thermal conductivity of ultradrawn polyethylene. *Journal of Polymer Science, Part B: Polymer Physics*, 1999.

Appendix A

Data

A.1 Small Angle Neutron Scattering Data for Section 3.3.1.3

Table A.1: Kuhn length and length measurements of fibres from SANS across one full temperature cycle.

	LiCl · **1**		$MgCl_2$ · **1**	
T (°C)	Kuhn Length (Å)	Length (Å)	Kuhn Length (Å)	Length (Å)
10	47 ± 1	Inf	40 ± 1	399 ± 1
15	80 ± 2	965 ± 35	60 ± 2	308 ± 5
20	60 ± 1	53 ± 1	260 ± 134	271 ± 58
25	37 ± 11	32 ± 1	175 ± 2	159 ± 2
30	38 ± 6	33 ± 1	48 ± 4	42 ± 3
25	49 ± 3	35 ± 1	44 ± 11	38 ± 1
20	39 ± 10	34 ± 1	42 ± 8	36 ± 1
15	48 ± 9	37 ± 1	237 ± 12	217 ± 20
10	78 ± 2	781 ± 18	228 ± 20	288 ± 20

Table A.2: Radii of fibres of $\mathbf{1} \cdot MgCl_2$ and $\mathbf{1} \cdot LiCl$ over the heat cycles, measured by small angle neutron scattering.

T (°C)	Radius ($\mathbf{1} \cdot MgCl_2$) (Å)	Radius ($\mathbf{1} \cdot LiCl$) (Å)
10	17.3 ± 0.2	8.5 ± 0.1
15	16.5 ± 0.1	9.6 ± 0.1
20	12.2 ± 0.1	8.1 ± 0.1
25	9.5 ± 0.1	8.2 ± 0.3
30	9.5 ± 0.2	7.5 ± 0.5
25	9.5 ± 0.2	8.1 ± 0.1
20	9.5 ± 0.2	8.5 ± 0.3
15	13.6 ± 0.1	8.5 ± 0.3
10	14.6 ± 0.1	11.2 ± 0.4

A.2 Small Angle Neutron Scattering Data for Section 3.3.2.2

Table A.3: Kuhn length and length measurements of fibres from SANS across one full temperature cycle.

T (°C)	Kuhn Length (Å)	Length (Å)	Radius (Å)
30-28	5.6 ± 1.1	21 ± 0.91	10 ± 0.028
28-26	17 ± 0.55	19 ± 0.47	10 ± 0.031
26-24	27 ± 0.14	17 ± 0.11	10 ± 0.018
24-22	27 ± 0.14	17 ± 0.11	10 ± 0.018
22-20	17 ± 0.69	18 ± 0.49	10 ± 0.031
20-18	27 ± 0.14	17 ± 0.11	11 ± 0.017
18-16	17 ± 0.66	18 ± 0.48	10 ± 0.03
16-14	110 ± 0.15	Inf	7.7 ± 0.010
14-12	90 ± 0.13	Inf	8.7 ± 0.011
12-10	89 ± 0.14	Inf	8.8 ± 0.011
10-12	88 ± 0.14	Inf	8.8 ± 0.011
12-14	89 ± 0.15	Inf	8.8 ± 0.011
14-16	88 ± 0.15	Inf	8.8 ± 0.011
16-18	88 ± 0.14	Inf	8.7 ± 0.011
18-20	89 ± 0.14	Inf	8.7 ± 0.011
20-22	46 ± 3.0	41 ± 0.15	8.8 ± 0.014
22-24	16 ± 0.30	32 ± 0.30	9.6 ± 0.025
24-26	27 ± 0.17	18 ± 0.12	10 ± 0.018
26-28	27 ± 0.17	18 ± 0.12	10 ± 0.018
28-30	17 ± 0.50	19 ± 0.46	10 ± 0.030

A.3 Optical Image of Mica Substrate With Gel Smear from Atomic Force Microscope

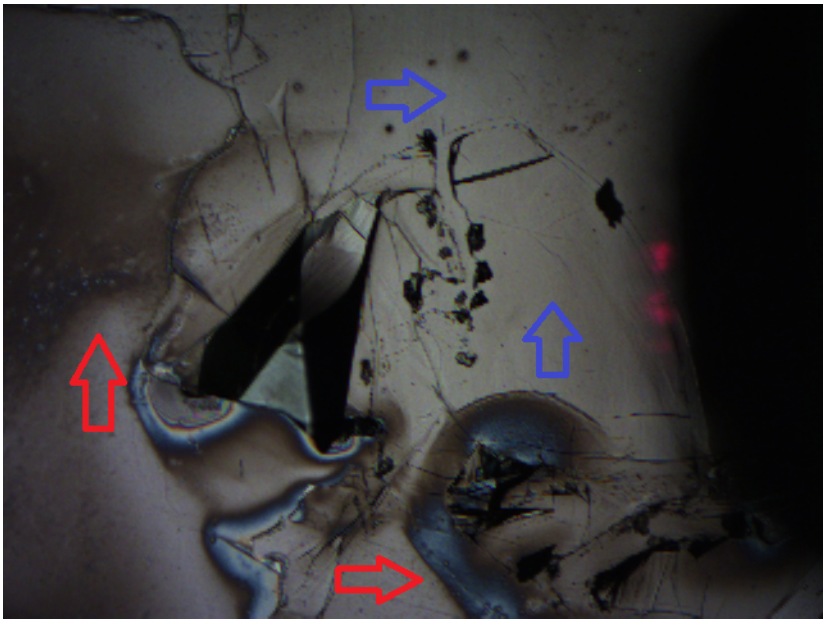

Figure A.1: Image taken with optical view of the Bruker Dimension FastScan instrument showing wetter (red) and drier areas (blue) of a gel smeared on mica.

A.4 Physical Properties of Proline Calix[4]arene Gel Fibres Calculated Using the NanoScope Matlab Utilities Toolbox

Table A.4: Physical Properties of gel fibres calculated using the Nanoscope Matlab Utility toolbox from Bruker for a **1** (27mM) · $MgCl_2$ (17mM) over a single heat and cool cycle. Measured using the PeakForce Quantitative Nanomechanical Mapping mode of Atomic Force Microscopy. All points above 0.5 nm were used to calculate the physical properties, this removes the points taken on the substrate. Error is standard deviation of measurements.

T (°C)	DMT Modulus (MPa)	Adhesion (nN)	Deformation (nm)	No. of Points
22.3	0.4472 ± 0.1053	-0.0922 ± 0.0321	42.1825 ± 4.9769	13599
21.4	0.5811 ± 0.1585	0.0562 ± 0.0593	34.8490 ± 5.5092	29964
20.6	0.4506 ± 0.1369	0.2533 ± 0.1596	38.3078 ± 9.5120	12292
20.8	0.2984 ± 0.1050	0.3966 ± 0.2089	44.1332 ± 15.6591	14198
23.7	0.5962 ± 0.1179	-0.6985 ± 0.1928	28.0165 ± 2.2224	8472
24.7	0.6423 ± 0.0963	-1.1370 ± 0.0997	40.1960 ± 40.1960	6515
25.7 - 30 - 23.3	no fibres observed			
22.1	1.9827 ± 0.2067	-0.0868 ± 0.0458	26.1758 ± 2.2678	5763
21.3	1.5132 ± 0.5702	0.0119 ± 0.0464	33.5799 ± 7.8402	8204
20.4	1.4612 ± 0.2711	0.0012 ± 0.1443	32.2473 ± 3.7868	29900

Table A.5: Physical Properties of gel fibres calculated using the Nanoscope Matlab Utility toolbox from Bruker for a **1** (27mM) · $MgCl_2$ (17mM) over a single heat and cool cycle in a repeated experiment. Measured using the PeakForce Quantitative Nanomechanical Mapping mode of Atomic Force Microscopy. All points above 0.5 nm were used to calculate the physical properties, this removes the points taken on the substrate. Error is standard deviation of measurements.

T (°C)	DMT Modulus (MPa)	Adhesion (nN)	Deformation (nm)	No. of Points
19.0	12.1936 ± 2.5007	0.6641 ± 0.1790	9.1776 ± 1.5303	13117
20.6	11.3462 ± 1.4746	0.5895 ± 0.1618	9.4440 ± 1.1063	31810
22.9	4.2854 ± 1.2414	-0.2183 ± 0.1195	14.6990 ± 9.9388	31274
24.6	4.4955 ± 1.0036	-0.6252 ± 0.1972	19.5407 ± 9.8793	31279
26.7	3.7001 ± 1.4459	-0.3382 ± 0.1136	22.5404 ± 10.8537	19012
27.0	17.1698 ± 4.4153	0.1701 ± 0.1857	8.4643 ± 7.2159	5230
27.0	18.9187 ± 4.8893	-0.0399 ± 0.2009	9.3414 ± 12.0306	2577
27.8	15.1924 ± 5.3797	0.0053 ± 0.2107	14.7785 ± 19.9781	2610
28.8	18.3400 ± 5.5375	0.2179 ± 0.2531	7.1281 ± 5.1800	1457
29.8	21.1520 ± 3.0111	0.5344 ± 0.2073	4.8610 ± 2.1703	7375
30.8 - 31.9 - 27.2	no fibres observed			
26.2	31.8444 ± 4.4585	0.0171 ± 0.1534	6.5441 ± 4.4891	5420
25.2	32.6142 ± 2.6117	0.4428 ± 0.1440	7.2024 ± 1.5066	4904
24.2	31.2079 ± 3.0394	0.1319 ± 0.1279	6.9369 ± 1.2568	5479
23.3	31.3296 ± 3.5479	0.0927 ± 0.1319	7.3727 ± 4.6956	4577
21.9	30.9752 ± 3.5598	0.1148 ± 0.1320	7.1564 ± 2.3227	5616
21.2	25.1457 ± 4.8450	0.0821 ± 0.1603	7.8712 ± 1.1122	12966
20.3	16.9639 ± 4.2992	0.2196 ± 0.3570	10.5331 ± 3.5634	25784

Appendix B

Rights and Permissions for Copyright Material

B.1 Permission Letters for Reproduction of Figures

PERMISSION TO USE COPYRIGHT MATERIAL AS SPECIFIED BELOW:

Amino acid functionalised calixarenes : crystal growth modifiers and low molecular weight gelators crystal growth modifiers and low molecular weight gelators. Figure 1.34

I hereby give permission for **Emily Barker** to include the abovementioned material(s) in his/her higher degree thesis for Curtin University, and to communicate this material via the espace institutional repository. This permission is granted on a non-exclusive basis and for an indefinite period.

I confirm that I am the copyright owner of the specified material.

Signed: 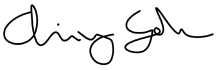

Name: Ching Yong Goh

Position: Technical Officer, Faculty of Science and Engineering, Curtin University

Date: 28/08/2020

Please return signed form to **Emily Barker, Emily.c.barker@student.curtin.edu.au.**

Regarding Incident 3773909 Permission to Reproduce Figures

S support@services.acs.org
Thu 27/08/2020 4:22 PM
To: Emily Barker

Dear Dr. Barker,

Thank you for contacting ACS Publications Support.

Your permission requested is granted and there is no fee for this reuse. In your planned reuse, you must cite the ACS article as the source, add this direct link <https://pubs.acs.org/doi/abs/10.1021/acs.biomac.7b00823>, and include a notice to readers that further permissions related to the material excerpted should be directed to the ACS.

Sincerely,

Budimir Jelic
ACS Publications
Customer Services & Information
Website: https://help.acs.org

Incident Information:

Incident #: 3773909
Date Created: 2020-08-27T09:11:03
Priority: 3
Customer: Emily Barker
Title: Permission to Reproduce Figures
Description: Hi,

I would like to request permission to use a single figure from the article "Drying Affects the Fiber Network in Low Molecular Weight Hydrogels" with DOI 10.1021/acs.biomac.7b00823. I would like to use parts a) and d) of figure 6 in my PhD thesis at Curtin University which is expected to be published on the university library website early next year. Please let me know if you need more information from me.

Kind regards,
Emily Barker.

{CMI: MCID1023423}

Reply | Forward

JOHN WILEY AND SONS LICENSE
TERMS AND CONDITIONS

Nov 18, 2020

This Agreement between Emily Barker ("You") and John Wiley and Sons ("John Wiley and Sons") consists of your license details and the terms and conditions provided by John Wiley and Sons and Copyright Clearance Center.

License Number	4896930921063
License date	Aug 27, 2020
Licensed Content Publisher	John Wiley and Sons
Licensed Content Publication	Journal of Applied Polymer Science
Licensed Content Title	Laser scanning confocal microscopy versus scanning electron microscopy for characterization of polymer morphology: Sample preparation drastically distorts morphologies of poly(2-hydroxyethyl methacrylate)-based hydrogels
Licensed Content Author	Murray V. Baker, Traian V. Chirila, Jeremy A. Shaw, et al
Licensed Content Date	May 31, 2012
Licensed Content Volume	127
Licensed Content Issue	6
Licensed	9

Content Pages	
Type of use	Dissertation/Thesis
Requestor type	University/Academic
Format	Electronic
Portion	Figure/table
Number of figures/tables	1
Will you be translating?	No
Title	Characterisation of Gelation by Atomic Force Microscopy
Institution name	Curtin University
Expected presentation date	Jan 2021
Portions	Figure 1
Requestor Location	Emily Barker 5 Bossea Place Ferndale, WA 6148 Australia Attn: Miss Emily Barker
Publisher Tax ID	EU826007151
Total	0.00 AUD

Terms and Conditions

TERMS AND CONDITIONS

This copyrighted material is owned by or exclusively licensed to John Wiley & Sons, Inc. or one of its group companies (each a"Wiley Company") or handled on behalf of a society with which a Wiley Company has exclusive publishing rights in relation to a particular work (collectively "WILEY"). By clicking "accept" in connection with completing this licensing transaction, you agree that the following terms and conditions apply to this transaction (along with the billing and payment terms and conditions established by the Copyright Clearance Center Inc., ("CCC's Billing and Payment terms and conditions"), at the time that you opened your RightsLink account (these are available at any time at http://myaccount.copyright.com).

Terms and Conditions

- The materials you have requested permission to reproduce or reuse (the "Wiley Materials") are protected by copyright.

- You are hereby granted a personal, non-exclusive, non-sub licensable (on a stand-alone basis), non-transferable, worldwide, limited license to reproduce the Wiley Materials for the purpose specified in the licensing process. This license, **and any CONTENT (PDF or image file) purchased as part of your order,** is for a one-time use only and limited to any maximum distribution number specified in the license. The first instance of republication or reuse granted by this license must be completed within two years of the date of the grant of this license (although copies prepared before the end date may be distributed thereafter). The Wiley Materials shall not be used in any other manner or for any other purpose, beyond what is granted in the license. Permission is granted subject to an appropriate acknowledgement given to the author, title of the material/book/journal and the publisher. You shall also duplicate the copyright notice that appears in the Wiley publication in your use of the Wiley Material. Permission is also granted on the understanding that nowhere in the text is a previously published source acknowledged for all or part of this Wiley Material. Any third party content is expressly excluded from this permission.

- With respect to the Wiley Materials, all rights are reserved. Except as expressly granted by the terms of the license, no part of the Wiley Materials may be copied, modified, adapted (except for minor reformatting required by the new Publication), translated, reproduced, transferred or distributed, in any form or by any means, and no derivative works may be made based on the Wiley Materials without the prior permission of the respective copyright owner.**For STM Signatory Publishers clearing permission under the terms of the STM Permissions Guidelines only, the terms of the license are extended to include subsequent editions and for editions in other languages, provided such editions are for the work as a whole in situ and does not involve the separate exploitation of the permitted figures or extracts,** You may not alter, remove or suppress in any manner any copyright, trademark or other notices displayed by the Wiley Materials. You may not license, rent, sell, loan, lease, pledge, offer as security, transfer or assign the Wiley Materials on a stand-alone basis, or any of the rights granted to you hereunder to any other person.

- The Wiley Materials and all of the intellectual property rights therein shall at all times remain the exclusive property of John Wiley & Sons Inc, the Wiley Companies, or their respective licensors, and your interest therein is only that of having possession of and the right to reproduce the Wiley Materials pursuant to Section 2 herein during the continuance of this Agreement. You agree that you own no right, title or interest in or to the Wiley Materials or any of the intellectual property rights therein. You shall have no rights hereunder other than the license as provided for above in Section 2. No right, license or interest to any trademark, trade name, service mark or other branding ("Marks") of WILEY or its licensors is granted hereunder, and you agree that you

shall not assert any such right, license or interest with respect thereto

- NEITHER WILEY NOR ITS LICENSORS MAKES ANY WARRANTY OR REPRESENTATION OF ANY KIND TO YOU OR ANY THIRD PARTY, EXPRESS, IMPLIED OR STATUTORY, WITH RESPECT TO THE MATERIALS OR THE ACCURACY OF ANY INFORMATION CONTAINED IN THE MATERIALS, INCLUDING, WITHOUT LIMITATION, ANY IMPLIED WARRANTY OF MERCHANTABILITY, ACCURACY, SATISFACTORY QUALITY, FITNESS FOR A PARTICULAR PURPOSE, USABILITY, INTEGRATION OR NON-INFRINGEMENT AND ALL SUCH WARRANTIES ARE HEREBY EXCLUDED BY WILEY AND ITS LICENSORS AND WAIVED BY YOU.

- WILEY shall have the right to terminate this Agreement immediately upon breach of this Agreement by you.

- You shall indemnify, defend and hold harmless WILEY, its Licensors and their respective directors, officers, agents and employees, from and against any actual or threatened claims, demands, causes of action or proceedings arising from any breach of this Agreement by you.

- IN NO EVENT SHALL WILEY OR ITS LICENSORS BE LIABLE TO YOU OR ANY OTHER PARTY OR ANY OTHER PERSON OR ENTITY FOR ANY SPECIAL, CONSEQUENTIAL, INCIDENTAL, INDIRECT, EXEMPLARY OR PUNITIVE DAMAGES, HOWEVER CAUSED, ARISING OUT OF OR IN CONNECTION WITH THE DOWNLOADING, PROVISIONING, VIEWING OR USE OF THE MATERIALS REGARDLESS OF THE FORM OF ACTION, WHETHER FOR BREACH OF CONTRACT, BREACH OF WARRANTY, TORT, NEGLIGENCE, INFRINGEMENT OR OTHERWISE (INCLUDING, WITHOUT LIMITATION, DAMAGES BASED ON LOSS OF PROFITS, DATA, FILES, USE, BUSINESS OPPORTUNITY OR CLAIMS OF THIRD PARTIES), AND WHETHER OR NOT THE PARTY HAS BEEN ADVISED OF THE POSSIBILITY OF SUCH DAMAGES. THIS LIMITATION SHALL APPLY NOTWITHSTANDING ANY FAILURE OF ESSENTIAL PURPOSE OF ANY LIMITED REMEDY PROVIDED HEREIN.

- Should any provision of this Agreement be held by a court of competent jurisdiction to be illegal, invalid, or unenforceable, that provision shall be deemed amended to achieve as nearly as possible the same economic effect as the original provision, and the legality, validity and enforceability of the remaining provisions of this Agreement shall not be affected or impaired thereby.

- The failure of either party to enforce any term or condition of this Agreement shall not constitute a waiver of either party's right to enforce each and every term and condition of this Agreement. No breach under this agreement shall be deemed waived or excused by either party unless such waiver or consent is in writing signed by the party granting such waiver or consent. The waiver by or consent of a party to a breach of any provision of this Agreement shall not operate or be construed as a waiver of or consent to any other or subsequent breach by such other party.

- This Agreement may not be assigned (including by operation of law or otherwise) by you without WILEY's prior written consent.

- Any fee required for this permission shall be non-refundable after thirty (30) days from receipt by the CCC.

- These terms and conditions together with CCC's Billing and Payment terms and conditions (which are incorporated herein) form the entire agreement between you and

WILEY concerning this licensing transaction and (in the absence of fraud) supersedes all prior agreements and representations of the parties, oral or written. This Agreement may not be amended except in writing signed by both parties. This Agreement shall be binding upon and inure to the benefit of the parties' successors, legal representatives, and authorized assigns.

- In the event of any conflict between your obligations established by these terms and conditions and those established by CCC's Billing and Payment terms and conditions, these terms and conditions shall prevail.
- WILEY expressly reserves all rights not specifically granted in the combination of (i) the license details provided by you and accepted in the course of this licensing transaction, (ii) these terms and conditions and (iii) CCC's Billing and Payment terms and conditions.
- This Agreement will be void if the Type of Use, Format, Circulation, or Requestor Type was misrepresented during the licensing process.
- This Agreement shall be governed by and construed in accordance with the laws of the State of New York, USA, without regards to such state's conflict of law rules. Any legal action, suit or proceeding arising out of or relating to these Terms and Conditions or the breach thereof shall be instituted in a court of competent jurisdiction in New York County in the State of New York in the United States of America and each party hereby consents and submits to the personal jurisdiction of such court, waives any objection to venue in such court and consents to service of process by registered or certified mail, return receipt requested, at the last known address of such party.

WILEY OPEN ACCESS TERMS AND CONDITIONS

Wiley Publishes Open Access Articles in fully Open Access Journals and in Subscription journals offering Online Open. Although most of the fully Open Access journals publish open access articles under the terms of the Creative Commons Attribution (CC BY) License only, the subscription journals and a few of the Open Access Journals offer a choice of Creative Commons Licenses. The license type is clearly identified on the article.

The Creative Commons Attribution License

The Creative Commons Attribution License (CC-BY) allows users to copy, distribute and transmit an article, adapt the article and make commercial use of the article. The CC-BY license permits commercial and non-

Creative Commons Attribution Non-Commercial License

The Creative Commons Attribution Non-Commercial (CC-BY-NC)License permits use, distribution and reproduction in any medium, provided the original work is properly cited and is not used for commercial purposes.(see below)

Creative Commons Attribution-Non-Commercial-NoDerivs License

The Creative Commons Attribution Non-Commercial-NoDerivs License (CC-BY-NC-ND) permits use, distribution and reproduction in any medium, provided the original work is properly cited, is not used for commercial purposes and no modifications or adaptations are made. (see below)

Use by commercial "for-profit" organizations

Use of Wiley Open Access articles for commercial, promotional, or marketing purposes requires further explicit permission from Wiley and will be subject to a fee.

Further details can be found on Wiley Online Library
http://olabout.wiley.com/WileyCDA/Section/id-410895.html

Other Terms and Conditions:

v1.10 Last updated September 2015

Questions? customercare@copyright.com or +1-855-239-3415 (toll free in the US) or +1-978-646-2777.

Copyright Clearance Center Marketplace™

Royal Society of Chemistry - License Terms and Conditions

This is a License Agreement between Emily Barker ("You") and Royal Society of Chemistry ("Publisher") provided by Copyright Clearance Center ("CCC"). The license consists of your order details, the terms and conditions provided by Royal Society of Chemistry, and the CCC terms and conditions.

All payments must be made in full to CCC.

Order Date	27-Aug-2020	**Type of Use**	Republish in a thesis/dissertation
Order license ID	1058552-1		
ISSN	1364-548X	**Publisher**	ROYAL SOCIETY OF CHEMISTRY
		Portion	Image/photo/illustration

LICENSED CONTENT

Publication Title	Chemical communications	**Country**	United Kingdom of Great Britain and Northern Ireland
Author/Editor	Royal Society of Chemistry (Great Britain)	**Rightsholder**	Royal Society of Chemistry
Date	01/01/1996	**Publication Type**	e-Journal
Language	English		

REQUEST DETAILS

Portion Type	Image/photo/illustration	**Distribution**	Worldwide
Number of images / photos / illustrations	1	**Translation**	Original language of publication
Format (select all that apply)	Electronic	**Copies for the disabled?**	No
		Minor editing privileges?	No
Who will republish the content?	Academic institution	**Incidental promotional use?**	No
Duration of Use	Current edition and up to 15 years	**Currency**	AUD
Lifetime Unit Quantity	Up to 499		
Rights Requested	Main product		

NEW WORK DETAILS

Title	Characterisation of Gelation by Atomic Force Microscopy	**Institution name**	Curtin University
		Expected presentation date	2021-01-01
Instructor name	Emily C Barker		

ADDITIONAL DETAILS

Order reference number	N/A	**The requesting person / organization to appear on the license**	Emily Barker

REUSE CONTENT DETAILS

Title, description or numeric reference of the portion(s)	Figure 1.3	**Title of the article/chapter the portion is from**	Chapter 1
Editor of portion(s)	N/A	**Author of portion(s)**	Royal Society of Chemistry (Great Britain)
Volume of serial or monograph	N/A	**Issue, if republishing an article from a serial**	N/A
Page or page range of portion	6	**Publication date of portion**	2021-01-01

CCC Republication Terms and Conditions

1. Description of Service; Defined Terms. This Republication License enables the User to obtain licenses for republication of one or more copyrighted works as described in detail on the relevant Order Confirmation (the "Work(s)"). Copyright Clearance Center, Inc. ("CCC") grants licenses through the Service on behalf of the rightsholder identified on the Order Confirmation (the "Rightsholder"). "Republication", as used herein, generally means the inclusion of a Work, in whole or in part, in a new work or works, also as described on the Order Confirmation. "User", as used herein, means the person or entity making such republication.

2. The terms set forth in the relevant Order Confirmation, and any terms set by the Rightsholder with respect to a particular Work, govern the terms of use of Works in connection with the Service. By using the Service, the person transacting for a republication license on behalf of the User represents and warrants that he/she/it (a) has been duly authorized by the User to accept, and hereby does accept, all such terms and conditions on behalf of User, and (b) shall inform User of all such terms and conditions. In the event such person is a "freelancer" or other third party independent of User and CCC, such party shall be deemed jointly a "User" for purposes of these terms and conditions. In any event, User shall be deemed to have accepted and agreed to all such terms and conditions if User republishes the Work in any fashion.

3. Scope of License; Limitations and Obligations.

    3.1. All Works and all rights therein, including copyright rights, remain the sole and exclusive property of the Rightsholder. The license created by the exchange of an Order Confirmation (and/or any invoice) and payment by User of the full amount set forth on that document includes only those rights expressly set forth in the Order Confirmation and in these terms and conditions, and conveys no other rights in the Work(s) to User. All rights not expressly granted are hereby reserved.

    3.2. General Payment Terms: You may pay by credit card or through an account with us payable at the end of the month. If you and we agree that you may establish a standing account with CCC, then the following terms apply: Remit Payment to: Copyright Clearance Center, 29118 Network Place, Chicago, IL 60673-1291. Payments Due: Invoices are payable upon their delivery to you (or upon our notice to you that they are available to you for downloading). After 30 days, outstanding amounts will be subject to a service charge of 1-1/2% per month or, if less, the maximum rate allowed by applicable law. Unless otherwise specifically set forth in the Order Confirmation or in a separate written agreement signed by CCC, invoices are due and payable on "net 30" terms. While User may exercise the rights licensed immediately upon issuance of the Order Confirmation, the license is automatically revoked and is null and void, as if it had never been issued, if complete payment for the license is not received on a timely basis either from User directly or through a payment agent, such as a credit card company.

    3.3. Unless otherwise provided in the Order Confirmation, any grant of rights to User (i) is "one-time" (including the editions and product family specified in the license), (ii) is non-exclusive and non-transferable and (iii) is subject to any and all limitations and restrictions (such as, but not limited to, limitations on duration of use or circulation) included in the Order Confirmation or invoice and/or in these terms and conditions. Upon completion of the licensed use, User shall either secure a new permission for further use of the Work(s) or immediately cease any new use of the Work(s) and shall render inaccessible (such as by deleting or by removing or severing links or other locators) any further copies of the Work (except for copies printed on paper in accordance with this license and still in User's stock at the end of such period).

    3.4. In the event that the material for which a republication license is sought includes third party materials (such as photographs, illustrations, graphs, inserts and similar materials) which are identified in such material as having been used by permission, User is responsible for identifying, and seeking separate

licenses (under this Service or otherwise) for, any of such third party materials; without a separate license, such third party materials may not be used.

3.5. Use of proper copyright notice for a Work is required as a condition of any license granted under the Service. Unless otherwise provided in the Order Confirmation, a proper copyright notice will read substantially as follows: "Republished with permission of [Rightsholder's name], from [Work's title, author, volume, edition number and year of copyright]; permission conveyed through Copyright Clearance Center, Inc. " Such notice must be provided in a reasonably legible font size and must be placed either immediately adjacent to the Work as used (for example, as part of a by-line or footnote but not as a separate electronic link) or in the place where substantially all other credits or notices for the new work containing the republished Work are located. Failure to include the required notice results in loss to the Rightsholder and CCC, and the User shall be liable to pay liquidated damages for each such failure equal to twice the use fee specified in the Order Confirmation, in addition to the use fee itself and any other fees and charges specified.

3.6. User may only make alterations to the Work if and as expressly set forth in the Order Confirmation. No Work may be used in any way that is defamatory, violates the rights of third parties (including such third parties' rights of copyright, privacy, publicity, or other tangible or intangible property), or is otherwise illegal, sexually explicit or obscene. In addition, User may not conjoin a Work with any other material that may result in damage to the reputation of the Rightsholder. User agrees to inform CCC if it becomes aware of any infringement of any rights in a Work and to cooperate with any reasonable request of CCC or the Rightsholder in connection therewith.

4. Indemnity. User hereby indemnifies and agrees to defend the Rightsholder and CCC, and their respective employees and directors, against all claims, liability, damages, costs and expenses, including legal fees and expenses, arising out of any use of a Work beyond the scope of the rights granted herein, or any use of a Work which has been altered in any unauthorized way by User, including claims of defamation or infringement of rights of copyright, publicity, privacy or other tangible or intangible property.

5. Limitation of Liability. UNDER NO CIRCUMSTANCES WILL CCC OR THE RIGHTSHOLDER BE LIABLE FOR ANY DIRECT, INDIRECT, CONSEQUENTIAL OR INCIDENTAL DAMAGES (INCLUDING WITHOUT LIMITATION DAMAGES FOR LOSS OF BUSINESS PROFITS OR INFORMATION, OR FOR BUSINESS INTERRUPTION) ARISING OUT OF THE USE OR INABILITY TO USE A WORK, EVEN IF ONE OF THEM HAS BEEN ADVISED OF THE POSSIBILITY OF SUCH DAMAGES. In any event, the total liability of the Rightsholder and CCC (including their respective employees and directors) shall not exceed the total amount actually paid by User for this license. User assumes full liability for the actions and omissions of its principals, employees, agents, affiliates, successors and assigns.

6. Limited Warranties. THE WORK(S) AND RIGHT(S) ARE PROVIDED "AS IS". CCC HAS THE RIGHT TO GRANT TO USER THE RIGHTS GRANTED IN THE ORDER CONFIRMATION DOCUMENT. CCC AND THE RIGHTSHOLDER DISCLAIM ALL OTHER WARRANTIES RELATING TO THE WORK(S) AND RIGHT(S), EITHER EXPRESS OR IMPLIED, INCLUDING WITHOUT LIMITATION IMPLIED WARRANTIES OF MERCHANTABILITY OR FITNESS FOR A PARTICULAR PURPOSE. ADDITIONAL RIGHTS MAY BE REQUIRED TO USE ILLUSTRATIONS, GRAPHS, PHOTOGRAPHS, ABSTRACTS, INSERTS OR OTHER PORTIONS OF THE WORK (AS OPPOSED TO THE ENTIRE WORK) IN A MANNER CONTEMPLATED BY USER; USER UNDERSTANDS AND AGREES THAT NEITHER CCC NOR THE RIGHTSHOLDER MAY HAVE SUCH ADDITIONAL RIGHTS TO GRANT.

7. Effect of Breach. Any failure by User to pay any amount when due, or any use by User of a Work beyond the scope of the license set forth in the Order Confirmation and/or these terms and conditions, shall be a material breach of the license created by the Order Confirmation and these terms and conditions. Any breach not cured within 30 days of written notice thereof shall result in immediate termination of such license without further notice. Any unauthorized (but licensable) use of a Work that is terminated immediately upon notice thereof may be liquidated by payment of the Rightsholder's ordinary license price therefor; any unauthorized (and unlicensable) use that is not terminated immediately for any reason (including, for example, because materials containing the Work cannot reasonably be recalled) will be subject to all remedies available at law or in equity, but in no event to a payment of less than three times the Rightsholder's ordinary license price for the most closely analogous licensable use plus Rightsholder's and/or CCC's costs and expenses incurred in collecting such payment.

8. Miscellaneous.

8.1. User acknowledges that CCC may, from time to time, make changes or additions to the Service or to these terms and conditions, and CCC reserves the right to send notice to the User by electronic mail or

otherwise for the purposes of notifying User of such changes or additions; provided that any such changes or additions shall not apply to permissions already secured and paid for.

8.2. Use of User-related information collected through the Service is governed by CCC's privacy policy, available online here:https://marketplace.copyright.com/rs-ui-web/mp/privacy-policy

8.3. The licensing transaction described in the Order Confirmation is personal to User. Therefore, User may not assign or transfer to any other person (whether a natural person or an organization of any kind) the license created by the Order Confirmation and these terms and conditions or any rights granted hereunder; provided, however, that User may assign such license in its entirety on written notice to CCC in the event of a transfer of all or substantially all of User's rights in the new material which includes the Work(s) licensed under this Service.

8.4. No amendment or waiver of any terms is binding unless set forth in writing and signed by the parties. The Rightsholder and CCC hereby object to any terms contained in any writing prepared by the User or its principals, employees, agents or affiliates and purporting to govern or otherwise relate to the licensing transaction described in the Order Confirmation, which terms are in any way inconsistent with any terms set forth in the Order Confirmation and/or in these terms and conditions or CCC's standard operating procedures, whether such writing is prepared prior to, simultaneously with or subsequent to the Order Confirmation, and whether such writing appears on a copy of the Order Confirmation or in a separate instrument.

8.5. The licensing transaction described in the Order Confirmation document shall be governed by and construed under the law of the State of New York, USA, without regard to the principles thereof of conflicts of law. Any case, controversy, suit, action, or proceeding arising out of, in connection with, or related to such licensing transaction shall be brought, at CCC's sole discretion, in any federal or state court located in the County of New York, State of New York, USA, or in any federal or state court whose geographical jurisdiction covers the location of the Rightsholder set forth in the Order Confirmation. The parties expressly submit to the personal jurisdiction and venue of each such federal or state court.If you have any comments or questions about the Service or Copyright Clearance Center, please contact us at 978-750-8400 or send an e-mail to support@copyright.com.

v 1.1

Copyright Clearance Center Marketplace™

Royal Society of Chemistry - License Terms and Conditions

This is a License Agreement between Emily Barker ("You") and Royal Society of Chemistry ("Publisher") provided by Copyright Clearance Center ("CCC"). The license consists of your order details, the terms and conditions provided by Royal Society of Chemistry, and the CCC terms and conditions.

All payments must be made in full to CCC.

Order Date	27-Aug-2020	**Type of Use**	Republish in a thesis/dissertation
Order license ID	1058558-1		
ISSN	1364-548X	**Publisher**	ROYAL SOCIETY OF CHEMISTRY
		Portion	Image/photo/illustration

LICENSED CONTENT

Publication Title	Chemical communications	**Country**	United Kingdom of Great Britain and Northern Ireland
Author/Editor	Royal Society of Chemistry (Great Britain)	**Rightsholder**	Royal Society of Chemistry
Date	01/01/1996	**Publication Type**	e-Journal
Language	English		

REQUEST DETAILS

Portion Type	Image/photo/illustration	**Distribution**	Worldwide
Number of images / photos / illustrations	2	**Translation**	Original language of publication
Format (select all that apply)	Print	**Copies for the disabled?**	No
		Minor editing privileges?	No
Who will republish the content?	Academic institution	**Incidental promotional use?**	No
Duration of Use	Current edition and up to 15 years	**Currency**	AUD
Lifetime Unit Quantity	Up to 499		
Rights Requested	Main product		

NEW WORK DETAILS

Title	Characterisation of Gelation by Atomic Force Microscopy	**Institution name**	Curtin University
		Expected presentation date	2021-01-01
Instructor name	Emily C Barker		

ADDITIONAL DETAILS

Order reference number	N/A	**The requesting person / organization to appear on the license**	Emily Barker

REUSE CONTENT DETAILS

Title, description or numeric reference of the portion(s)	Figure 1.4	**Title of the article/chapter the portion is from**	Chapter 1
Editor of portion(s)	N/A	**Author of portion(s)**	Royal Society of Chemistry (Great Britain)
Volume of serial or monograph	N/A	**Issue, if republishing an article from a serial**	N/A
Page or page range of portion	7	**Publication date of portion**	2021-01-01

CCC Republication Terms and Conditions

1. Description of Service; Defined Terms. This Republication License enables the User to obtain licenses for republication of one or more copyrighted works as described in detail on the relevant Order Confirmation (the "Work(s)"). Copyright Clearance Center, Inc. ("CCC") grants licenses through the Service on behalf of the rightsholder identified on the Order Confirmation (the "Rightsholder"). "Republication", as used herein, generally means the inclusion of a Work, in whole or in part, in a new work or works, also as described on the Order Confirmation. "User", as used herein, means the person or entity making such republication.

2. The terms set forth in the relevant Order Confirmation, and any terms set by the Rightsholder with respect to a particular Work, govern the terms of use of Works in connection with the Service. By using the Service, the person transacting for a republication license on behalf of the User represents and warrants that he/she/it (a) has been duly authorized by the User to accept, and hereby does accept, all such terms and conditions on behalf of User, and (b) shall inform User of all such terms and conditions. In the event such person is a "freelancer" or other third party independent of User and CCC, such party shall be deemed jointly a "User" for purposes of these terms and conditions. In any event, User shall be deemed to have accepted and agreed to all such terms and conditions if User republishes the Work in any fashion.

3. Scope of License; Limitations and Obligations.

    3.1. All Works and all rights therein, including copyright rights, remain the sole and exclusive property of the Rightsholder. The license created by the exchange of an Order Confirmation (and/or any invoice) and payment by User of the full amount set forth on that document includes only those rights expressly set forth in the Order Confirmation and in these terms and conditions, and conveys no other rights in the Work(s) to User. All rights not expressly granted are hereby reserved.

    3.2. General Payment Terms: You may pay by credit card or through an account with us payable at the end of the month. If you and we agree that you may establish a standing account with CCC, then the following terms apply: Remit Payment to: Copyright Clearance Center, 29118 Network Place, Chicago, IL 60673-1291. Payments Due: Invoices are payable upon their delivery to you (or upon our notice to you that they are available to you for downloading). After 30 days, outstanding amounts will be subject to a service charge of 1-1/2% per month or, if less, the maximum rate allowed by applicable law. Unless otherwise specifically set forth in the Order Confirmation or in a separate written agreement signed by CCC, invoices are due and payable on "net 30" terms. While User may exercise the rights licensed immediately upon issuance of the Order Confirmation, the license is automatically revoked and is null and void, as if it had never been issued, if complete payment for the license is not received on a timely basis either from User directly or through a payment agent, such as a credit card company.

    3.3. Unless otherwise provided in the Order Confirmation, any grant of rights to User (i) is "one-time" (including the editions and product family specified in the license), (ii) is non-exclusive and non-transferable and (iii) is subject to any and all limitations and restrictions (such as, but not limited to, limitations on duration of use or circulation) included in the Order Confirmation or invoice and/or in these terms and conditions. Upon completion of the licensed use, User shall either secure a new permission for further use of the Work(s) or immediately cease any new use of the Work(s) and shall render inaccessible (such as by deleting or by removing or severing links or other locators) any further copies of the Work (except for copies printed on paper in accordance with this license and still in User's stock at the end of such period).

    3.4. In the event that the material for which a republication license is sought includes third party materials (such as photographs, illustrations, graphs, inserts and similar materials) which are identified in such material as having been used by permission, User is responsible for identifying, and seeking separate

licenses (under this Service or otherwise) for, any of such third party materials; without a separate license, such third party materials may not be used.

3.5. Use of proper copyright notice for a Work is required as a condition of any license granted under the Service. Unless otherwise provided in the Order Confirmation, a proper copyright notice will read substantially as follows: "Republished with permission of [Rightsholder's name], from [Work's title, author, volume, edition number and year of copyright]; permission conveyed through Copyright Clearance Center, Inc. " Such notice must be provided in a reasonably legible font size and must be placed either immediately adjacent to the Work as used (for example, as part of a by-line or footnote but not as a separate electronic link) or in the place where substantially all other credits or notices for the new work containing the republished Work are located. Failure to include the required notice results in loss to the Rightsholder and CCC, and the User shall be liable to pay liquidated damages for each such failure equal to twice the use fee specified in the Order Confirmation, in addition to the use fee itself and any other fees and charges specified.

3.6. User may only make alterations to the Work if and as expressly set forth in the Order Confirmation. No Work may be used in any way that is defamatory, violates the rights of third parties (including such third parties' rights of copyright, privacy, publicity, or other tangible or intangible property), or is otherwise illegal, sexually explicit or obscene. In addition, User may not conjoin a Work with any other material that may result in damage to the reputation of the Rightsholder. User agrees to inform CCC if it becomes aware of any infringement of any rights in a Work and to cooperate with any reasonable request of CCC or the Rightsholder in connection therewith.

4. Indemnity. User hereby indemnifies and agrees to defend the Rightsholder and CCC, and their respective employees and directors, against all claims, liability, damages, costs and expenses, including legal fees and expenses, arising out of any use of a Work beyond the scope of the rights granted herein, or any use of a Work which has been altered in any unauthorized way by User, including claims of defamation or infringement of rights of copyright, publicity, privacy or other tangible or intangible property.

5. Limitation of Liability. UNDER NO CIRCUMSTANCES WILL CCC OR THE RIGHTSHOLDER BE LIABLE FOR ANY DIRECT, INDIRECT, CONSEQUENTIAL OR INCIDENTAL DAMAGES (INCLUDING WITHOUT LIMITATION DAMAGES FOR LOSS OF BUSINESS PROFITS OR INFORMATION, OR FOR BUSINESS INTERRUPTION) ARISING OUT OF THE USE OR INABILITY TO USE A WORK, EVEN IF ONE OF THEM HAS BEEN ADVISED OF THE POSSIBILITY OF SUCH DAMAGES. In any event, the total liability of the Rightsholder and CCC (including their respective employees and directors) shall not exceed the total amount actually paid by User for this license. User assumes full liability for the actions and omissions of its principals, employees, agents, affiliates, successors and assigns.

6. Limited Warranties. THE WORK(S) AND RIGHT(S) ARE PROVIDED "AS IS". CCC HAS THE RIGHT TO GRANT TO USER THE RIGHTS GRANTED IN THE ORDER CONFIRMATION DOCUMENT. CCC AND THE RIGHTSHOLDER DISCLAIM ALL OTHER WARRANTIES RELATING TO THE WORK(S) AND RIGHT(S), EITHER EXPRESS OR IMPLIED, INCLUDING WITHOUT LIMITATION IMPLIED WARRANTIES OF MERCHANTABILITY OR FITNESS FOR A PARTICULAR PURPOSE. ADDITIONAL RIGHTS MAY BE REQUIRED TO USE ILLUSTRATIONS, GRAPHS, PHOTOGRAPHS, ABSTRACTS, INSERTS OR OTHER PORTIONS OF THE WORK (AS OPPOSED TO THE ENTIRE WORK) IN A MANNER CONTEMPLATED BY USER; USER UNDERSTANDS AND AGREES THAT NEITHER CCC NOR THE RIGHTSHOLDER MAY HAVE SUCH ADDITIONAL RIGHTS TO GRANT.

7. Effect of Breach. Any failure by User to pay any amount when due, or any use by User of a Work beyond the scope of the license set forth in the Order Confirmation and/or these terms and conditions, shall be a material breach of the license created by the Order Confirmation and these terms and conditions. Any breach not cured within 30 days of written notice thereof shall result in immediate termination of such license without further notice. Any unauthorized (but licensable) use of a Work that is terminated immediately upon notice thereof may be liquidated by payment of the Rightsholder's ordinary license price therefor; any unauthorized (and unlicensable) use that is not terminated immediately for any reason (including, for example, because materials containing the Work cannot reasonably be recalled) will be subject to all remedies available at law or in equity, but in no event to a payment of less than three times the Rightsholder's ordinary license price for the most closely analogous licensable use plus Rightsholder's and/or CCC's costs and expenses incurred in collecting such payment.

8. Miscellaneous.

8.1. User acknowledges that CCC may, from time to time, make changes or additions to the Service or to these terms and conditions, and CCC reserves the right to send notice to the User by electronic mail or

otherwise for the purposes of notifying User of such changes or additions; provided that any such changes or additions shall not apply to permissions already secured and paid for.

8.2. Use of User-related information collected through the Service is governed by CCC's privacy policy, available online here:https://marketplace.copyright.com/rs-ui-web/mp/privacy-policy

8.3. The licensing transaction described in the Order Confirmation is personal to User. Therefore, User may not assign or transfer to any other person (whether a natural person or an organization of any kind) the license created by the Order Confirmation and these terms and conditions or any rights granted hereunder; provided, however, that User may assign such license in its entirety on written notice to CCC in the event of a transfer of all or substantially all of User's rights in the new material which includes the Work(s) licensed under this Service.

8.4. No amendment or waiver of any terms is binding unless set forth in writing and signed by the parties. The Rightsholder and CCC hereby object to any terms contained in any writing prepared by the User or its principals, employees, agents or affiliates and purporting to govern or otherwise relate to the licensing transaction described in the Order Confirmation, which terms are in any way inconsistent with any terms set forth in the Order Confirmation and/or in these terms and conditions or CCC's standard operating procedures, whether such writing is prepared prior to, simultaneously with or subsequent to the Order Confirmation, and whether such writing appears on a copy of the Order Confirmation or in a separate instrument.

8.5. The licensing transaction described in the Order Confirmation document shall be governed by and construed under the law of the State of New York, USA, without regard to the principles thereof of conflicts of law. Any case, controversy, suit, action, or proceeding arising out of, in connection with, or related to such licensing transaction shall be brought, at CCC's sole discretion, in any federal or state court located in the County of New York, State of New York, USA, or in any federal or state court whose geographical jurisdiction covers the location of the Rightsholder set forth in the Order Confirmation. The parties expressly submit to the personal jurisdiction and venue of each such federal or state court.If you have any comments or questions about the Service or Copyright Clearance Center, please contact us at 978-750-8400 or send an e-mail to support@copyright.com.

v 1.1

B.2 Co-author Attribution Statement

Emily C Barker, Adam D Martin, Christopher J Garvey, Ching Yong Goh, Franca Jones, Mauro Mocerino, Brian W Skelton, Mark I Ogden and Thomas Becker. Thermal annealing behaviour and gel to crystal transition of a low molecular weight hydrogelator. *Soft Matter*, 13(5):1006 1011, 2017.

	Concept and Design	Acquisition of Data and Method	Data Conditioning and Manipulation	Analysis and Statistical Method	Interpretation and Discussion	Final Approval
Emily C Barker	☒	☒	☒	☒	☒	☒
I acknowledge that these represent my contribution to the above research output: EBarker 28/11/2020						
Adam D Martin	☐	☒	☒	☒	☒	☒
I acknowledge that these represent my contribution to the above research output: Amartin 30/11/20						
Christopher J Garvey	☐	☒	☒	☒	☒	☒
I acknowledge that these represent my contribution to the above research output: cjgarvey 28/11/2020						
Ching Yong Goh	☐	☒	☐	☐	☐	☐
I acknowledge that these represent my contribution to the above research output: 29/11/2020						
Franca Jones	☐	☐	☐	☐	☒	☒
I acknowledge that these represent my contribution to the above research output: 29/11/2020						
Mauro Mocerino	☒	☐	☐	☐	☐	☒
I acknowledge that these represent my contribution to the above research output: M.Mocerino 30/11/2020						
Brian W Skelton	☐	☒	☒	☐	☐	☐
I acknowledge that these represent my contribution to the above research output: BWSkelton 30/11/2020						
Mark I Ogden	☒	☐	☐	☐	☒	☒
I acknowledge that these represent my contribution to the above research output: M. Ogden 01/12/2020						
Thomas Becker	☒	☒	☐	☐	☒	☒
I acknowledge that these represent my contribution to the above research output: Thomas Becker 30.11.2020						